Clemson University
TigerPrints

All Dissertations | Dissertations

5-2007

DEVELOPMENT AND IN VITRO EXAMINATION OF MATERIALS FOR OSSEOINTEGRATION

Sahil Jalota
Clemson University, sjalota@clemson.edu

Follow this and additional works at: https://tigerprints.clemson.edu/all_dissertations

 Part of the Materials Science and Engineering Commons

Recommended Citation
Jalota, Sahil, "DEVELOPMENT AND IN VITRO EXAMINATION OF MATERIALS FOR OSSEOINTEGRATION" (2007). *All Dissertations*. 78.
https://tigerprints.clemson.edu/all_dissertations/78

This Dissertation is brought to you for free and open access by the Dissertations at TigerPrints. It has been accepted for inclusion in All Dissertations by an authorized administrator of TigerPrints. For more information, please contact kokeefe@clemson.edu.

DEVELOPMENT AND *IN VITRO* EXAMINATION OF MATERIALS FOR OSSEOINTEGRATION

A Dissertation
Presented to
the Graduate School of
Clemson University

In Partial Fulfillment
of the Requirements for the Degree
Doctor of Philosophy
Materials Science and Engineering

---

by
Sahil Jalota
May 2007

Accepted by:
Dr. Sarit B. Bhaduri, Committee Chair
Dr. Burtrand Lee
Dr. Jian Luo
Dr. Thomas Boland

ABSTRACT

Bone is a connective tissue with nanosized particles of carbonated apatitic calcium phosphate dispersed in a hydrated collagen matrix. With the ageing of the baby boomer population, an increasing number of people sustain bone fractures and defects. Hence, efforts are underway to develop materials to hasten the healing and repairing of such defects. These materials are termed as artificial bone substitutes.

This study represents innovative techniques for development of bone implant materials and improving the existing substitute materials. Emphasis was on three different kinds of materials: Metals (titanium and alloys), Ceramics (calcium phosphates), and Polymers (collagen). The bioactivity of titanium and alloys, resorptivity of calcium phosphates and biocompatibility of collagen were the major issues with these materials. These issues are appropriately addressed in this dissertation. For titanium and alloys, biomimetic coating methodology was developed for uniformly and evenly coating 3-D titanium structures. Cracks were observed in these coatings and a protocol was developed to form crack-free biomimetic coatings. In calcium phosphates, increasing the resorption rate of HA (hydroxyapatite) and decreasing the resorption rate of β-TCP (β-tricalcium phosphate) were studied. HA-based ceramics were synthesized with Na^{+} and CO_3^{2-} ions dopings, and development of biphasic mixtures of HA-β-TCP and HA-Rhenanite was performed. Similarly, β-TCP ceramics were synthesized with Zn^{2+} ion doping and development of β-TCP-HA biphasic mixtures was performed. In case of collagen, a biomimetic coating process was developed that decreased the time to coat the collagen substrates and also increased biocompatibility, as determined by the response of mouse osteoblasts.

DEDICATION

I dedicate this work to my wife Mrs. Satvinder Jalota, my parents Dr. M.L. Jalota and Dr. Kanta Jalota, my brother Mr. Capri Jalota, sister-in-law Mrs. Rashmi Jalota, and the rest of my family members and friends. This dissertation was not possible without their love, encouragement and support.

ACKNOWLEDGEMENTS

My deepest and sincerest gratitude and appreciation go out to Dr. Sarit B. Bhaduri and Dr. A. Cuneyt Tas. Thank you for all the guidance and support throughout my dissertation work.

I would also thank my committee members Dr. Burtrand Lee, Dr. Jian Luo and Dr. Thomas Boland for their able support and guidance. Each of you were instrumental in the completion of my dissertation. Both of you provided me with additional knowledge and a better understanding of the subject.

My appreciation to Ms. Kim Ivey, Chemist, School of Materials Science and Engineering for her continuous support in doing FT-IR analyses. A special thanks to EM facility (Joan Hudson and Amar Khumbar) for lending support and teaching me the operation of scanning electron. Also would also like to thank Cassie Gregory for performing the *in vitro* osteoblast cell culture experiments.

My gratitude extends forward to my laboratory team members, Dr. C.H. Jung, Muralithran Kutty, Jake Jokisaari, Baris Kokuoz, Ken Evans, and Tarang Desai for helping and providing support at various stages during my dissertation. Thank you for all wonderful times we have had together and the given memories that I will cherish for the rest of my life.

TABLE OF CONTENTS

Table of Contents (Continued)

Page

Table of Contents (Continued)

Page

LIST OF TABLES

LIST OF FIGURES

List of Figures (Continued)

List of Figures (Continued)

Figure Page

List of Figures (Continued)

Figure Page

CHAPTER 1

INTRODUCTION

Bone graft or osteal implant surgery has been a topic of research for many years due to ever-increasing demand for bone substitutes. An estimated 2 million people sustain bone fractures each year in the United States as a result of activity or trauma.[1] This procedure replaces missing bone with material from either the patient's own body (autograft), natural substitute (allograft) or a synthetic material (artificial graft). The most desirable implants are those which are autogenous and allogenic since no immune rejection occurs. However, sufficient material cannot always be derived from the patient or a suitable donor and current medical technologies are not yet able to synthesize these materials. As a consequence, artificial materials are substituted. In contrast to the previous methods, abundant resources are available to produce artificial replacements. *In this research, emphasis is laid on three kinds of artificial materials: Metal (Titanium and alloys), Ceramics (calcium phosphates) and Polymer-Ceramic Composite (collagen-calcium phosphates).*

1.1 Titanium and alloys

Titanium and alloys are important materials for biomedical and dental implants due to **t**heir lower modulus, superior biocompatibility and better corrosion resistance when compared to more conventional stainless and cobalt-based alloys. This is due to the factor that titanium (and alloys) readily forms a thin surface oxide layer upon contact with either air or fluids. They are generally regarded to have good biocompatibility but are relatively bioinert, that is, they do not bond to bone. Upon implantation, titanium (and alloys) is thereby recognized as a foreign material and the body tries to isolate it by encasing in fibrous tissues.

The process of fibrous encapsulation is described as follows.[2,3,4] After implanted into body, neutrophils and macrophages are first noted on the implants,

followed by the formation of foreign body giant cells from activated macrophages. It is generally accepted that osteoprogenitor cells migrate to the implant site and differentiate into osteoblasts that make bone. After the materials have been implanted into the body, the first stage in the reaction (after interaction with water and ions) is non-specific protein adsorption. Afterwards, neutrophils and macrophages interrogate the implant. The macrophage interaction and cytokines released by the macrophages are believed to attract fibroblasts and drive the foreign body encapsulation process.[2,3,4]

This leads to poor adhesion of titanium implant with the bone which is attributed only to the mechanical interlocking of titanium surface roughness and pores of bone. It was noted that the implant and bone is separated by a thin non-mineral layer.[5] The material surface plays an extremely important role in the response of the biological environment to the artificial implants. In order to make titanium biologically bond to bones, surface modification methods have been proposed to improve the bioactivity of titanium (and alloys).

Surface modifications can be performed by either physical or chemical methods. The physical methods are used to deposit a layer of bioactive calcium phosphates on the titanium surface. The most preferred calcium phosphate coating that is performed is that of hydroxyapatite because of its similarity to the mineral phase of natural hard tissues. [6-9] Current hydroxyapatite physical coating methods can be broadly categorized as follows: (1) Plasma Spraying,[10-12] (2) Dip Coating,[13-17] (3) Sputtering,[18-27] (4) Electrophoretic Deposition,[28-35] and (5) Pulsed Laser Ablation[36-38]. Due to use of very high temperatures in most of these processes, a change in chemical composition and structure of the hydroxyapatite coating takes place, reducing its adhesion to the substrate, decreasing its bioactivity, and thereby limiting its use.[2] This disadvantage is overcome by using chemical methods that are performed at relatively lower temperatures.

Current chemical modification techniques involves treating the surface with either acid,[39-42] hydrogen peroxide,[43-47] or a strong base[48-55] followed by a heat treatment step which converts the layer from amorphous to crystalline. The layer produced induces apatite forming ability on the metal surface and exhibits

bone-bonding ability. Other common ways of chemical treatments are sol-gel coatings,[56-59] anodic oxidation,[60-64] and SBF-based biomimetic coating[65-69] techniques. Of these processes, only SBF-based biomimetic coatings employ physiological conditions that is, in a solution at a pH 7.4 and 37°C, to coat. The most important advantage is that the formed coatings retain carbonates and are similar to the biological apatites. In a recent study it was shown that SBF-coated titanium substrates behaved better with the osteoblast cells than alkali-treated or pristine titanium substrates.[69]

The biomimetic coatings are formed by soaking an alkali pre-treated titanium (or an alloy) substrate in a simulated body fluid (SBF) solution. The alkali pre-treatment is a crucial step, which forms a hydrous sodium or potassium titanate layer (depending upon the alkali used) on the substrate.[68,70-72] The as-formed sodium (or potassium) titanate on soaking in SBF exchanges Na^+ (K^+) ions with the H_3O^+ ions and forms Ti-OH groups on the surface that increases the ionic activity of apatite in SBF.[73] During soaking, nanometer sized apatitic calcium phosphate globules rapidly nucleate on the sodium (or potassium) titanate layer and then grow to a few microns by consuming Ca and P ions from the SBF solution.[71]

There are several different SBF solutions recipes available in the literature.[74-78] It was found out that different SBFs lead to different amount and type of coating. Recently, the apatite inducing abilities of 3 different SBF solutions referred to as *c*-SBF, *t*-SBF and *r*-SBF on these alkali treated titanium substrates was investigated.[69] *c*-[74] and *r*-SBF[75,76] are conventional and revised versions of SBF, as developed by Kokubo. *t*-SBF[77,78] is the formulation developed by Tas. The compositions of the three SBF solutions and the important differences between them are given in ref 69. It was noted that *t*-SBF solutions with an HCO_3^- concentration of 27mM are able to coat titanium strips more quickly than c-SBF solutions.[69] Another important conclusion from this study was that the osteoblast response was better for coatings produced by *t*-SBF than *r*-SBF solutions.[69] *These initial results were taken into consideration and a biomimetic coating methodology was developed for uniformly and evenly coating 3-D*

structures utilizing t-SBF (Chapter 2).

In spite of all the advantages of biomimetic coatings, it was noted that cracks were persistently present on these apatitic calcium phosphate coatings irrespective of the composition of the coating solution. A major consequence of the presence of these cracks substantially increases the chances of delamination. Thereby, decreasing the coating's bonding ability with the natural bone. Hence, *reasons for the formation of such cracks was found and a protocol for producing crack-free homogeneous biomimetic coating on Ti6Al4V utilizing t-SBF was established (Chapter 3).*

1.2 Calcium Phosphates

Apart from titanium and alloys, several other ceramic materials have been discovered that have good biocompatibility. These are known as Bioceramics. Materials that can be classified as bioceramics are: Alumina, Zirconia, Calcium phosphates, Silica based glasses or glass ceramics, and Pyrolytic carbons.[79] This research work consists focusing on research and development of calcium phosphate materials for implants. There are several calcium phosphates that found use in the biomedical field and are as follows: tetra-calcium phosphate [TTCP, $Ca_4(PO_4)_2O$], tri-calcium phosphate [α-TCP, α-$Ca_3(PO_4)_2$ and β-TCP, β-$Ca_3(PO_4)_2$], di-calcium phosphate anhydrous [DCPA, monetite, $CaHPO_4$] and di-calcium phosphate dihydrate [DCPD, brushite, $CaHPO_4.2H_2O$]. However, most commonly used calcium phosphate as substitute material is sintered HA. This is because HA is closely similar in chemical composition, structure, and physicochemical properties to the mineral component of the osseous tissue.[80,81] Another calcium phosphate that has recently become a subject of increased interest is sintered TCP, due to its increased resorption rate.[82,83] But both these materials experience some problems, which are highlightened in this section and appropriate solutions are suggested.

Before proceeding further, it is important here to understand the bone material and its remodeling process. Bone is a connective tissue with extracellular substance consisting of a carbonated, apatitic calcium phosphate nanosize mineral

dispersed in what is essentially a hydrated collagen matrix.[84-86] All bones consist of living cells embedded in the mineralized organic matrix, which are: the matrix-forming osteoblasts, the tissue-resorbing osteoclasts, and the osteocytes.[86,87] Osteoblasts are the cells present in bones which actually build the extracellular matrix and regulate its mineralization. The lifespan of an osteoblast ranges up to 8 weeks in humans, during which time it lays down 0.5 to 1.5 prm osteoid per day.[86-88] Osteoclasts, on the other hand, are able to resorb fully mineralized bone as they are equipped with a variety of enzymes which lower the local pH to values between 3 and 4. Osteocytes are the principal (they account for about 90% of all cells in the adult skeleton) cells present in adult bones, and their special construction may actually orchestrate the spatial and temporal recruitment of the cells that form and resorb bone. Modeling is the processes whereby bone is laid down onto available surfaces, whereas in remodeling, osteoclastic resorption of bone leaves pockets that are then filled by osteoblast activity.[87] When the bones no longer have any osteoblasts or osteoclasts, the modeling/remodeling processes would cease.

Calcium phosphate-based bone substitute materials should ideally be implanted with the design consideration that the osteoclastic resorption will be able to slowly and gradually degrade the bone substitute material, and in the pockets created by the osteoclasts, new bone will be deposited by the osteoblasts.[86,87] If a material is not resorbed by the osteoclasts, then it can not be used as a bone substitute bioceramic, which can take part in bone turnover. On the other hand, if an implant material is simply soluble in physiological fluids, then it can not help much in the bone remodeling processes. This is due to the lack of that precise interaction and crosstalk between the resorbing osteoclasts and depositing osteoblasts, which must occur.[86]

Following observation of the behavior of bioceramics *in vivo*, it was determined that the essential requirement[86] for bonding of the implant is that it should:

1. readily take part in bone remodeling (i.e., osteoconduction the direct anchorage of an implant by bony tissue surrounding it, without the growth of fibrous tissue at the bone implant interface),
2. itself cause the formation of bone tissues (i.e., osteoinduction), even if it is not in interfacial contact with natural bones,
3. maintain its mechanical strength during the intermediate stages of cellular (i.e., osteoclasts) active resorption, and
4. be gradually but fully replaced, within 48 to 52 weeks, by new bone (i.e., osseointegration) at the implantation site.

HA or β-TCP implants exhibit relatively good tissue compatibility, and new bone is formed directly on the implants with no fibrous encapsulation.[89] However, sintered and well-crystallized HA ceramics usually demonstrated minimal *in vivo* resorption, with resorption times lagging the new bone formation rates.[90-94] Literature reports the lack of full participation of sintered HA implants in the bone remodeling processes even a year after their implantation.[95] Kilian et al.[96] showed that nonsintered HA could even be phagocytized and dissolved by macrophages and osteoclasts, while sintered ceramics did not degrade and remained at the site of implantation for years following the surgery. β-TCP, on the other hand, has a significantly high solubility[97,98] and typically fades away from the defect site even before the completion of new bone formation. . It was shown that the dissolution rate of β-TCP (i.e., 1.26×10^{-4} mol/m^{-2} min^{-1}) in an aqueous solution at a pH of about 6 was about 89 times greater than that of carbonated apatite (1.42×10^{-6} mol/m^{-2} min^{-1}).[97] As an implant the higher dissolution rate of β-TCP may result in premature loss of mechanical strength.

An ideal skeletal repair implant should readily take part in the bone remodeling processes, and also allow for the direct anchorage by the bony tissues surrounding it (osteoconduction).[99] If the skeletal repair implant itself causes the *in situ* formation of the mineral part of the bone tissues (osteoinduction) rich in carbonated, apatitic calcium phosphates,[100] while it is continuously resorbing (*in vivo* osseointegration), this could be its most effective repair method of the defect

site.[86,101-103] This is similar to the mineral phase of human bones. Loty et al.[104] described the mechanism of the binding between bones and the bone-like apatite layer. The osteoblast cells proliferate on the bone-like apatite layers, and form a biological matrix containing apatite and collagen whilst consuming the apatite in the bone-like apatite layer and then remodeling the layer. This bonding process between artificial materials and natural bone is identical to that involved in the bonding between natural bones.[104] Therefore, efforts in the direction of developing calcium phosphate-based bone substitutes of higher *in vivo* resorbability and osteoinductive/osteoconductive capabilities are still needed.

Therefore, the main line of research for HA-containing biomaterials was to increase the resorption/solubility rate of the implant material. This can be achieved by:

(1) *Preparation of nonstoichiometric HA by modification of the HA structure with foreign ions (Na^+ / K^+ / Mg^{2+} / CO_3^{2-})*; and

(2) *Design of poly-mineral composites incorporating HA and other calcium phosphates*.

In the first instance, resorption depends on the structural perfection of HA: nonstoichiometry, type of solid solutions, site occupancies, and distribution of the effective charge in the presence of foreign cations. The apatite structure is very hospitable and allows substitutions of Ca^{2+}, PO_4^{2-} or OH^- sites with other ions.[79-81] There is evidence in literature that substitution results in changes in properties like lattice parameters, morphology, and most importantly solubility without significantly changing the hexagonal symmetry.[79] Undoubtedly, HA doped with low concentrations of select elements may promote bonding of orthopedic/dental implants to juxtaposed bone due to its similarity with the biological apatite / bone mineral. Therefore, *our aim was first, to synthesize HA ceramics with Na^+ and CO_3^{2-} ions dopings and then, to evaluate their bioactivity and biocompatibility (Chapter 4).*

As for the second line of research, a composite is formed of HA with other calcium phosphates. The log K_{sp} values for all calcium phosphates is shown in

Table 1.1. The table clearly shows that HA has the lowest dissolution rate whereas all other calcium phosphates dissolve much faster than HA. Therefore, making a composite of HA with other calcium phosphate will definitely improve the resorption rate of the material *in vivo*. However, β-TCP has been a choice of material since it fully resorbs in human tissue, whereas other phosphates experience weak resorption and belong to the class of resistive compounds. Jarcho[105,106] points out that the resorption rate of implants is proportional to the TCP content: increasing the fraction of HA reduces the resorption rate.

Other materials can also be used to make a composite. The criterion followed in selecting these materials is that they should (1) promote bioactivity, (2) enhance cellular proliferation, and (3) possess high solubility and increase the degradation rate of the composite. Thus, *innovative techniques were employed to synthesize HA-TCP (Chapter 4) and HAP-Rhenanite composites (Chapter 5).*

For β-TCP-containing biomaterials, the line of research followed consists of:

(1) *Design of poly-mineral composites of β-TCP and HA*;

(2) *Stabilizing the structure of β-TCP*.

Table 1.1 Solubility products of different calcium phosphates

Chemical Formula	**Name**	**Ca/P**	**-log K_{sp} at 25ºC**
$Ca(H_2PO_4)_2$	MCPA	0.5	highly soluble
$Ca(H_2PO_4)_2.H_2O$	MCPM	0.5	highly soluble
$CaHPO_4$	DCPA	1.0	6.90
$CaHPO_4.2H_2O$	DCPD	1.0	6.59
$Ca_8H_2(PO_4)_6.5H_2O$	OCP	1.33	96.6
α-$Ca_3(PO4)_2$	α-TCP	1.5	25.5
β-$Ca_3(PO4)_2$	β-TCP	1.5	28.9
$Ca_{10}(PO_4)_6(OH)_2$	HA,	1.67	58.4
$Ca_4(PO_4)_2O$	TTCP	2.0	38.0

The first one is similar to that of HA, wherein composites of β-TCP and HA are formed which lead to an optimal resorption rate and enhanced cellular proliferation *(Chapter 4)*. The second line of research depends on the stabilization of the β-TCP structure. It was shown that when the β-TCP structure was stabilized, the dissolution rate decreases, providing better mechanical properties. This stability in structure can be achieved by substituting the larger Ca^{2+} (0.099 nm) ions with smaller divalent cations, such as Zn^{2+} (0.074 nm)[107,108] or Mg^{2+} (0.072 nm)[109] ions. Therefore, *different range of Zn-doping from pure β-TCP to 1.0 wt% Zn-doped β-TCP was synthesized and we examined the effect of Zn-doping on dissolution and biocompatibility (Chapter 6).*

1.3 Collagen-Calcium Phosphates Composite

A composite of collagen and apatite is of special interest because of their compositional similarity with bone.[110-113] In recent years, there is an increased effort to produce apatite-collagen composite materials by innovative biomimetic processing.[113-120] Biomimetic coating process is employed to coat collagen substrates to synthesize the apatite-collagen composites.[121-129] This process is similar to that employed for titanium and alloys, which involves soaking the substrate in a SBF solution, wherein several-micron-thick bioactive layers of apatitic calcium phosphate nano-aggregates is deposited. It was noted that even after 4 weeks of soaking time, the collagen surface was not fully covered by apatitic calcium phosphates.[122] Several modifications to the biomimetic coating process were employed by altering the normal soaking procedures, which led to increase in bioactivity.[121-129] These methods include either changing the chemistry of collagen or adding a compound to SBF solutions. Even after these attempted modifications, the process appeared lengthy and the problem of the dissolution of collagen in the liquid medium posed a relevant issue. Therefore, *our aim was to develop a biomimetically coating process that decreased the time to coat the collagen substrates (Chapter 7)*.

1.4 References

1. P. Ullom-Minnich. Prevention of osteoporosis and fractures. *Am Fam Physician* **60** (1999) 194-202.

2. X. Liu, P.K. Chu, C. Dinga. Surface modification of titanium, titanium alloys, and related materials for biomedical applications. *Mater Sci Eng R* **47** (2004) 49–121.

3. J.M. Anderson, in: B.D. Ratner, A.S. Hoffman, F.J. Lemons (Eds.), Biomaterials Science: An Introduction to Materials in Medicine, Academic Press, San Diego, (1996) 165–173.

4. B.D. Ratner, in: D.M. Brunette, P. Tengvall, M. Textor, P. Thomsen (Eds.), Titanium in Medicine, Springer, Berlin (2001) 1–12.

5. P. Thomsen, C. Larsson, L.E. Ericson, L. Sennerby, J. Lausmaa, B. Kasmo. Structure of the interface between rabbit cortical bone and implants of gold, zirconium and titanium. *J Mater Sci Mater Med* **8** (1997) 653.

6. W.L. Jaffe, D.F. Scott. Current concepts review: total hip arthroplasty with hydroxyapatite-coated prostheses. *J Bone Jt Surg* **78A** (1996), pp. 1918–1934.

7. K.A. Thomas. Hydroxyapatite coatings. *Orthopedics* **17** (1994), pp. 267–278.

8. P. Ducheyne, J.M. Cuckler. Bioactive ceramic prosthetic coatings. *Clin Orthop Rel Res* **276** (1992), pp. 102–114.

9. R.J. Furlong, J.F. Osborn. Fixation of hip prostheses by hydroxyapatite ceramic coatings. *J Bone Jt Surg* **73B** (1991), pp. 741–745.

10. Y. Yang, J.L. Ong, K. Bessho. Plasma-sprayed hydroxyapatite-coated and plasma-sprayed titanium-coated implants. In: M.J. Yaszemski, D.J. Trantolo, K. Lewandrowski, V. Hasirci, D.E. Altobelli and L. Wise Donald, Editors, *Biomaterials in orthopedics*, Marcel Dekker Inc., New York (2004), pp. 401–423.

11. M.J. Filiaggi, N.A. Coombs, R.M. Pilliar. Characterization of the interface in the plasma-sprayed HA coating/Ti-6Al-4V implant system. *J Biomed Mater Res* **25** (1991) 1211–1229.

12. V. Palka, E. Postrkova, H.K. Koerten. Some characteristics of hydroxylapatite powders after plasma spraying. *Biomaterials* **19** (1998) 1763–1772.

13. W. Weng, J.L. Baptisa. Alkoxide route for preparing hydroxyapatite and its coatings. *Biomaterials* **19** (1998) 125–131.

14. J. Choi, D. Bogdanski, M. Koller, S.A. Esenwein, D. Muller, G. Muhr, M. Epple. Calcium phosphate coating of nickel-titanium shape-memory alloys. Coating procedure and adherence of leukocytes and platelets. *Biomaterials* **24** (2003) 3689–3696.

15. D. Shi, G. Jiang, J. Bauer. The effect of structural characteristics on the *in vitro* bioactivity of hydroxyapatite. *J Biomed Mater Res (Appl Biomater)* **63** (2002) 71–78.

16. G. Jiang, D. Shi. Coating of hydroxyapatite on highly porous Al_2O_3 substrate for bone substitutes. *J Biomed Mater Res (Appl Biomater)* **43** (1998) 77–81.

17. A.A. Campbell, L. Song, X.S. Li, B.J. Nelson, C. Bottoni, D.E. Brooks, E.S. DeJong. Development, characterization, and anti-microbial efficacy of hydroxyapatite chlorhexidine coatings produced by surface-induced mineralization. *J Biomed Mater Res (Appl Biomater)* **53** (2000) 400–407.

18. S. Ding. Properties and immersion behavior of magnetron-sputtered multi-layered hydroxyapatite/titanium composite coatings. *Biomaterials* **24** (2003) 4233–4238.

19. S. Ding, C. Ju, J.C. Lin. Characterization of hydroxyapatite and titanium coatings sputtered on Ti-6Al-4V substrate. *J Biomed Mater Res* **44** (1999) 266–279.

20. J.G.C. Wolke, J.P.C.M. van der Waerden, H.G. Schaeken, J.A. Jansen. In vivo dissolution behavior of various RF magnetron-sputtered Ca-P coatings on roughened titanium implants. *Biomaterials* **24** (2003) 2623–2629.

21. C. Massaro, M.A. Baker, F. Cosentino, P.A. Ramires, S. Klose, E. Milella. Surface and biological evaluation of hydroxyapatite-based coatings on titanium deposited by different techniques. *J Biomed Mater Res (Appl Biomater)* **58** (2001) 651–657.

22. J.L. Ong, L.C. Lucas. Post-deposition heat treatment for ion beam sputter deposited calcium phosphate coatings. *Biomaterials* **15** (1994) 337–341.

23. J.L. Ong, L.C. Lucas, G.N. Raikar, J.J. Weimer, J.C. Gregory. Surface characterization of ion-beam sputter-deposited Ca-P coatings after *in vitro* immersion. *Col and Surf* **87** (1994) 151–162.

24. J.G.C. Wolke, K. van Dijk, H.G. Schaeken, K. de Groot, J.A. Jansen. Study of the surface characteristics of magnetron-sputter calcium phosphate coatings. *J Biomed Mater Res* **28** (1994) 1477–1484.

25. K. van Dijk, H.G. Schaeken, J.G.C. Wolke, C.H.M. Maree, F.H.P.M. Habraken, J. Verhoven, J.A. Jansen. Influence of discharge power level on the properties of hydroxyapatite films deposited on Ti6Al4V with RF magnetron sputtering. *J Biomed Mater Res* **29** (1995) 269–276.

26. K. van Dijk, H.G. Schaeken, J.G.C. Wolke, J.A. Jansen. Influence of annealing temperature on RF magnetron sputtered calcium phosphate coatings. *Biomaterials* **17** (1996) 405–410.

27. J.G. Wolke, J.P. van der Waerden, H.G. Schaeken, J.A. Jansen. In vivo dissolution behavior of various RF magnetron-sputtered Ca-P coatings on roughened titanium implants. *Biomaterials* **24** (2003) 2623–2629.

28. P. Ducheyne, W. Van Raemdonck, J.C. Heughebaert, M. Heughebaert. Structural analysis of hydroxyapatite coatings on titanium. *Biomaterials* **7** (1986) 97–103.

29. Y. Han, K. Xu, J. Lu, Z. Wu. The structural characteristics and mechanical behaviors of nonstoichiometric apatite coatings sintered in air atmosphere. *J Biomed Mater Res* **45** (1999) 198–203.

30. Y. Han, T. Fu, J. Lu, K. Xu. Characterization and stability of hydroxyapatite coatings prepared by an electrodeposition and alkaline-treatment process. *J Biomed Mater Res* **54** (2001) 96–101.

31. X. Zhu, K. Kim,Y. Jeong. Anodic oxide films containing Ca and P of titanium biomaterials. *Biomaterials* **22** (2001) 2199–2206.

32. L.A. De Sena, M.C. de Andrade, A.M. Rossi, G.D.A. Soares. Hydroxyapatite deposition by electrophoresis on titanium sheets with different surface finishing. *J Biomed Mater Res* **60** (2002) 1–7.

33. J. Ma, C. Wang, K.W. Peng. Electrophoretic deposition of porous hydroxyapatite scaffold. *Biomaterials* **24** (2003) 3505–3510.

34. X. Nie, A. Leyland, A. Matthews, J.C. Jiang, E.I. Meletis. Effects of solution pH and electrical parameters on hydroxyapatite coatings deposited by a plasma-assisted electrophoresis technique. *J Biomed Mater Res* **57** (2001) 612–618.

35. M. Manso, C. Jimenez, C. Morant, P. Herrero, J.M. Martinez-Duart. Electrodeposiiton of hydroxyapatite coatings in basic conditions. *Biomaterials* **21** (2000) 1755–1761.

36. L. Cleries, E. Martinez, J.M. Fernandez-Pradas, G. Sardin, J. Esteve, J.L. Morenza. Mechanical properties of calcium phosphate coatings deposited by laser ablation. *Biomaterials* **21** (2000) 967–971.

37. J.M. Fernandez-Pradas, L. Cleries, E. Martinez, G. Sardin, J. Esteve and J.L. Morenza. Influence of thickness on the properties of hydroxyapatite coatings deposited by KrF laser ablation. *Biomaterials* **22** (2001) 2171–2175.

38. H. Zeng, W.R. Lacefield. The study of surface transformation of pulsed laser deposited hydroxyapatite coatings. *J Biomed Mater Res* **50** (2000) 239–247.

39. A. Nanci, J.D. Wuest, L. Peru, P. Brunet, V. Sharma, S. Zalzal, M.D. McKee. Chemical modification of titanium surfaces for covalent attachment of biological molecules. *J Biomed Mater Res* **40** (1998) 324-335.

40. Z. Schwartz, J.Y. Martin, D.D. Dean, J. Simpson, D.L. Cochran, B.D. Boyan. Effect of titanium surface roughness on chondrocyte proliferation, matrix production, and differentiation depends on the state of cell maturation. *J Biomed Mater Res* **30** (1996) 145-155.

41. H.B. Wen, J.G. Wolke, J.R. Wijn, Q. Liu, F.Z. Cui, K. de Groot. Fast precipitation of calcium phosphate layers on titanium induced by simple chemical treatments. *Biomaterials* **18** (1997) 1471-1478.

42. H.B. Wen, Q. Liu, J.R. Wijn, K. de Groot. Preparation of bioactive microporous titanium surface by a new two-step chemical treatment. *J Mater Sci Mater Med* **9** (1998) 121-128.

43. P. Tengvall, I. Lundstrom. Physico-chemical considerations of titanium as a biomaterial. *Clin Mater* **9** (1992) 115-134.

44. P. Tengvall, I. Lundstrom, L. Sjoqvist, H. Elwing, L.M. Bjursten. Titanium-hydrogen peroxide interaction: model studies of the influence of the inflammatory response on titanium implants. *Biomaterials* **10** (1989) 166-175.

45. P. Tengvall, H. Elwing, L. Sjoqvist, I. Lundstrom, L.M. Bjursten. Interaction between hydrogen peroxide and titanium: a possible role in the biocompatibility of titanium. *Biomaterials* **10** (1989) 118-120.

46. B. Walivaara, I. Lundstrom, P. Tengvall. An in-vitro study of H_2O_2-treated titanium surfaces in contact with blood plasma and a simulated body fluid. *Clin Mater* **12** (1993) 141-148.

47. B. Walivaara, B.O. Aronsson, M. Rodahl, J. Lausmma, P. Tengvall. Titanium with different oxides: *in vitro* studies of protein adsorption and contact activation. *Biomaterials* **15** (1994) 827-834.

48. H.M. Kim, F. Miyaji, T. Kokubo, T. Nakamura. Preparation of bioactive Ti and its alloys via simple chemical surface treatment. *J Biomed Mater Res* **32** (1996) 409.

49. B.C. Yang, J. Weng, X.D. Li, X.D. Zhang, The order of calcium and phosphate ion deposition on chemically treated titanium surfaces soaked in aqueous solution. *J Biomed Mater Res* **47** (1999) 213-219.

50. L. Jonasova, F.A. Muller, A. Helebrant, J. Strnad, P. Greil. Biomimetic apatite formation on chemically treated titanium. *Biomaterials* **25** (2004) 1187-1194.

51. C.X. Wang, M. Wang, X. Zhou. Nucleation and growth of apatite on chemically treated titanium alloy: an electrochemical impedance spectroscopy study. *Biomaterials* **24** (2003) 3069-3077.

52. C.X. Wang, M. Wang. Electrochemical impedance spectroscopy study of the nucleation and growth of apatite on chemically treated pure titanium *Mater Lett* **54** (2002) 30-36.

53. F. Liang, L. Zhou, K. Wang. Enhancement of the bioactivity of alkali-heat treated titanium by pre-calcification. *J Mater Sci Lett* **22** (2003) 1665-1667.

54. L. Jonasova, F.A. Muller, A. Helebrant, J. Strnad, P. Greil. Hydroxyapatite formation on alkali-treated titanium with different content of Na^+ in the Surface Layer. *Biomaterials* **23** (2002) 3095.

55. X. Lu, Y. Leng. TEM Study of Calcium Phosphate Precipitation on Bioactive Titanium Surfaces. *Biomaterials* **25** (2004) 1779-1786.

56. P. Li, K. Grrot, T. Kokubo, Bioactive $Ca_{10}(PO_4)_6(OH)_4$-TiO_2 composite coating prepared by sol-gel process. *J Sol-Gel Sci Technol* **7** (1996) 27–34.

57. M. Manso, M. Langlet, C. Jimenez, J.M. Martinez-Duart, Microstructural study of areosol-gel derived hydroxyapatite coatings. *Biomol Eng* **19** (2002) 63–66.

58. D. Liu, Q. Yang, T. Troczynski, Sol-gel hydroxyapatite coatings on stainless steel substrates. *Biomaterials* **23** (2002) 691–698.

59. C.S. Chai, K.A. Gross, B. Ben-Nissan, Critical ageing of hydroxyapatite sol-gel solutions. *Biomaterials* **19** (1998) 2291–2296.

60. B. Yang, M. Uchida, H.-M. Kim, X. Zhang, T. Kokubo. Preparation of bioactive titanium metal via anodic oxidation treatment. *Biomaterials* **25** (2004) 1003-1010.

61. H. Ishizawa, M. Ogino. Formation and characterization of anodic titanium oxide films containing Ca and P. *J Biomed Mater Res* **29** (1995) 65-72.

62. H. Ishizawa, M. Ogino. Characterization of thin hydroxyapatite layers formed on anodic titanium oxide films containing Ca and P by hydrothermal treatment. *J Biomed Mater Res* **29** (1995) 1071-1079.

63. X. Zhu, K.-H. Kim, Y. Jeong. Anodic oxide films containing Ca and P of titanium biomaterial. *Biomaterials* **22** (2001) 2199-2206.

64. X. Zhu, J.L. Ong, S. Kim, K. Kim. Surface characteristics and structure of anodic oxide films containing Ca and P on a titanium implant material. *J Biomed Mater Res* **60** (2002) 333-338.

65. W.-Q. Yan, T. Nakamura, K. Kawanabe, S. Nishigochi, M. Oka, T. Kokubo. Apatite layer-coated titanium for use as bone bonding implants. *Biomaterials* **18** (1997) 1185-1190.

66. W.-Q. Yan, T. Nakamura, M. Kobayashi, H.-M. Kim, F. Miyaji, T. Kokubo. Bonding of chemically treated titanium implants to bone. *J Biomed Mater Res* **37** (1997) 267-275.

67. P. Habibovic, F. Barrere, C.A. van Bliterswijk, K. de Groot, P. Layrolle, Biomimetic hydroxyapatite coating on metal implants. *J Am Ceramic Soc* **85** (2002) 517–522.

68. A.C. Tas, S.B. Bhaduri. Rapid coating of Ti6Al4V at room temperature with a calcium phosphate solution similar to 10× simulated body fluid. *J Mater Res* **19** (2004) 2742-2749.

69. S. Jalota, S.B. Bhaduri, A.C. Tas. Effect of carbonate content and buffer used in SBF solutions on calcium phosphate formation on Ti6Al4V. *J Mater Sci Mater M* **17** (2006) 697-707.

70. P. Li, I. Kangasniemi, K. de Groot, T. Kokubo. Bone-like hydroxyapatite induction by a gel-derived titania on a titanium substrate. *J Am Ceram Soc* **77** (1994) 1307-1312.

71. T. Kokubo, F. Miyaji, H.-M. Kim, T. Nakamura. Spontaneous formation of bone-like apatite layer on chemically treated titanium metals. *J Am Ceram Soc* **79** (1996) 1127-1129.

72. H.-M. Kim, F. Miyaji, T. Kokubo, T. Nakamura. Apatite forming ability of alkali-treated Ti metal in body environment. *J Ceram Soc Jpn* **105** (1997) 111-116.

73. H. Takadama, H.-M. Kim, T. Kokubo, T. Nakamura. TEM-EDX study of mechanism of bonelike apatite formation on bioactive titanium metal in simulated body fluid. *J Biomed Mater Res* **57** (2001) 441-448.

74. T. Kokubo. Surface chemistry of bioactive glass-ceramics. *J Non-Cryst Solids* **120** (1990) 138-151.

75. A. Oyane, K. Onuma, A. Ito, H.-M. Kim, T. Kokubo, T. Nakamura. Formation and growth of clusters in conventional and new kinds of simulated body fluids. *J Biomed Mater Res A* **64** (2003) 339-348.

76. H.-M. Kim, K. Kishimoto, F. Miyaji, T. Kokubo, T. Yao, Y. Suetsugu, J. Tanaka, T. Nakamura. Composition and structure of apatite formed on organic polymer in simulated body fluid with a high content of carbonate ion. *J Mater Sci Mater M* **11** (2000) 421-426.

77. D. Bayraktar, A.C. Tas. Chemical preparation of carbonated calcium hydroxyapatite powders at 37°C in urea-containing synthetic body fluids. *J Eur Ceram Soc* **19** (1999) 2573-2579.

78. A.C. Tas. Synthesis of biomimetic Ca-hydroxyapatite powders at 37°C in synthetic body fluids. *Biomaterials* **21** 1429-1438 (2000).

79. L.L. Hench, J. Wilson, An Introduction to Bioceramics, Advanced Series in Ceramics – Vol.1, World Scientific Publishing Co. Pte. Ltd., (1993) 1-24.

80. A. S. Posner. The Mineral of Bone. *Clin Orthop Relat Res* **87** (1985) 99.

81. A. S. Posner. The Structure of Bone Apatite Surfaces. *J Biomed Mater Res* **19** (1985) 241-250.

82. J.C. Heughebaert, G. Bonel. Composition, stuctures and properties of calcium phosphates of biological interest. In: Christel P, Meunier A, Lee AJC (eds); *Biological and Biomechanical Performance of Biomaterials* (Elsevier Science Publishers), 9-14 (1986).

83. C.E. Rawlings, J.A. Persing, J.M. Tew. Modern bone substitutes with emphasis on calcium-phosphate ceramics and osteoinductors. *Neurosurgery* **33** (1993) 935-938.

84. L.L. Hench. Bioceramics: From concept to clinic. *J Am Ceram Soc* **74** (1991) 1487.

85. D.D. Lee, C. Rey, M. Aiolova, A. Tofighi. US Patent, No. 6 117 456, Sep. 12, 2000.

86. A.C. Tas. Participation of calcium phosphate bone substitutes in the bone remodeling process: Influence of materials chemistry and porosity. *Key Eng Mater* **264 –268** (2004) 1969 –1972.

87. R. Gunzburg, M. Szpalski, N. Passuti, M. Aebi. The Use of Bone Substitutes in Spine Surgery (Springer-Verlag, Germ any, 2002).

88. G. Bourne. The Biochemistry and Physiology of Bone (Academic Press, USA, 1972).

89. M. Spector. Anorganic bovine bone and ceramic analogs of bone mineral as implants to facilitate bone regeneration. *Clin Plast Surg* **21** (1994) 437– 444.

90. D.S. Metsger, T.D. Driskell, J.R. Paulsrud. Tricalcium phosphate ceramic—A resorbable bone implant: Review and current status. *J Am Dent Assoc* **105** (1982) 1035–1038.

91. J.P. Schmitz, J.O. Hollinger, S.B. Milam. Reconstruction of bone using calcium phosphate bone cements: A critical review. *J Oral Maxillofac Surg* **57** (1999) 1122–1126.

92. S. Joschek, B. Nies, R. Krotz, A. Goepferich. Chemical and physicochemical characterization of porous hydroxyapatite ceramics made of natural bone. *Biomaterials* **21** (2000) 1645–1658.

93. K.A. Hing, S.M. Best, K.E. Tanner, W. Bonfield, P.A. Revell. Mediation of bone ingrowth in porous hydroxyapatite bone graft substitutes. *J Biomed Mater Res A* **68** (2004)187–200.

94. S. Kamakura, Y. Sasano, T. Shimizu, K. Hatori, O. Suzuki, M. Kagayama, K. Motegi. Implanted octacalcium phosphate is more resorbable than β-tricalcium phosphate and hydroxyapatite. *J Biomed Mater Res* **59** (2002) 29–34.

95. Y. Shinto, A. Uchida, F. Korkusuz, N. Araki, K. Ono. *J Bone Joint Surg B* **74** (1992) 600.

96. O. Kilian, S. Wenisch, C. Heiss, U. Horas, E. Dingeldein, R. Schnettler. Einfluss von Ostim kombiniert mit autologen thrombozytaeren Wachstumsfaktoren. *Biomaterialien* **3** (2002) 126–132.

97. R. Tang, M. Hass, W. Wu, S. Gulde, G.H. Nancollas. Constant composition dissolution of mixed phases. II. Selective dissolution of calcium phosphates. *J Colloid Interface Sci* **260** (2003) 379–384.

98. S.H. Kwon, Y.K. Jun, S.H. Hong, H.E. Kim. Synthesis and dissolution behavior of β-TCP and HA/β-TCP composite powders. *J Eur Ceram Soc* **23** (2003) 1039 –1045.

99. A. Hoshikawa, N. Fukui, A. Fukuda, T. Sawamura, M. Hattori, K. Nakamura, H. Oda. Quantitative analysis of the resorption and osteoconduction process of a calcium phosphate cement and its mechanical effect for screw fixation. *Biomaterials* **24** (2003) 4967– 4975.

100. H.P. Yuan, Z.J. Yang, Y.B. Li, X.D. Zhang, J.D. De Bruijn, K. de Groot. Osteoinduction by calcium phosphate biomaterials. *J Mater Sci Mater Med* **9** (1998) 723–726.

101. E. Goyenvalle, N.J.M. Guyen, E. Aguado, N. Passuti, G. Daculsi. Bilayered calcium phosphate coating to promote osseointegration of a femoral stem prosthesis. *J Mater Sci Mater Med* **14** (2003) 219 –227.

102. M. Szpalski, R. Gunzburg. Applications of calcium phosphate-based cancellous bone void fillers in trauma surgery. *Orthopedics* 25 (2002) S601–S609.

103. W.F. Neuman, M.W. Neuman. The Chemical Dynamics of Bone Mineral. Chicago: Chicago University Press; 1958.

104. C. Loty, J.-M. Sautier, H. Boulekbache, T. Kokubo, H.-M. Kim, N. Forest. *In vitro* bone formation on a bone-like apatite layer prepared by a biomimetic process on a bioactive glass-ceramic. *J Biomed Mater Res* **49** (2000) 423 – 434.

105. M. Jarcho. Calcium Phosphate Ceramics as Hard Tissue, *Clin. Orthop. Rel. Res.*, **157** (1981) 260–278.

106. A. Yu. Malysheva, B. I. Beletskii. Biocompatibility of Apatite-Containing Implant Materials. *Inorg Mater* **37** (2001) 180–183.

107. A. Ito, H. Kawamura, S. Miyakawa, P. Layrolle, N. Kanzaki, G. Treboux, K. Onuma, S. Tsutsumi. Resorbability and solubility of zinc-containing tricalcium phosphate. *J Biomed Mater Res* **60** (2002) 224-31.

108. A. Bigi, E. Foresti, M. Gandolfi, M. Gazzano, N. Roveri. Isomorphous substitutions in beta-tricalcium phosphate: The different effects of zinc and strontium. *J Inorg Biochem* **66** (1997) 259-65.

109. I. Manjubala, T.S.S. Kumar. Preparation of biphasic calcium phosphate doped with magnesium fluoride for osteoporotic applications. *J Mater Sci Lett* **20,** (2001) 1225-7.

110. L.L. Hench. Bioceramics: From concept to clinic. *J Am Ceram Soc* **74** (1991) 1487-1510.

111. D.D. Lee, C. Rey, M. Aiolova, and A. Tofighi. Methods and products related to the physical conversion of reactive amorphous calcium phosphate. US Patent, No. 6117456, 2000.

112. A. Rovira, R. Bareille, I. Lopez, F. Rouais, L. Bordenave, C. Rey and M. Rabaud. Preliminary reports on a new composite material made of calcium phosphate, elastin peptides and collagens. *J Mater Sci Mater Med* **4** (1993) 372-380.

113. N.J. Mathers and J.T. Czernuszka. Growth of hydroxyapatite on type 1 collagen. *J. Mater. Sci. Lett.* **10** (1991) 992-993.

114. S.-T. Liu. Composite materials for hard tissue replacement. U.S. Patent No. 5320844, 1994.

115. R.Z. Wang, F.Z. Cui, H.B. Lu, H.B. Wen, C.L. Ma and H.D. Li. Synthesis of nanophase hydroxyapatite/collagen composite. *J Mater Sci Lett* **14** (1995) 490-492.

116. Y. Doi, T. Horiguchi, Y. Moriwaki, H. Kitago, T. Kajimoto and Y. Iwayama. Formation of apatite-collagen complexes. *J Biomed Mater Res* **31** (1996) 43-49.

117. M. K. Kwan, S.D. Pacetti and R. K. Yamamoto. Bone grafting matrix. U.S. Patent No. 6187047, 2001.

118. R.K. Yamamoto, M. K. Kwan, S.D. Pacetti. Tissue repair matrix. U.S. Patent No. 6764517, 2004.

119. L.A. Sena, P. Serricella, R. Borojevic, A.M. Rossi, G.A. Soares. Synthesis and characterization of hydroxyapatite on collagen gel. *Key Eng Mater* **254-256** (2004) 493-496.

120. B.-H. Yoon, H.-W. Kim, S.-H. Lee, C.-J. Bae, Y.-H. Koh, Y.-M. Kong, H.-E. Kim. Stability and cellular responses to fluorapatite–collagen composites. *Biomaterials* **26** (2005) 2957–2963.

121. S.-H. Rhee, J. Tanaka. Hydroxyapatite coating on a collagen membrane by a biomimetic method. *J Am Ceram Soc* **81** (1998) 3029-3031.

122. S.-H. Rhee, J.D. Lee, J. Tanaka. Nucleation of hydroxyapatite crystal through chemical interaction with collagen. *J Am Ceram Soc* **83** (2000) 2890-2892.

123. L.-J. Zhang, X.-S. Feng, H.-G. Liu, D.-J. Qian, L. Zhang, X.-L. Yu, F.-Z. Cui. Hydroxyapatite/collagen composite materials formation in simulated body fluid environment. *Mater Lett* **58** (2004) 719-722.

124. A. L. Andrade, J. M. F. Ferreira, R.Z. Domingues. Zeta potential measurement in bioactive collagen. *Mater Res* **7** (2004) 631-634.

125. D. Lickorish, J.A. Ramshaw, J.A. Werkmeister, V. Glattuer, C.R. Howlett. Collagen-hydroxyapatite composite prepared by biomimetic process. *J Biomed Mater Res A* **68** (2004) 19-27.

126. N. Kobayashi, K. Onuma, A. Oyane, A. Yamazaki. The role of phosvitin for nucleation of calcium phosphates on collagen. *Key Eng Mater* **254-256** (2004) 537-540.

127. X. Li, J. Chang. Preparation and characterization of bioactive collagen/wollastonite composite scaffolds. *J Mater Sci Mater Med* **16** (2005) 361-365.

128. D. Eglin, S. Maalheem, J. Livage, T. Coradin. *In vitro* apatite forming ability of type I collagen hydrogels containing bioactive glass and silica sol-gel particles. *J Mater Sci Mater M.* **17** (2006) 161– 167.

129. X.Y. Lin, H.S. Fan, X.D. Li, M. Tang, X.D. Zhang. Evaluation of bioactivity and cytocompatibility of nano-HA/collagen composite *in vitro*. *Key Eng Mater* **284-286**, (2005) 553-556.

CHAPTER 2

OSTEOBLAST PROLIFERATION ON NEAT AND APATITE-LIKE CALCIUM PHOSPHATE-COATED TITANIUM FOAM SCAFFOLDS

Abstract

The biocompatibility and the load-bearing ability of lightweight titanium made it possible to be used as a biomaterial, especially in hip revision and fixation surgery. It was initially shown that sand-blasted or surface-roughened titanium implants had an improved bone-bonding ability over the bioinert metallic surfaces. Plasma-spraying of a phase mixture of loosely-attached calcium phosphates on titanium implants further improved their in vivo bone-bonding ability. However, stoichiometric calcium hydroxyapatite ceramic of high crystallinity is known to have poor in vivo resorbability, and is shy of taking part in bone remodeling and of being resorbed by the osteoclasts. Supersaturated calcium phosphate (CaP) solutions, such as synthetic body fluids (SBF), on the other hand, are able to form "carbonated, hydrophilic and apatite-like" CaP nano-aggregates on titanium surfaces. A Tris-buffered SBF solution with an HCO_3^- concentration of 27mM was used in this study. Neat, NaOH-etched, and SBF-coated (biomimetic coating) titanium foams were compared with *in vitro* cell culture experiments by using rat osteoblasts. SBF-coated foams were found to yield the highest protein concentration at the end of the *in vitro* culture tests. Such biomimetic coatings were easily formed on flat strips, springs, or 3D foams of titanium, without any geometric constraints. The coated titanium springs and foams were characterized by using XRD, SEM, and FTIR.

(This work is published in *Mater Sci Eng C* 27 (2007) 432–440)

2.1. Introduction

Human blood plasma has a Ca/P molar ratio of 2.50. On the other hand, the same molar ratio becomes 1.556, 1.316×10^{-3}, and 5.20 for the human extracellular, intracellular, and cerebrospinal fluids, respectively.[1] Acellular SBF (synthetic body fluid) solutions try to mimic the ionic concentrations of human blood plasma, therefore, SBF is supersaturated with respect to the precipitation of carbonated, non-stoichiometric, poorly-crystallized or nanocrystalline apatite-like calcium phosphate.[2,3] Ringer's[4], Earle's (EBSS, Earle's Balanced Salt Solution[5]) and Hank's (HBSS[6]) solutions are most popular and are the guiding force for the development of synthetic body fluid solutions of today. In contrast to the earlier solutions, such as Ringer's, Earle's and Hanks solutions, the pH values of SBF solutions were fixed at the physiological value of 7.4 by using organic buffers, such as TRIS (tris-hydroxymethyl-aminomethane)[2,3] or HEPES (2-(4-(2-hydroxyethyl)-1-piperazinyl)ethane sulphonic acid)[7–9].

c-SBF[2] was essentially a TRIS–HCl-buffered variant of HBSS[6]. *c*-SBF formulation raised the Ca/P molar ratio to 2.50, in comparison to 1.62 in HBSS. Moreover, HBSS and *c*-SBF solutions have exactly the same low carbonate ion concentrations (i.e., 4.2mM), which is far from imitating that of the human plasma (i.e., 27mM). Tas et al.[3,10] have been the first to raise the HCO_3^- concentration in a TRIS–HClbuffered SBF solution (i.e., *tas*-SBF) to 27 mM, while Bigi et al.[7] were the first to do the same in a HEPES–NaOH-buffered SBF solution (i.e., *Bigi*-SBF) of 27mM HCO_3^-. SBF solutions were found to be able to induce apatite-like calcium phosphate formation on numerous metallic, ceramic or polymeric surfaces (only after proper surface pretreatments) immersed in them.[11] Oyane et al.[9], who developed the HEPES-buffered *r*-SBF recipe with ion concentrations exactly equal to those of human plasma, reported that *r*-SBF would release CO_2 gas from the fluid, causing a decrease in HCO_3^- concentration, and an increase in pH value, when the storage period was long. Furthermore, these authors stated that r-SBF would not be suitable for long-term use in the biomimetic coating processes owing to its instability.[9] The buffering agent TRIS present in conventional SBF (*c*- and *tas*-SBF) formulations, for instance, was

reported[12] to form soluble complexes with several cations, including Ca^{2+}, which further reduces the concentration of free Ca^{2+} ions available for the real time calcium phosphate coating. To our knowledge, this behavior has not yet been reported for HEPES.

The term biomimetic coating stands for the formation of several micron-thick layer of hydrated calcium phosphate nano-aggregates on any suitable substrate (either metallic, ceramic or polymeric) at the human body temperature (36.5–37°C) from a supersaturated or metastable solution, whose ionic composition and pH value mimic those of human plasma. As implied by this definition, the coating process shall not necessarily be instantaneous and may progress within the long physiological timeframes as well. Calcium phosphate deposits observed on explanted intraocular lenses[13], silicon mammary prostheses[14], and heart valves and arteries[15] do all form in vivo working examples of natural biomimetic coating or calcification processes. In stark contrast to what numerous researchers keep naming in the open literature, the calcium phosphate aggregates deposited by the biomimetic coating processes are not simply calcium hydroxyapatite (HA: $Ca_{10}(PO_4)_6(OH)_2$ = 3 $Ca_3(PO_4)_2{\cdot}Ca(OH)_2$). Biomimetic coating processes do not have the high enough pH to form a hydroxide material. Biomimetic coating deposits contain Ca^{2+}, HPO_4^{2-}, and PO_4^{3-} ions, but the Ca/P molar ratio of those were found to be greater than 1.7, typically between 1.7 and 2.7.[16] Moreover, biomimetic CaP deposits were found to lack OH^- ions like the human bones,[17] and contain CO_3^{2-} ions (between 19 and 40 wt.%)[16]. Characteristic micro-globules or spherulites deposited by the biomimetic coating consist of intermingling nanoplatelets of CaP resembling a porcupine architecture with high surface area. The thickness of the formed biomimetic coating nanoplatelets is very much comparable with that of the apatite-like nanocrystals (20–30nm) observed in bone mineral.[18] Biomimetic coating surfaces represent a microtopographical complexity, which create a greater surface area to which bone cell-mediated proteins could adsorb.[19] Therefore, the deposits obtained by the biomimetic coating are best described by using the following; “carbonated, hydrated, apatite-like calcium phosphate nanoplatelet aggregates.” Characteristic

nanotexture of such biomimetic CaP deposits on Ti6Al4V has been documented in the open literature.[20,21] Regardless of the concentration of the SBF solution used, whether it is 1×SBF[2,3] or 10×SBF[21], the unique nanomorphology observed in the deposited layers did not change. Habibovic et al.[22] coated Ti6Al4V foams (produced by polyurethane sponge-burn out method) in 3 days by using a TRIS- or HEPES-free 5×SBF (i.e., a solution five times more concentrated than *c*-SBF recipe) solution, and reported that when the CaP-coated foams were implanted into the back muscles of goats, they caused ectopic bone formation in 6 to 12 weeks. *Tas*-SBF solutions with an HCO_3^- concentration of 27mM are able to coat titanium strips more quickly than c-SBF solutions[23]. The goal of this study was to test the rat osteoblast attachment and proliferation on surfaces of approximately 85% porous (with interconnected pore sizes in the range of 400 to 500μm) titanium foams. Neat, NaOH-treated (60°C, 24h) and SBF-soaked (37°C, 7 days) titanium foam samples were prepared and the cell culture tests were performed on those in a comparative manner. Synthetic body fluid used in this study was a TRIS-buffered *Tas*-SBF solution of 27mM HCO_3^- concentration.

2.2. Experimental Procedure

2.2.1. ***Substrate preparation*.** Titanium foam pieces (Selee Corp., Hendersonville, NC), with dimensions of 10×10×1.25mm, were used as substrates in biomimetic coating. The foam pieces were washed, respectively, with acetone, ethanol and deionized water in an ultrasonic bath, followed by immersion in 50mL of a 5M NaOH solution at 60°C for 24h in sealed glass bottles. After alkali treatment, each foam piece was washed with an ample supply of water. In-house Ti6Al4V springs were prepared as follows; an approximately 1-mm-thick and 7-cm-long strip was first cut from a Ti6Al4V sheet, and then coiled around a steel rod (diameter 6mm) to form the spiral/spring shape. Such spring-like samples were used to evaluate the efficiency of the 3D surface coverage of the biomimetic coating process.

2.2.2. ***SBF solution preparation*.** SBF solutions were prepared according to the detailed protocol given elsewhere.[3,10] The basic SBF recipe was hereby

concentrated by 1.5 times, therefore, the solutions used in this study were named as 1.5×*Tas*-SBF. Reagent-grade chemicals (all from Fisher Scientific, NJ) were used in preparing the solutions; NaCl (>99.0%), $NaHCO_3$ (>99.7%), KCl (>99.5%), Na_2HPO_4 (>99.0%), $MgCl_2{\cdot}6H_2O$ (>99.5%), Na_2SO_4 (>99.0%), $(CH_2OH)_3CNH_2$ (>99.8%), $CaCl_2{\cdot}2H_2O$ (>99.5%) and HCl (37vol.%). 20mg/L Na-azide was also added to the solutions to prevent bacteria growth. When not in use, SBF solutions were stored in glass jars in a domestic refrigerator at 4°C.

2.2.3. ***Coating process*.** The springs or foams were soaked in 100mL of 1.5 × *tas*-SBF solutions kept at 37°C in sealed Pyrex® bottles of 100-mL capacity for a period of 7days. SBF solutions were completely replenished with fresh solutions every 48h. Prior to replenishment, fresh SBF solutions of pH 7.4 were heated to 37°C. At the end of 7days of soaking, samples were removed from the SBF solutions, followed by washing first with 100mL of deionized water and then with 10mL of 98% pure ethanol.

2.2.4. ***Sample characterization*.** For phase analysis, the surfaces of the uncoated and coated foams were investigated by an X-ray diffractometer (XRD; Model XDS 2000, Scintag Corp., Sunnyvale, CA), operated at 40kV and 30mA with monochromated Cu Kα radiation. The foams were also analyzed by using Fourier-transformed infrared spectroscopy (FTIR; Nicolet 550, Thermo-Nicolet, Woburn, MA). FTIR was equipped with an Endurance Foundation Series single-bounce diamond ATR (50° incidence angle) and 32 scans were collected at a resolution of 4cm−1. Scanning electron microscopy (FESEM; S4700, Hitachi Corp., Tokyo, Japan) was used to monitor the changes in the surface morphology of the foams before and after SBF-soaking.

2.2.5. ***Cell culture*.** 7F2 rat osteoblast cells (CRL-12557, American Type Culture Collection, Rockville, MD) were grown in 75cm2 culture flasks at 37°C and 5% CO2 in an alpha-minimum essential medium (α-MEM, Sigma Inc.) with 2mM 1-glutamine and 1mM sodium pyruvate, without ribonucleosides and deoxyribonucleosides, augmented with 10% FBS. The culture medium was changed every other day until the cells reached a confluence of 90–95%, as determined visually with an inverted microscope. The cells then were passaged

using trypsin (2.5 g/L)/EDTA (25mM) solution (Sigma). Obtained cells were then seeded at a concentration of 5000cells/well on 1cm2 samples for the various assays. Two control samples were used, one was the pristine foam and the second was the alkali-treated foam. Cell viability was assessed after 72h, and total protein amount was measured after 7days in a 24-well cell culture plate. Further details of the cell culture procedures were given elsewhere.[23] Cell attachment studies were also performed on the foams by visual observation via FESEM. Prior to FESEM investigations, cells were fixed by using 3.5% glutaraldehyde. Osteoblasts were dehydrated through sequential washings in 50%, 75%, 95% ethanol solutions and 2 times with 100% ethanol. Samples were then critical point-dried. Samples were sputter-coated with a thin layer of Pt prior to the FESEM observations performed at 5kV. For statistics, all experiments were performed in triplicate, where n=3.

2.3. Results and Discussion

The pore sizes (400 to 500μm) and strut morphology of the as-received titanium foams were depicted in Figure 2.1a. These foams have been produced using the polymeric sponge impregnation method with titanium powders. The high magnification inset in Figure 2.1a showed the characteristic kinks and steps of recrystallization phenomenon which took place during the sintering of the foam precursors. However, the NaOH-treatment of those foams completely removed those kinks and replaced the surface with nanoporous hydrated Na-titanate phase(s) as shown in Figure 2.1b. Hydrated Na-titanate layers on Ti with a slightly basic surface were believed to further enhance the biomimetic coating process.[20] SEM photomicrographs of Figure 2.2 showed that the foams were fully covered with apatite-like calcium phosphates; consisting of micron-size CaP globules with nanoporous surfaces. FTIR data (not shown) of the TRIS-buffered, 27mM HCO_3^- SBF-soaked (7 days) foam samples showed that all the coatings consisted of carbonated (CO_3^{2-} ion absorption bands seen at 1470–1420 and 875cm^{-1}) calcium phosphates. The absence of the stretching and the vibrational modes of the O–H group at 3571 and 639cm^{-1} confirmed that these coatings might not simply be named as hydroxyapatite. We prefer to call them as

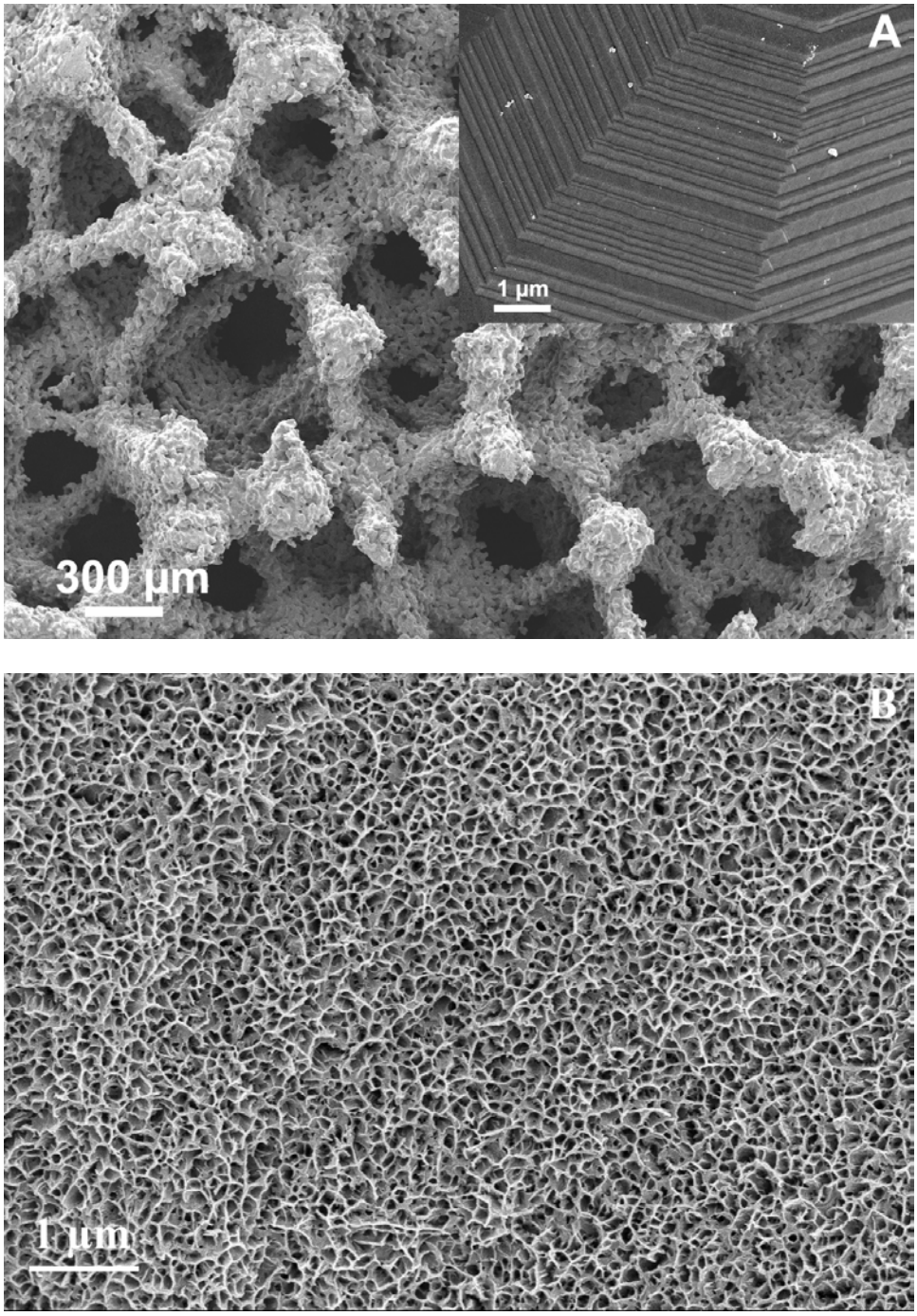

Fig. 2.1 SEM micrographs of Ti foams prior to SBF-soaking; (a) neat surface, (b NaOH-treated surface.

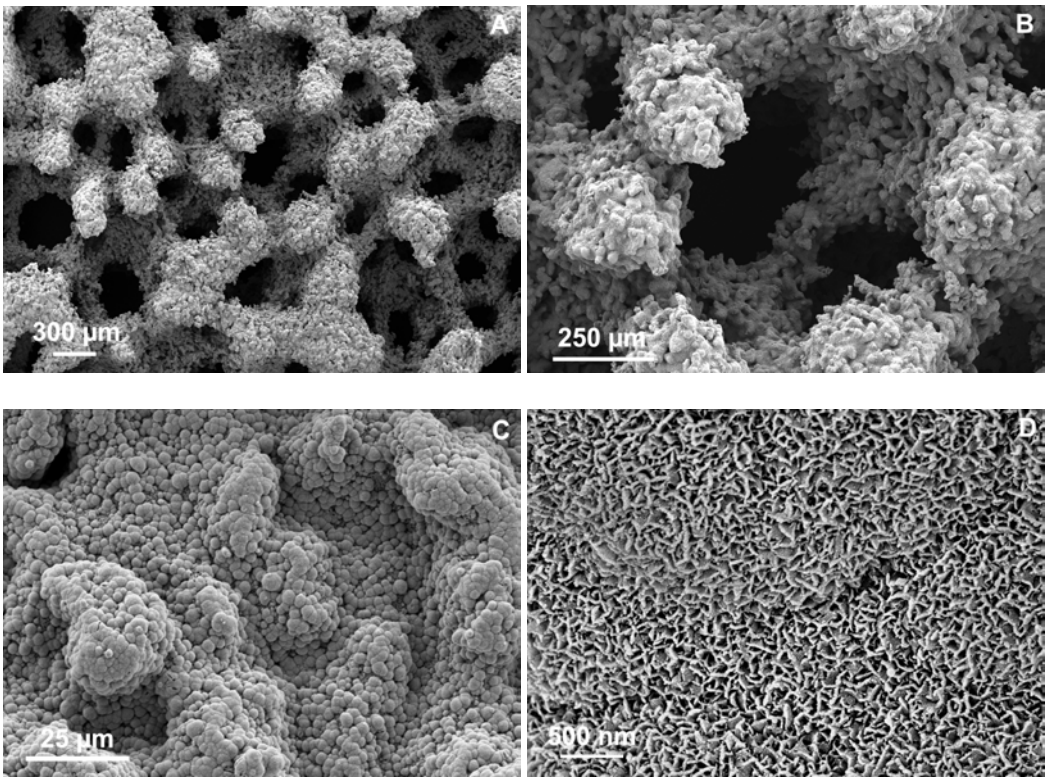

Fig. 2.2 (a–d) SEM micrographs of 27mM HCO3-Tris-SBF-coated (7days) titanium foams at various magnifications; characteristic CaP globules (c) and their nano-porous texture (d) were readily visible.

carbonated, apatite-like CaP. Micrographs of the SBF-coated titanium springs are given in Figure 2.3.

SEM micrographs given in Figures 2.4, 2.5, and 2.6 depicted the osteoblast proliferation and attachment on neat titanium foams, NaOH-treated foams and the SBF-coated foams, respectively. *In vitro* cell culture results given in Figure 2.7 revealed that all three groups of samples were statistically and strikingly different from one another, and the cytotoxicity of the NaOH-treated samples was found to be the highest (Fig. 2.7a). In the specific comparison of pristine titanium foams with those treated in NaOH, it was evident that the former performed much better, which meant that the surface roughness or nano-topography (or nanotexture) was not a sole factor in determining the advance of osteoblast attachment, spreading and proliferation. Here the surface chemistry strongly prevailed in the sense that the neat, nonporous, low surface area titanium foams turned out to be less cytotoxic than high surface area, nano-porous, NaOH-treated foams with a surface layer of hydrated, basic Na-titanates.[20]

SBF-coated titanium foams, on the other hand, were found to have the highest protein concentration and cell viability levels (Fig. 2.7). While in the case of neat titanium foams the osteoblasts were only able to attach and then extend their filopodia over the available surface (Figure 2.4c and d), the osteoblast cells on SBF-coated foams were able to proliferate to the extent that even the vinculin adhesion plaques and the actin cytoskeleton and stress fibers became visible (Fig. 2.6d). Throughout its cell culture tests, this study concurrently investigated the same titanium foam material with three different surfaces, i.e., neat, NaOH-treated, and apatite-like CaP deposited from an SBF solution. The response of osteoblasts to a given surface can be regarded as the sum of their ability to attach, proliferate, and differentiate. In the attachment stage, osteoblast filopodia explored the substrate topography (Fig. 2.4) for areas to which a greater surface area of the cell can adhere. These filopodia were used in sensing the substrate, and they extended over significant distances to find areas appropriate for attachment. As was the case with NaOH treated titanium foams, cells were seen to produce

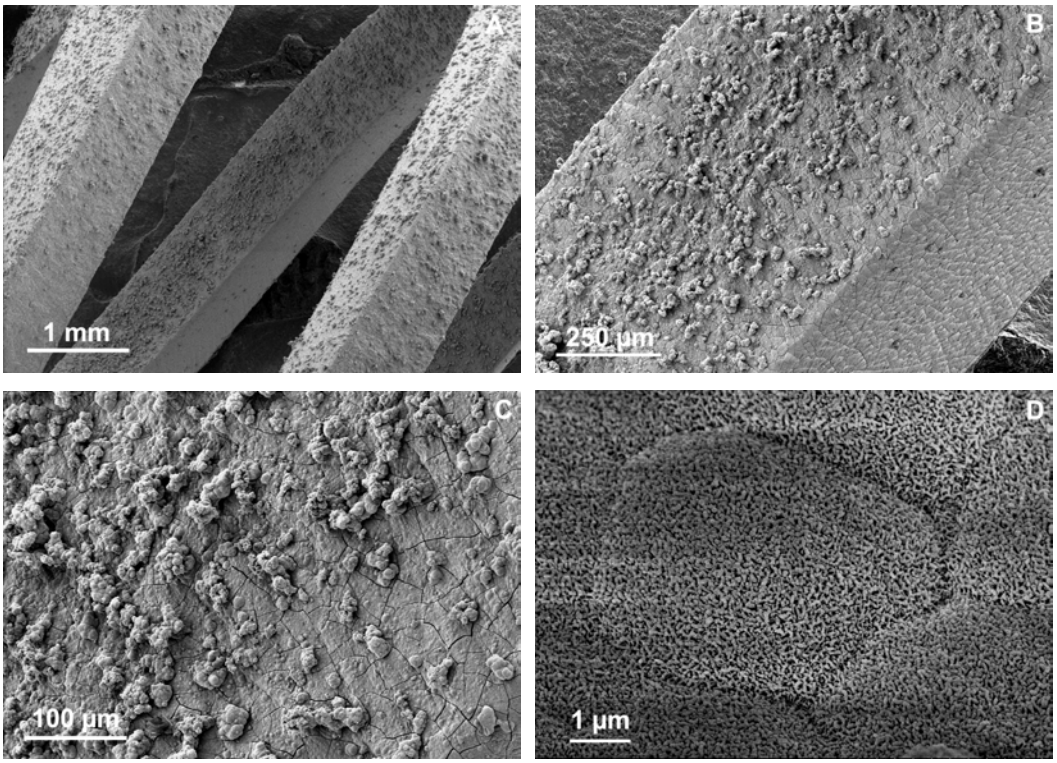

Fig. 2.3 SEM micrographs of 27mM HCO_3^- Tris-SBF-coated (7 days) titanium springs/spirals.

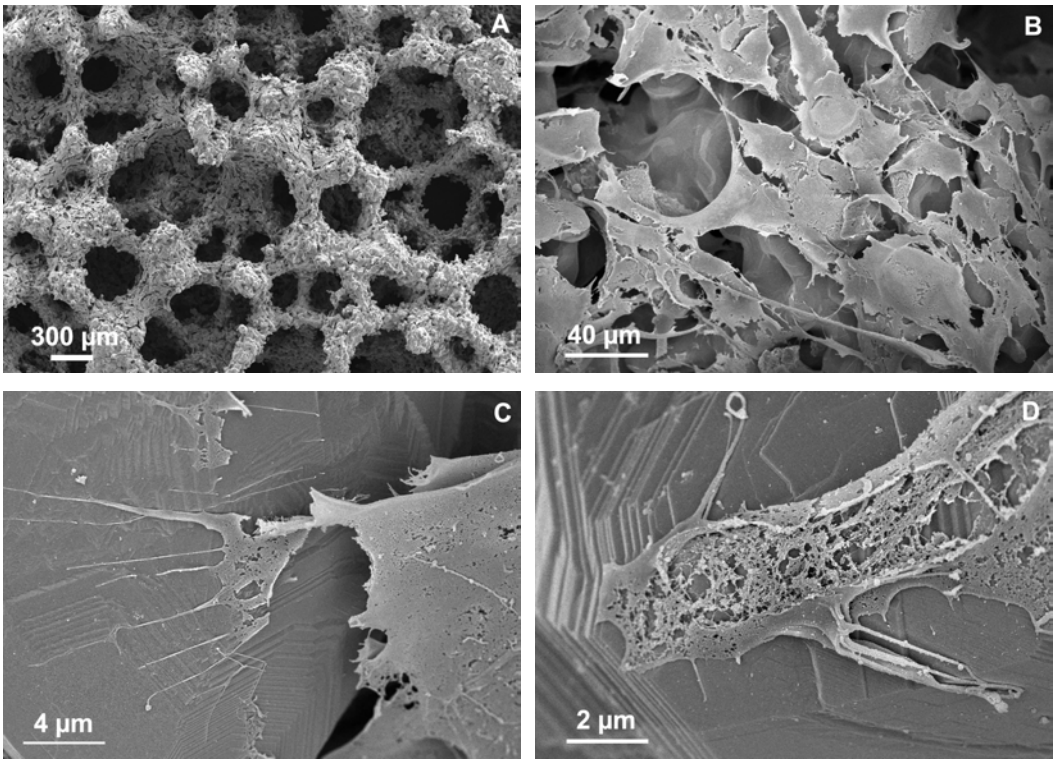

Fig. 2.4 Osteoblast proliferation and attachment on neat titanium foam surfaces.

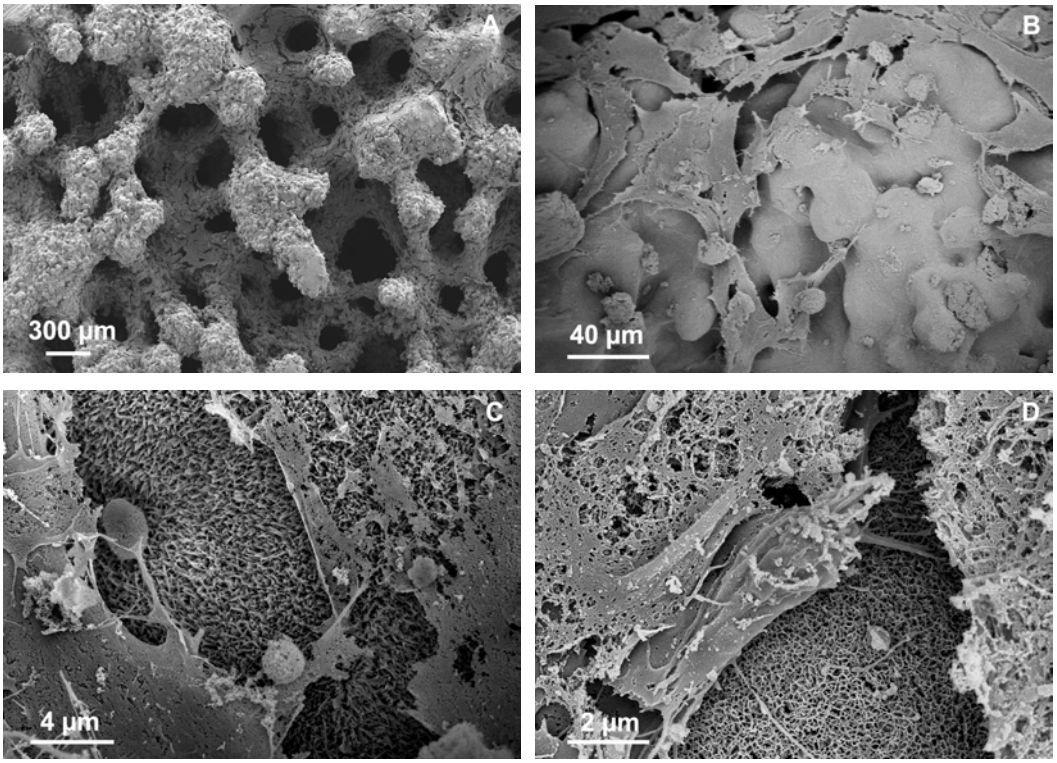

Fig. 2.5 Osteoblast proliferation and attachment on NaOH-treated titanium foams.

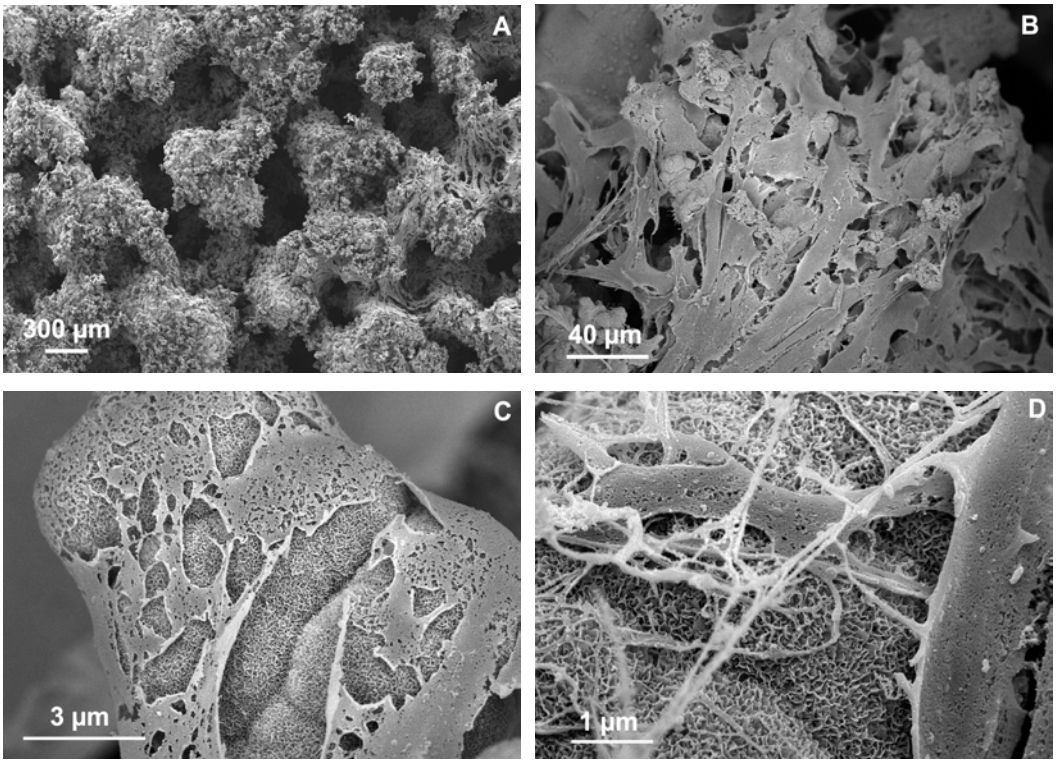

Fig. 2.6 Osteoblast proliferation and attachment on 27mM HCO3-Tris-SBF-coated titanium foams.

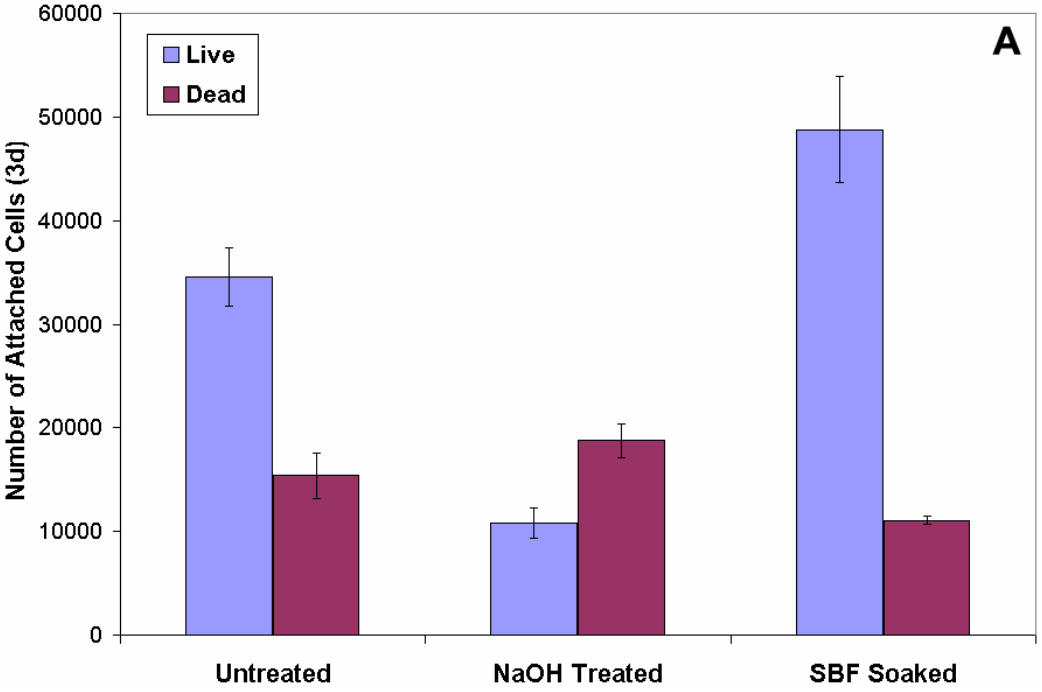

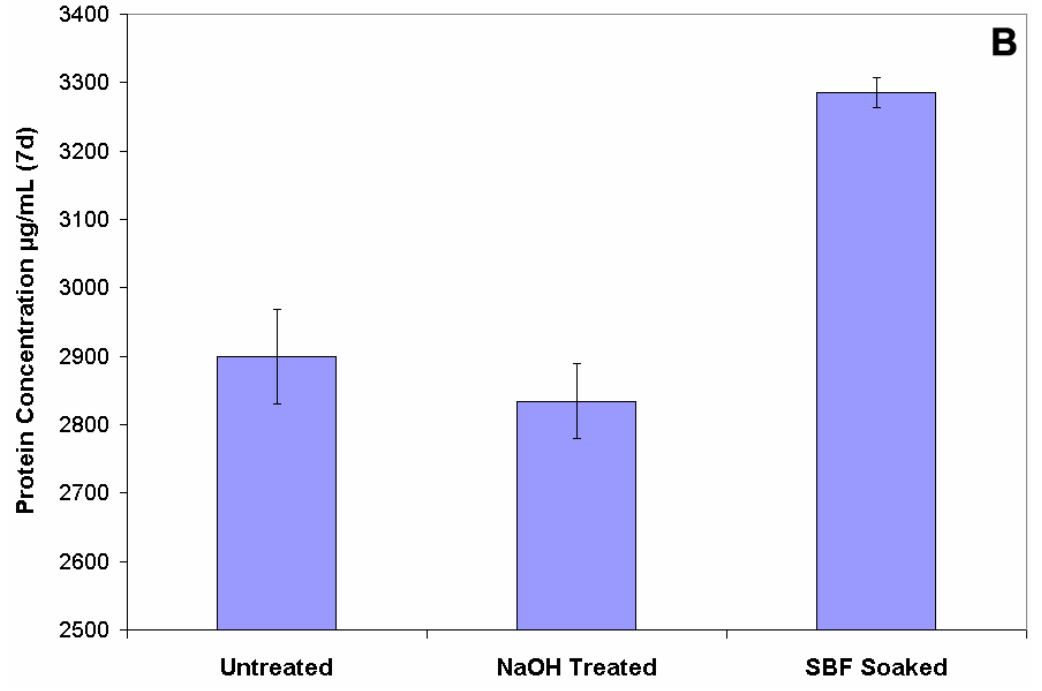

Fig. 2.7 *In vitro* (a) cell viability and (b) protein concentration histograms for the samples of Figures 2.4–2.6.

fewer adhesion plaques while still in the process of migration than ones permanently settled in place (Fig. 2.5). SEM micrographs given in Figures 2.4b, 2.5b, and 2.6b alone can also be used as a concise visual comparison tool for the osteoblast proliferation behavior on three different titanium surfaces of this study.

How does biomimetic coating proceed via SBF solutions? If a simple aqueous solution, which only contains 2.5mM $CaCl_2 \cdot H_2O$ dissolved in it, is exposed to a gaseous CO_2 atmosphere, it will start precipitating submicron particles of $CaCO_3$ (calcite and/or vaterite) within the following few hours of ageing at room temperature.[24] CO_2 gas leads initially to the formation of carbonic acid, H_2CO_3, and it will dissociate into HCO_3^- and CO_3^{2-} aqueous species. The reversal of these dissociation reactions will cause the release of CO_2 gas out of the solution, with an accompanied increase in the pH value. The HCO_3^-/CO_3^{2-} pair exerts a buffering effect. However, if one adds 27mM $NaHCO_3$ to this Ca-chloride solution, this will eliminate the necessity of exposing it to a gaseous CO_2 atmosphere, and again, it would only form submicron $CaCO_3$ precipitates.[25] If one adds 1mM Na_2HPO_4 into the above carbonated Ca-chloride solution (Ca/P=2.50) together with 112mM NaCl, this solution of ionic strength of 149.5mM will precipitate carbonated calcium phosphates instead of pure $CaCO_3$. This solution is saturated with respect to the formation of apatite-like calcium phosphates, and it contains Ca^{2+}, HPO_4^{2-}, HCO_3^-, Na^+, and Cl^- ions. The main question here is whether the resultant precipitates still contain $CaCO_3$ at their cores or not. Does the precipitation proceed by a topotactic reaction of heavily carbonated CaP growing on $CaCO_3$ (vaterite perhaps) particles? These questions must be addressed prior to calling the SBF deposited CaP layers simply as "hydroxyapatite." When the pH of the above solution is brought down to the range of 5 to 6, for instance, by adding tiny droplets of dilute HCl, it will only precipitate $CaHPO_4 \cdot 2H_2O$ (i.e., brushite, DCPD, dicalcium phosphate dihydrate). If the pH value of that solution is kept at the physiological value of 7.4 or higher, it would nucleate carbonated, apatite-like calcium phosphates. Over the pH range of 6.2 to 10, HCO_3^- is the most stable carbonate species in aqueous solutions. The

precipitation of carbonated, apatite-like calcium phosphates from such a solution may be described by using the following reaction[26]:

According to the above B-type substitution scheme (which is typically observed for low-temperature apatites) of Eq. (1), HPO_4^{2-} and CO_3^{2-} ions replace the PO_4^{3-} tetrahedra. The charge imbalance created by these substitutions will be compensated by the Ca-vacancies. Monovalent Na^+ ions will also substitute over a certain fraction of the Ca-sites. Bone mineral, with extremely small sizes of biological apatite-like crystals (i.e., 20 to 30nm), contains substantial amounts of CO_3^{2-} (4 to 6 wt.%), 0.5% Mg^{2+}, 0.7% Na^+, is about 10% Ca-deficient with the accompanying increase in reactivity related to this condition[27], and moreover, the presence of HCO_3^- in aqueous environments is known to reduce the apatitic growth rate[28]. As seen from Eq. (1), precipitation of apatite-like calcium phosphates may also be accompanied by a slight pH decrease. All the precipitated calcium phosphate powders, therefore, may possess, to a certain extent, Ca-deficiency, HPO_4^{2-} and CO_3^{2-} ions in their nanocrystalline moieties. Carbonate ion doping into the phosphate tetrahedra of apatite-like calcium phosphates will result in the creation of charge compensating Ca-vacancies, and this is the reason for the observed Ca-deficiency of CaPs synthesized in body fluids.[10,29] Astala and Stott[29], based on their electron density function calculations, recently reported that CO_3^{2-} ions and the Ca-vacancies are strongly related with one another and form a cluster complex in the crystallographic unit cell of apatite-like calcium phosphates.

The addition of 5mM K^+ and/or 0.5mM SO_4^{2-} ions (since these ions are present in the human blood plasma) into a solution as described above do not change the nature of the precipitates formed. Increasing the amount of Na^+ and Cl^- ions to the levels present in human blood plasma (i.e., 142 and 103mM, respectively) would just increase the ionic strength of the new solution. For instance, the ionic strength of the *Tas*-SBF (27mM HCO_3^- Tris-buffered) used in this study is 160.5mM. Theoretically, if a solution has a low ionic strength, this means that the ionic diffusion will be enhanced in such a solution. Therefore, in a solution of low ionic strength and high ionic diffusion, there will be more

nucleation sites for the precipitation reactions. CO_2 would be released from an aqueous solution at a faster rate if the solution has a low ionic strength.[30] The presence of NaCl in human blood plasma is for the purpose of fixing the ionic strength at the value of 149.5mM. If one increases the ionic strength of an SBF solution to above 1100mM, its rate of CO_2 release would be slowed down significantly.[21] If one adds 1.5mM Mg^{2+} into the above solution, this would slow down the growth rate of apatitic calcium phosphates, and also favor the formation of poorly-crystallized (i.e., in terms of their XRD spectra—not shown here), non-stoichiometric calcium phosphates.[16] Mg is, therefore, an important additive in SBF solutions and chemically incorporated into the SBF-formed CaP precipitates.[16]

Yin and Stott[31] pointed out that an amorphous calcium phosphate (ACP) precursor would always be present during the precipitation of apatite-like calcium phosphates from highly supersaturated solutions, such as the SBF solutions used here. Posner and Betts[27] proposed that the process of ACP formation in solution involved the formation first of $Ca_9(PO_4)_6$ clusters which then aggregated randomly to produce the larger spherical particles or globules (Figs. 2.2 and 2.6), while the intercluster space is being filled with water. Such clusters (with a diameter of about 0.95nm[31]) were the transient solution precursors to the formation of carbonated apatite-like calcium phosphate precipitates as described in Eq. (1) above. The passage from the angstrom-size Posner's clusters in solution to the solid nanoaggregates of carbonated-CDHA (i.e., $Ca_9(PO_4)_5$-CO_3OH) or dahllite ($Ca_{10}(PO_4)_6CO_3$=$3Ca_3(PO_4)_2{\cdot}CaCO_3$) or a solid solution of those should be the key concept of biomimetic coating by the use of SBF or supersaturated CaP calcification solutions (SCS). One proton to be released by the aqueous bicarbonate ion (i.e., $HCO_3^- \rightarrow CO_3^{2-} + H^+$) can readily be consumed in forming the hydrogen phosphate groups of CDHA. c-SBF solutions (which are similar to the HBBS solution in terms of ionic concentrations) of low HCO_3^- concentration (4.2mM) are slow in forming CDHA in comparison to *Tas*-SBF of 27mM HCO_3^-. c-SBF solutions require more than 2weeks (typically 3weeks) to completely cover a given titanium surface.[2,8,11,20] If the formation of dahllite or a precursor phase

like that is indeed required, then the sluggish response of c-SBF solutions becomes understandable. The concentration of the carbonate ions in synthetic body fluid formulations does significantly influence the advance of the biomimetic coating process. Onuma and Ito[32] have demonstrated, by using dynamic light scattering, the presence of such calcium phosphate clusters from 0.7 to 1.0nm in size in transparent-looking synthetic body fluids. They reported that calcium phosphate clusters were present in SBF even when there was no precipitation. This was true after 5 months of storage at RT. Since these nanoclusters are always present even in supersaturated SBF solutions, the insertion of, for instance, a suitable alkali solution-treated titanium surface into the solutions triggers the hexagonal packing[32] of those nanoclusters to form apatite-like CaP aggregates.

ACP can also be present together with the nanocrystalline apatite-like CaP, as confirmed by the previous TEM studies performed on the SBF-coating layers.[33] The role of alkali-treated Ti6Al4V surfaces in stimulating the SBF-coating process has been explained in great detail by Kokubo et al.[11,20] Continuation of this phase separation process from the SBF solutions will be conditional upon the smooth supply of Ca^{2+}, HPO_4^{2-} and CO_3^{-} ions to the metal-solution interface. These colloidal precipitates (as a result of the hexagonal packing of the nanoclusters[32]) are formed by a homogeneous nucleation and precipitation process. The presence of these initial precipitates within the solution further accelerates the coarsening of the micron-sized calcium phosphate globules (see Figs. 2c, 3c and 6c). Precipitation observed in SBF solutions is closely related to the HCO_3^{-} (aq) concentration. A certain fraction of dissolved carbonate ions will be lost as CO_2 (g), followed by an increase in solution pH to above 7.5, and then this loss would decrease the level of supersaturation of the solution.[34] This explains the lesser amount of coating formed on titanium surfaces when the solutions were not replenished, let us say, for 1week. TRIS-buffered SBF solutions (1.5SBF) of 27mM HCO_3^{-} concentration were able to form those substratebound precipitates by the end of 2nd day of soaking at 37°C. However, when the HCO_3^{-} concentration was lower (i.e., 4.2mM; *c*-SBF) in the SBF, the

rate of formation of these precipitates is decreased. Since the Ca/P molar ratio of the SBF solutions were 2.50, they are not stable against carbonated, apatite-like CaP, dahllite or OCP (octacalcium phosphate; $Ca_8(HPO_4)_2(PO_4)_4{\cdot}5H_2O$) precipitation when the solution pH is higher than 6.3.[16,35] On the other hand, OCP typically forms, in comparison to CDHA, carbonated-CDHA or dahllite, at slightly lower pH values and much lower Ca/P molar ratios[36]. It should be noted that since the crystallinity of such hydrated and hydrophilic biomimetic coatings is extremely poor, it may be rather difficult to distinguish and quantify (e.g., by XRD) the amounts of mixed apatite-like CaP, dahllite and OCP phases in the deposited layers.[37] Dorozhkina and Dorozhkin[16] determined the water and carbonate contents of SBF-formed precipitates to be 10 and 15 wt.%, respectively. With the advance of precipitate formation the inherent level of supersaturation in the solution decreases, eventually the CaP nanoaggregate formation comes to a halt, and hence this is where one would need replenishing the SBF solution. If one does not replenish the SBF solution used in biomimetic coating for more than several days or 1week, then due to the abovementioned loss in supersaturation and as exemplified by Iimori et al.[38], one would start seeing the deposition of calcite ($CaCO_3$) crystals. However, $CaCO_3$ (nacre, aragonite, vaterite and calcite) is one of the mostly preferred and biocompatible materials used by mother nature in aquatic life forms.

2.4. Conclusions

Titanium foams with interconnected pores were coated biomimetically with apatite-like calcium phosphates in 7 days by using TRIS-buffered, 27mM HCO_3^- containing 1.5×*Tas*-SBF solution. Titanium springs/spirals were also coated with the same solution. Biomimetic coating process was able to cover all the surfaces and struts of the samples. *In vitro* cell culture tests with rat osteoblasts were used to compare the neat, NaOH-treated and SBF-coated surfaces of titanium foams. In terms of osteoblast attachment, protein production and cell proliferation, NaOH-treated surface has the least amount of cells attached, whereas the SBF-coated surfaces had the most. Untreated, neat titanium

foam surfaces were found to be less cytotoxic to the osteoblasts in comparison to NaOH-treated titanium surfaces. Of the three surfaces compared, SBF-coated surfaces exhibited the highest protein production and cell attachment figures. Biomimetic coating is a practical and robust way of increasing the biocompatibility of titanium foams or spring-like shapes by coating them with bone-like, carbonated, nanotextured apatite-like calcium phosphates.

2.5. References

1. F.C.M. Driessens, Mineral Aspects of Dentistry, S. Karger, Basel, 1982.

2. T. Kokubo. Surface chemistry of bioactive glass-ceramics. *J Non-Cryst Solids* **120** (1990) 138-151.

3. D. Bayraktar, A.C. Tas. Chemical preparation of carbonated calcium hydroxyapatite powders at 37°C in urea-containing synthetic body fluids. *J Eur Ceram Soc* **19** (1999) 2573-2579.

4. S. Ringer. A further contribution regarding the influence of the different constituents of the blood on the contraction of the heart. *J Physiol* **4** (1883) 29-42.

5. W. Earle, E. Schilling, T. Stark, N. Straus, M. Brown, E. Shelton. Production of malignancy *in vitro*: IV. The mouse fibroblast culture and changes seen in the living cells. *JNCI* **4** (1943) 165–212.

6. J.H. Hanks, R.E. Wallace. Relation of oxygen and temperature in the preservation of tissues by refrigeration. *Proc Soc Exp Biol Med* **71** (1949) 196-200.

7. A. Bigi, E. Boanini, S. Panzavolta, N. Roveri. Biomimetic Growth of Hydroxyapatite on Gelatin Films Doped with Sodium Polyacrylate. *Biomacromolecules* **1** (2000) 752-756.

8. H.M. Kim, K. Kishimoto, F. Miyaji, T. Kokubo, T. Yao, Y. Suetsugu, J. Tanaka, T. Nakamura. Composition and structure of apatite formed on organic polymer in simulated body fluid with a high content of carbonate ion *J Mater Sci Mater Med* **11** (2000) 421-426.

9. A. Oyane, K. Onuma, A. Ito, H.M. Kim, T. Kokubo, T. Nakamura. Formation and growth of clusters in conventional and new kinds of simulated body fluids. *J Biomed Mater Res A* **64** (2003) 339-348.

10. A.C. Tas. Synthesis of Biomimetic Ca-Hydroxyapatite Powders at 37°C in Synthetic Body Fluids. *Biomaterials* **21** (2000) 1429-1438.

11. T. Kokubo. Apatite formation on surfaces of ceramics, metals and polymers in body environment. *Acta Mater* **46** (1998) 2519-2527.

12. A.P. Serro, B. Saramago. Influence of sterilization on the mineralization of titanium implants induced by incubation in various biological model fluids. *Biomaterials* **24** (2003) 4749-4760.

13. S.Y. Lin, K.H. Chen, M.J. Li, W.T. Cheng, S.L. Wang. Evidence of octacalcium phosphate and Type-B carbonated apatites deposited on the surface of explanted acrylic hydrogel intraocular lens. *J Biomed Mater Res B* **70** (2004) 203-208.

14. C. Rolland, R. Guidoin, R. Ledoux, A. Zerguini, P.E. Roy. Carbonate-hydroxylapatite, hopeite, and parascholzite in fibrous capsules surrounding silicone breast implants. *Can Mineral* 29 (1991) 337-345.

15. C.L. Higgins, S.A. Marvel, J.D. Morrisett. Quantification of Calcification in Atherosclerotic Lesions. *Arterioscler Thromb Vasc Biol* **25** (2005) 1567-1576.

16. E.I. Dorozhkina, S.V. Dorozhkin. Structure and Properties of the Precipitates **...** Simulated Body Fluid. *J Biomed Mater Res* **67A** (2003) 578-581.

17. C.K. Loong, C. Rey, L.T. Kuhn, C. Combes, Y. Wu, S.H. Chen, M.J. Glimcher. Evidence of Hydroxyl-Ion Deficiency in Bone Apatites: An Inelastic Neutron Scattering Study. *Bone* **26** (2000) 599-602.

18. Z. Molnar. Additional Observations on Bone Crystal Dimensions. *Clin Orthop* **17** (1960) 38-42.

19. L. Kikuchi, J.Y. Park, C. Victor, J.E. Davies. Platelet interactions with calcium-phosphate-coated surfaces. *Biomaterials* **26** (2005) 5285-5295.

20. T. Kokubo, H.M. Kim, M. Kawashita, T. Nakamura. Bioactive metals: preparation and properties. *J Mater Sci Mater Med* **15** (2004) 99-107.

21. A.C. Tas, S.B. Bhaduri. Rapid coating of Ti6Al4V at room temperature with a calcium phosphate solution similar to 10x simulated body fluid. *J Mater Res* **19** (2004) 2742-2749.

22. P. Habibovic, C.M. van der Kalk, C.A. van Blitterswijk, K. De Groot, G. Meijer. Influence of octacalcium phosphate coating on osteoinductive properties of biomaterials. *J Mater Sci Mater Med* **15** (2004) 373-380.

23. S. Jalota, S.B. Bhaduri, and A.C. Tas. Effect of carbonate content and buffer used in SBF solutions on calcium phosphate formation on Ti6Al4V. *J Mater Sci Mater Med* **17** (2006) 697-707.

24. D. Rautaray, K. Sinha, S.S. Shankar, S.D. Adyanthaya, M. Sastry. Aqueous Foams as Templates for the Synthesis of Calcite Crystal Assemblies of Spherical Morphology. *Chem Mater* **16** (2004) 1356-1361.

25. O. Grassmann, P. Loebmann. Biomimetic nucleation and growth of $CaCO_3$ in hydrogels incorporating carboxylate groups. *Biomaterials* **25** (2004) 277-282.

26. T. Leventouri, B.C. Chakoumakos, N. Papanearchou, V. Perdikatsis. A Comparison of Crystal Structure Parameters of Natural and Synthetic Apatites from Neutron Powder Diffraction. *J Mater Res* **16** (2001) 2600.

27. A.S. Posner, F. Betts. Synthetic amorphous calcium phos- phate and its relation
to bone mineral structure. *Acc Chem Res* **8** (1975) 273-281.

28. H. Newesely. Changes in crystal types of low solubility calcium phosphates in the presence of accompanying ions. *Arch Oral Biol* **6** (1961) 174-180.

29. R. Astala, M.J. Stott. First Principles Investigation of Mineral Component of Bone: CO_3 Substitutions in Hydroxyapatite. *Chem Mater* **17** (2005) 4125-4133.

30. F. Barrere, C.A. van Blitterswijk, K. de Groot, P. Layrolle. Influence of ionic strength and carbonate on the Ca-P coating formation from SBFx5 solution. *Biomaterials* **23** (2002) 1921-1930.

31. X. Yin, M.J. Stott. Biological Calcium Phosphates and Posner's Cluster. *J Chem Phys* **118** (2003) 3717-3723.

32. K. Onuma, A. Ito. Cluster Growth Model for Hydroxyapatite. *Chem Mater* **10** (1998) 3346-3351.

33. Y.F. Chou, W.A. Chiou, Y. Xu, J.C.Y. Dunn, B.M. Wu. The Effect of pH on the Structural Evolution of Accelerated Biomimic Apatite. *Biomaterials* **25** (2004) 5323-5331.

34. P.A.A.P. Marques, M.C.F. Magalhaes, R.N. Correia. Inorganic plasma with physiological CO_2/HCO_3^- buffer. *Biomaterials* **24** (2003) 1541-1548.

35. L.C. Chow, S. Takagi, "Self-setting calcium phosphate cements and methods for preparing and using them," US Patent No. 5,525,148, June 11, 1996.

36. M. Iijima, Octacalcium phosphate, ed. L. C. Chow and. E. D. Eanes. Monogr Oral Sci S Karger, Basel, (2001) 17-49.

37. X. Lu, Y. Leng. TEM Study of Calcium Phosphate Precipitation on Bioactive Titanium Surfaces. *Biomaterials* **25** (2004) 1779-1786.

38. Y. Iimori, Y. Kameshima, K. Okada, S. Hayashi. Comparative study of apatite formation on CaSiO3 ceramics in simulated body fluids with different carbonate concentrations. *J Mater Sci Mater M* **16** (2005) 73-79.

CHAPTER 3

A PROTOCOL TO DEVELOP CRACK-FREE BIOMIMETIC COATINGS ON Ti6Al4V SUBSTRATES

Abstract

Biomimetic coating of titanium and related alloys with carbonated apatitic calcium phosphate is an important area of research in implantology. One step in the protocol involves an intermediate alkali treatment of Ti6Al4V to form a sodium titanate layer on the alloy surface. This pre-treatment enhances the formation of the coating from simulated body fluid (SBF) solutions. Many papers in the biomimetic coating literature demonstrate presence of cracks in coatings, irrespective of the SBF compositions, and placement of the substrates. The presence of cracks may result in degradation and delamination of coatings. To the best of our knowledge, this issue remains unresolved. Therefore, the aim of this study was: (1) to examine and understand the reasons for cracking and (2) based on the results, to develop a protocol for producing crack-free apatitic calcium phosphate coatings on Ti6Al4V substrates. In this study, the authors focused their attention to the alkali treatment procedure and the final drying step. It is hypothesized that these two steps of the process affect the crack formation the most. In the first case, the surfaces of alkali treated substrates were examined with/without water soaking treatment before immersing in SBF. This water treatment modifies the sodium titanate surface layer. In the second case, two different drying techniques (after soaking in SBF) were employed. In one procedure, the coated substrates were dried rapidly and in the other, they were dried slowly. It was observed that the water treatment, irrespective of the drying method, provides a surface, which on subsequent soaking in SBF forms a crack-free apatitic calcium phosphate coating. Based on these results, we suggest a protocol incorporating a water soaking treatment after the alkali treatment and prior to the SBF soaking treatment to obtain crack-free coatings.

(This work is *in print* in *J Mater Res* **22** (Jun 2007)

3.1 Introduction

Coating carbonated apatitic calcium phosphate layer on titanium and its alloys has been of increasing interest due to their ability to directly bond with bone.[1,2] Of the many coating processes available today, the biomimetic coating technique has many advantages including producing carbonated apatitic calcium phosphate coatings, which is otherwise impossible to produce. The coatings are formed by soaking an alkali pre-treated titanium (or an alloy) substrate in a simulated body fluid (SBF) solution.[3-6] The alkali pre-treatment is a crucial step, which forms a hydrous sodium or potassium titanate layer (depending upon the alkali used) on the substrate.[3-6] The as-formed sodium (or potassium) titanate on soaking in SBF exchanges Na^+ (K^+) ions with the H_3O^+ ions and forms Ti-OH groups on the surface that increases the ionic activity of apatite in SBF.[7] During soaking, nanometer sized apatitic calcium phosphate globules rapidly nucleate on the sodium (or potassium) titanate layer and then grow to a few microns by consuming Ca and P ions from the SBF solution.[4]

In spite of all the advantages of the biomimetic coating process, the phenomenon of cracking persists. Furthermore, the reason for cracking of such coatings remains unresolved. The present paper is an attempt to examine this issue. Previously, the present authors investigated the apatite inducing abilities of different SBF solutions referred to as *c*-SBF, *t*-SBF and *r*-SBF on these alkali treated titanium substrates.[8] *c*-[9] and *r*-SBF[10,11] are conventional and revised versions of SBF, as developed by Kokubo. *t*-SBF is the formulation developed by Tas[12,13]. The compositions of the three SBF solutions and the important differences between them are given in ref 8. The authors noted that cracks were persistently present on these apatitic calcium phosphate coating irrespective of the composition of the coating solution.[8] Also, the placement of the substrates (e.g., horizontal or vertical) was examined as a parameter affecting the formation of cracks in the coatings.[8] These cracks were present on all the substrates irrespective of their placements.[8] A major consequence of the presence of these cracks substantially increases the chances of delamination. Thereby, decreasing the coating's bonding ability with the natural bone.

The SEM micrographs, as reported by the present authors[8] and other researchers[14-22] indicate that these cracks are not just surface cracks and are rather deep. However, in the references[14-20], the authors did not mention the cause of these deep cracks. In other papers, drying is cited as a potential reason for their formation.[6,8,21,22] The main reason for this argument is that the water entrapped does not readily escape during low temperature drying and leads to deep cracks.[6,8,21,22] It is known that in the SBF solution, Posner's clusters are the dominant transient phase during the formation of calcium deficient carbonated calcium phosphates.[23,24,25] Since Posner's clusters already have water molecules in their intercluster spaces, the aggregates of these clusters forming the nano-porous coating layers on Ti6Al4V surfaces also entrap a sizable amount of water.[23,24,25] Yet another explanation is attributed to the presence of thermal expansion coefficient mismatch between the Ti6Al4V substrates and the calcium phosphate coating layers.[26] Most of these explanations are hypothetical in nature and are not based on concrete experimental results.

The broad objective of the present work was to find the reasons for the formation of such cracks and to establish a protocol for producing crack-free homogeneous biomimetic coating on Ti6Al4V utilizing *t*-SBF. The reasons for using *t*-SBF are given in ref. 8. Since the cracks appear to be deep, the authors hypothesize that the hydrous sodium titanate layer[4] formed on the Ti6A14V substrate has a role in the formation of cracks in the coatings. Thus in this careful study, we modified the pre-treatment procedure and subsequently examined its effect on formation of cracks in the coatings. Also, we attempted new drying procedures to examine the effect of drying on the crack formation. The rate of removal of water differentiates the new and the conventionally used procedures. The new procedure leads to the rapid removal of water as compared to the conventional method, in which the entrapped water does not readily escape.

3.2 Experimental Procedure

3.2.1 ***Substrate Preparation and Alkali Pre-treatment.*** Ti6Al4V strips (Grade 5, McMaster-Carr), with the dimensions of 10 x 10 x 1 mm, were used as

substrates in the SBF coating. The substrates were first abraded with a #100 SiC paper (FEPA P#1000, Struers) and then washed three times respectively with acetone, ethanol, and deionized water in an ultrasonic bath. Each substrate was then immersed in 50 mL of 5M NaOH solution at 60ºC for 24 hours. At the end of this alkali treatment, substrates were given two different treatments to check the effect on change of composition of treated layer on coating cracks. The first treatment involved the most commonly used practice of drying the substrates at 40ºC for 24 hours after alkali treatment. The second treatment consisted of immersing the substrates in water at RT for 24 hours after the alkali treatment and then drying them at 40ºC for 24 hours.

3.2.2 ***SBF Solution Preparation.*** The details of SBF preparation routines are given in Table 3.1. Freshly prepared *t*-SBF solution[12,13] was used in coating experiments. We concentrated the basic SBF recipe by 1.5 times, as per common practice in the biomimetic coating of Ti6Al4V. The order of addition of the reagents to 700 mL of water is given in the second column of Table 3.1. A total of 65 mL of 1M HCl was consumed for pH adjustments during the preparation of 1 l of 1.5 x *t*-SBF solution. A 15 mL aliquot of this acid solution was added just before the addition of the sixth reagent, $CaCl_2.2H_2O$. Otherwise, the solution would display slight turbidity. The remaining part of the HCl solution was used during the subsequent titration. Following the addition of the eighth reagent, tris(hydroxymethyl) aminomethane, the solution temperature was raised from

Table 3.1 Preparation of *t*-SBF solution (1 L)[12,13]

Reagent	*Weight (g)*	*Ion*	*Human Plasma(mM)*	*SBF (mM)*
NaCl	6.547	Na^+	142	142
$NaHCO_3$	2.268	Cl^-	103	125
KCl	0.373	HCO_3^-	27	27
$Na_2HPO_4{\cdot}2H_2O$	0.178	K^+	5	5.0
$MgCl_2{\cdot}6H_2O$	0.305	Mg^{2+}	1.5	1.5
$CaCl_2{\cdot}2H_2O$	0.368	Ca^{2+}	2.5	2.5
Na_2SO_4	0.071	HPO_4^{2-}	1	1.0
$(CH_2OH)_3CNH_2$	6.057	SO_4^{2-}	0.5	0.5

ambient temperature to 37ºC. This solution was then titrated with 1 M HCl to a pH of 7.4 at 37ºC. During the titration process, the solution was also continuously diluted with consecutive additions of deionised water to make the final volume equal to 1 l.

3.2.3 ***Coating and Drying Process*****.** For coating purposes, the pre-treated substrates were soaked vertically in 100 mL of *t*-SBF at 37ºC in tightly sealed Pyrex bottles of 100 mL capacity for a period of 7 days. The reason for using vertical placement (by hanging in the solution bottle via a stainless steel wire) is given in ref. 7. The SBF solution was replenished at every 48 hours. Prior to replenishment, fresh SBF solutions of pH 7.4 were heated to 37ºC. The substrates were removed from the SBF solution followed by gentle washing with approximately 100 mL deionized water and then dried using two different techniques. The first technique involved the commonly used method for drying the biomimetically coated substrates that is, drying the substrates at 40 º C for 24 hours. The second technique involved water soaking, followed by rinsing with 50 mL of 99.5% ethanol and then placing the substrates at RT for 15 minutes to evaporate ethanol.

3.2.4 ***Sample Characterization*****.** For phase analysis, the surfaces of the uncoated and coated substrates were investigated by X-Ray Diffraction (XDS 2000, Scintag Corp., CA) using monochromated Cu K_α radiation generated at a voltage and power of 40 kV and 30 mA, respectively. The substrates were also analyzed by using Fourier-transformed infrared spectroscopy (Nicolet 550, Thermo-Nicolet, MA). FTIR was equipped with an Endurance Foundation Series single-bounce diamond ATR (50º incidence angle) and 32 scans were performed at a resolution of 4 cm^{-1}. In order to analyze the substrate surface, before and after every treatment for cracks, scanning electron microscope (FESEM, S-4700, Hitachi Corp., Tokyo, Japan) operated at 5 kV was used. To determine the amount of sodium present in the surface layer, samples were characterized using inductively coupled plasma-atomic emission spectroscopy (ICP-AES, Model 61E, Thermo Electron, Madison, WI).

3.3 Results

The results of this study are divided into two groups: a) an alkali pre-treatment before soaking in SBF solution and b) a drying step after soaking in SBF solution.

3.3.1 *Alkali pre-treatment before soaking in SBF solution*:

After the alkali treatment, substrates were divided in two sets of samples; the first set was oven-dried at 40ºC for 24 hours and the second set was soaked in water and then oven-dried at 40ºC for 24 hours. After completing these procedures, the substrates were examined by XRD, FTIR, and SEM. Figure 3.1 shows the XRD patterns of (a) as-received Ti6Al4V substrates; (b) substrates after polishing, NaOH-treatment, and drying at 40ºC for 24 hours; and (c) substrates after polishing, NaOH-treatment, water-treatment, and then drying at 40ºC for 24 hours. Ti6Al4V readily forms titanium oxide (TiO_2) layer on the surface on exposure to air. Prior to any treatment, titanium oxide was present on the as-received Ti6Al4V strips of this study as determined by the XRD pattern shown in Figure 3.1a. All rutile (TiO_2) peaks are marked as (*) on the pattern. A hydrated layer of sodium titanate (marked as ^) and titanium oxide (Rutile, TiO_2) was reported to form on the exposed surfaces of Ti6Al4V strips after 24 hours of immersion in a 5M NaOH solution at 60ºC.[3,4,16] This layer was indeed found to be present on both NaOH treated and water treated Ti6Al4V strips. Both the patterns have similar peaks and respective intensities, and no significant difference was found in the XRD patterns (Figs. 3.1a and b). The FTIR pattern of NaOH-treated Ti6Al4V strips (Fig. 3.2b) shows that they were hydrated in nature with a huge band of H_2O present from 3700-2400 cm^{-1} and one present at 1640 cm^{-1}. Both of these bands were also present on the substrates after water treatment (Fig. 3.2c), thus, confirming their hydrated nature. The most important difference in the FTIR pattern was the presence of carbonates in the NaOH treated surface layer. FTIR pattern showed the presence of carbonate bands (CO_3^{2-}) between 1470-1410 and at 870 cm^{-1} in the NaOH-treated substrates (Fig. 3.2b) whereas these bands were absent after water treatment (Fig. 3.2c) as shown. Inductively coupled plasma analyses showed significant differences in the amount Na present on the surface

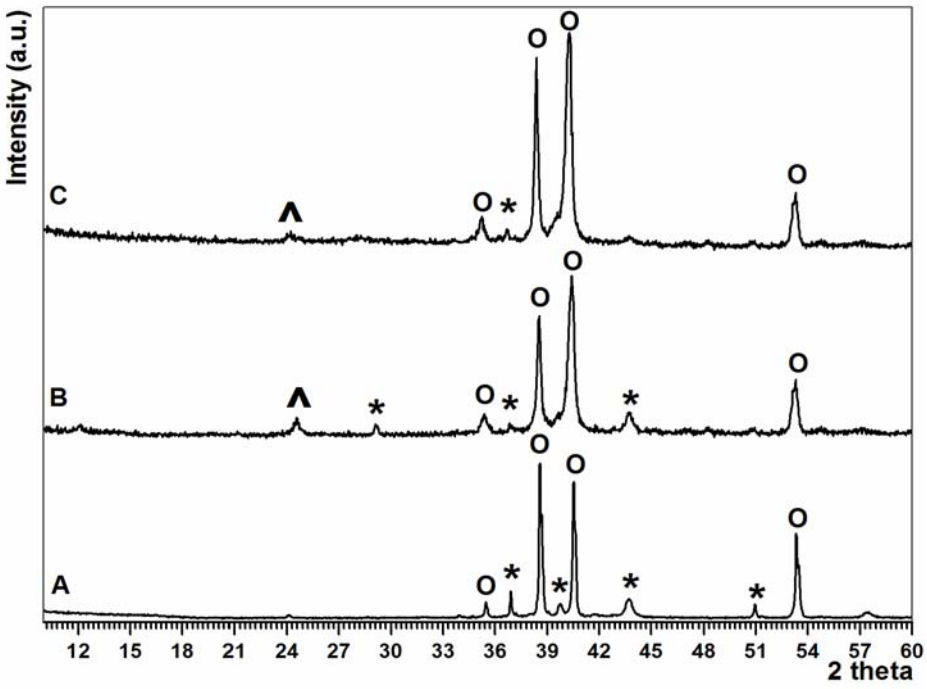

Fig. 3.1 XRD pattern of (a) as-received Ti6Al4V, (b) 5M NaOH treated and then dried at 40ºC, and (c) 5M NaOH treated and then soaked in water (O: Titanium, *: Rutile, and ^: Sodium Titanate)

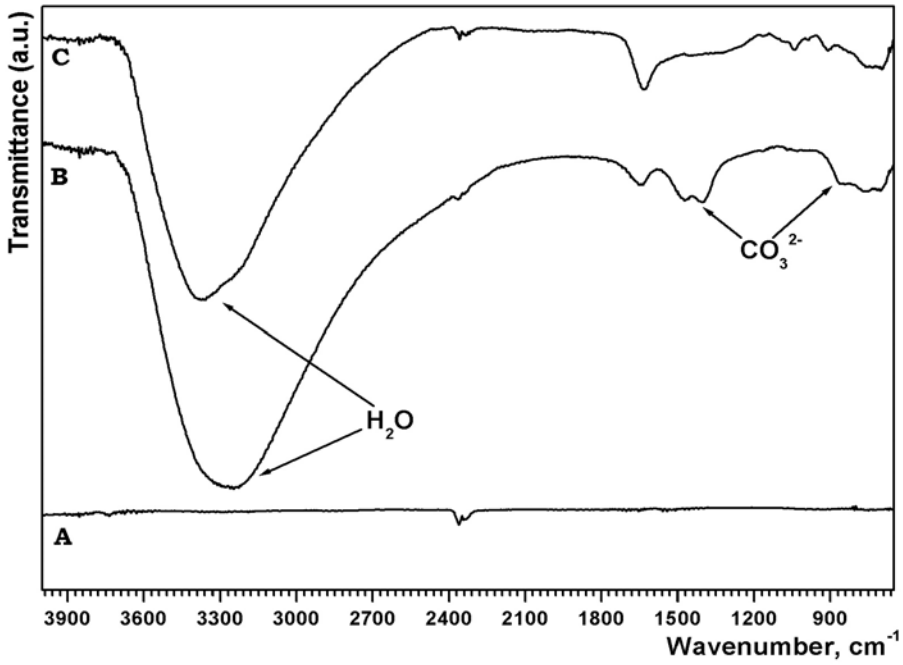

Fig. 3.2 FTIR pattern of (a) as-received Ti6Al4V, (b) 5M NaOH treated and then dried at 40ºC, and (c) 5M NaOH treated and then soaked in water (arrows point the H_2O and CO_3^{2-} bands).

layer of the NaOH treated and water treated samples. As expected during water treatment, sodium was released from the substrate surface into the water in which they were immersed. The amount of Na present in the hydrous sodium titanate layer of NaOH-treated substrates was 8.25 wt.% whereas, in water treated substrates, the amount decreased to 3.6 wt.%.

Examination of these differently treated substrates under the SEM also showed variations in microstructure. The alkali treatment, prior to soaking in SBF solution, provided the substrate with a certain nano-scale roughness as shown in the SEM micrographs of Figure 3.3a. The nano-porous structure formed by the NaOH treatment was unchanged after water treatment (Fig. 3.3b). But the water treatment had a considerable effect on the microstructure. The NaOH-treated substrates that were dried at 40ºC subsequently showed large number of cracks (Fig. 3.3a), which were persistent throughout the surface of the hydrated sodium titanate layer. These cracks might have formed during the drying process at 40ºC due to the release of either water or carbonates from the layer. However, cracks could not be seen in the low magnification micrographs (inset in Fig. 3.3), only in the high magnification micrographs, they (cracks) become detectable. In contrast, the water treated substrates were crack-free as shown in Figure 3.3b. To summarize, it is clear that water soaking after alkali treatment forms a hydrate sodium titanate layer without carbonates and cracks, and with a lower sodium content. All other features remain the same.

3.3.2 *Drying step after soaking in SBF solution*:

This section describes the results obtained after the alkali treated substrates (with/without water treatment) were soaked in 1.5 times *t*-SBF solution. Upon soaking, calcium phosphates covered the surface of these substrates within 7 days (Fig. 3.4). The alkali treated substrates with/without water treatment after SBF coating were dried in two different methods to see the effect of kinetics of drying. One method was to dry the substrates by placing them at 40ºC for 24 hour; and the other was to wash the coated substrates with ethanol and then dry them at room temperature. The former method is slower than the latter. Figure 3.4a shows that the NaOH-treated substrate coated with apatitic calcium

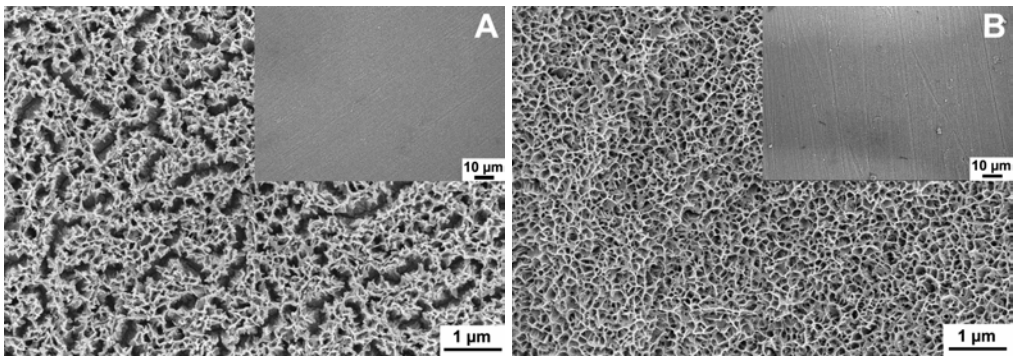

Fig. 3.3 SEM micrographs of Ti6Al4V strips treated with 5M NaOH at 60ºC for 24 hours then (a) dried at 40ºC for 24 hours, and (b) soaked in deionized water for 24 hours (inset shows low magnification view).

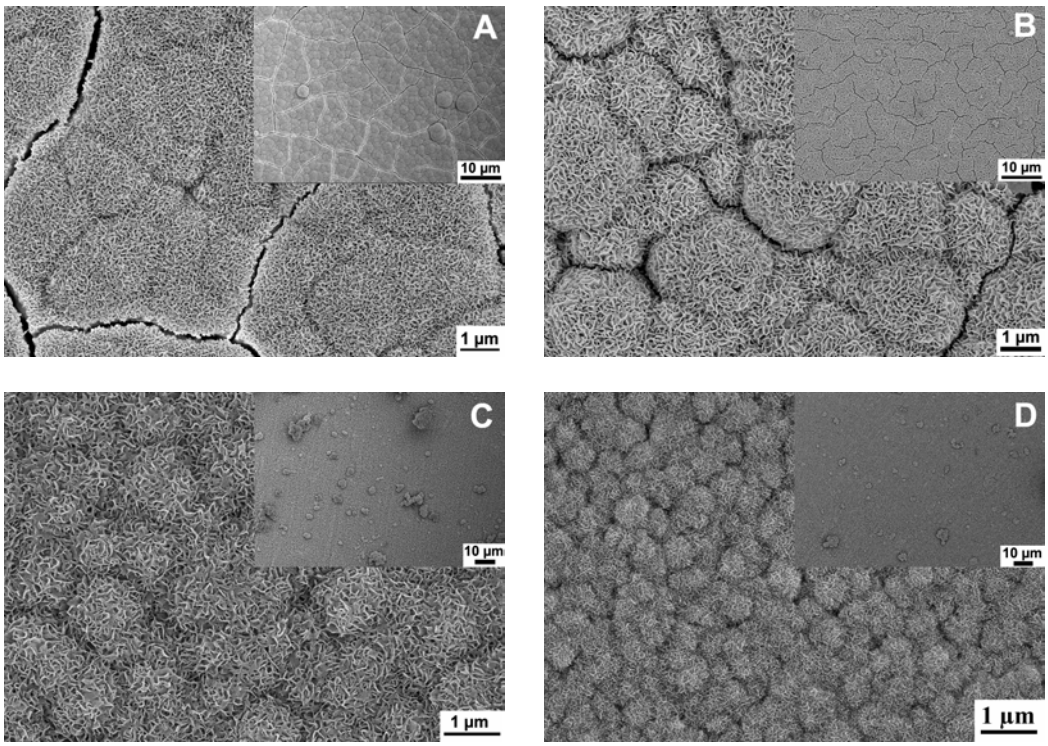

Fig. 3.4 Substrates after alkali treatment dried at 40ºC for 24 hours, then soaked in *t*-SBF for 7 days and then (a) dried at 40ºC for 24 hours and (b) dried with ethanol. Substrates after alkali treatment were soaked in deionized water for 24 hours, soaked in *t*-SBF for 7 days, and then (c) dried at 40ºC for 24 hours, and (d) dried with ethanol (inset shows low magnification view).

phosphate developed deep cracks after drying it at 40ºC for 24 hours. Because these cracks have previously been referred to as "drying cracks", or those formed while drying, the second method of drying was used. The SEM micrographs (Fig. 3.4b) showed morphology and cracks similar to those shown in Figure 3.4a. Thus, this ethanol treatment was unsuccessful in removing the cracks from the coating surface. Figure 3.4c and d show the substrates that were water treated after alkali treatment and then soaked in SBF for 7 days. Subsequently, the substrates were washed with water and then dried at 40ºC for 24 hours (shown in Fig. 3.4c). The SEM micrographs at both high and low magnification (shown in inset) show a crack-free coating surface, and also showed no significant difference in the morphology of the apatitic calcium phosphate coatings. The micrograph depicts the round globules with needle-like intermingled nano-size calcium phosphates on the surface of Ti6Al4V strips. At the end of the soaking time, the substrates (shown in Fig. 3.4d) were first washed with water and then rinsed with ethanol. The micrograph is very similar to that in Figure 3.4c, which also shows a crack-free apatitic calcium phosphate coating.

The calcium phosphate coatings formed on substrates after different pre-treatments retained a similar XRD pattern (Fig. 3.5). The broadening of the 211, 112 and 300 reflections between 30-34º and the relatively high intensity of the 002 reflection at 25.9º confirms the nano-nature and the low crystallinity of the coatings. The titanium peaks were still visible and these are marked as (*) in the XRD pattern (Fig. 3.5). FTIR patterns (Fig. 3.6) were also similar for all coated samples and showed that all the coatings consisted of carbonated, (CO_3^{2-} ion absorption bands seen at 1470-1420 and 875 cm^{-1}) calcium phosphates. The absence of the stretching and vibrational modes of the O-H group at 3571 and 639 cm^{-1} confirmed that these coatings might not be simply termed as hydroxyapatite. These characteristics are similar to the coatings that we came across in our earlier experiments.[8] Thus, the coatings retain all the expected characteristics but remain crack-free, when soaked in water after alkali treatment.

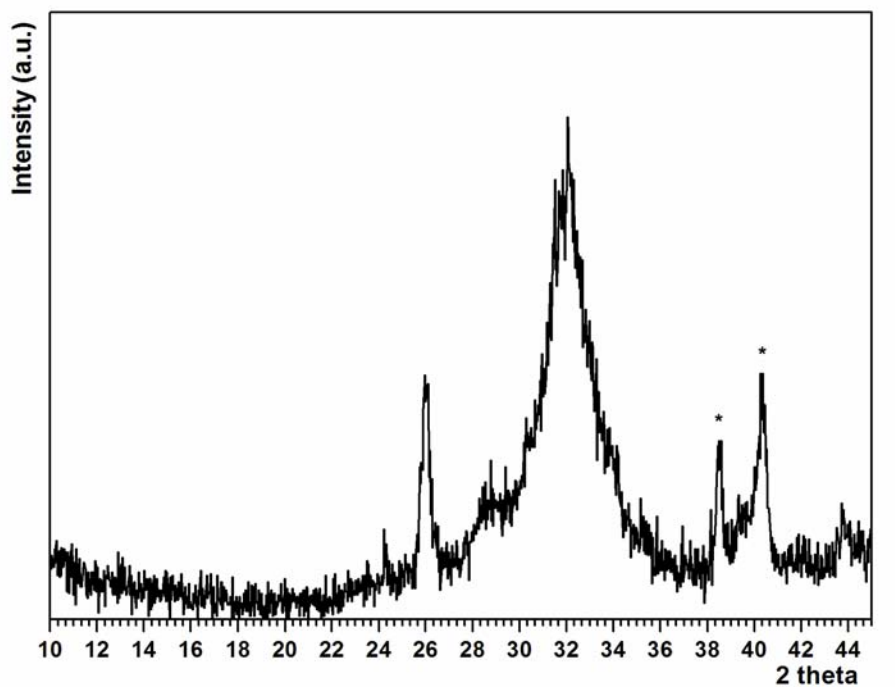

Fig. 3.5 XRD pattern of alkali treated Ti6Al4V soaked in 1.5x *t*-SBF for 7 days

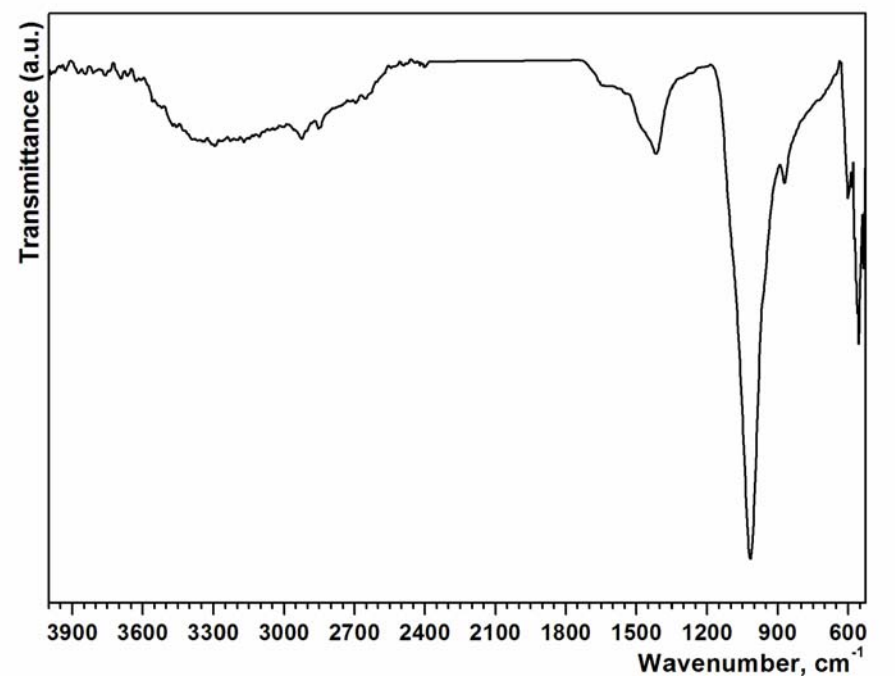

Fig. 3.6 FTIR pattern of alkali treated Ti6Al4V soaked in 1.5x *t*-SBF for 7 days

3.4 Discussion

The deionized water, which normally has a neutral pH of 7.0, now has an acidic pH of approximately 5.7 when exposed to air. Carbon dioxide dissolves slightly in water to form carbonic acid, H_2CO_3, a weak acid, according to the following reaction:

$$H_2O + CO_2 = H_2CO_3$$

When sodium hydroxide is added to this deionized water, some of it reacts with the carbonic acid to form sodium bi-carbonate, as follows:

$$H_2CO_3 + NaOH = NaHCO_3 + H_2O$$

The pH of the solution is increased to 9. The bi-carbonate ion is relatively unstable in comparison to the carbonate ion at this pH. Thus, it leads to the formation of sodium carbonate, as per the following:

$$NaHCO_3 + NaOH = Na_2CO_3 + H_2O$$

Thus, the alkali solution now contains mostly NaOH with small amounts of dissolved Na_2CO_3. The mechanism of the reaction of the titanium alloy with this alkaline solution has been previously explained by Kokubo et al. [4]. On soaking the substrates in alkali solution, the negatively charged hydrated titanate forms, with incorporated sodium ions in it.[4] A hydrated layer of sodium titanate and titanium oxide has been reported to form on the exposed surfaces of Ti6Al4V strips after 24 hours of immersion in a 5M NaOH solution at 60ºC.[3,4,16] The formation of this hydrous sodium titanate after alkali treatment was confirmed by the XRD pattern as shown in Figure 3.1. Since this solution contains small amounts of Na_2CO_3, it also plays a role in the etching process of the Ti6Al4V strips. There is a tendency to form either a compound containing carbonates in it or a complex with sodium titanate on the surface layer. Although no additional phase was detected by XRD, the presence of carbonates in the treated surface is confirmed by FTIR pattern as shown in Figure 3.2b. To summarize, it is clear that the surface layer of NaOH treated Ti6Al4V consists a mixture of hydrated, carbonated sodium titanate and titanium dioxide (rutile).

One possible explanation can be presented when the alkali treated substrates were immersed in deionized water for 24 hours at RT. The deionized

water has a pH of 5.7, at which carbonic acid is the most stable ion phase. On soaking the NaOH treated substrates in deionized water, there is a tendency for the CO_3^{2-} ions present in the surface layer to react with the H^+ ions of water and form carbonic acid, as follows:

$$2H^+ + CO_3^{2-} = H_2CO_3.$$

After 24 hours of soaking time, all the carbonates from the substrate surface go through the reaction. After drying, the substrate is a carbonate-free surface. This effect of carbonate release from the surface with water treatment is substantiated by the FTIR pattern shown in Figure 3.2c. Thus, the data presented in this study highlights differences in the compositions of surface layers after two different surface treatments. The data show that the substrates, before and after water treatment, differ in the (a) sodium, and (b) carbonate contents in the surface treated layer.

The water soaking treatment leads to a decrease in the amount of sodium in the alkali treated layer from 8.25 to 3.6 wt. %. In the present study, the water treatment was performed in large amounts of water for 24 hours at RT. Though performing the water soaking treatment with a small quantity of water at RT for 1 minute results in a decrease in the amount of sodium, it does not remove the carbonates from the surface. Jonasova et al.[17] studied the effect of washing the alkali treated substrates with water at RT on their apatite inducing ability. No significant difference in the rate of apatite formation was observed but the Na amount was lowered from 9.6 to 3.5 at. %.[17] When the water treatment is performed with large amounts of water for 48 hours at 80°C, Uchida et al.[27] observed an increase in apatite formation on titanium metal. However, this enhancement of the apatite forming ability is due to the formation of anatase, formed from the conversion of sodium titanate gel after water treatment at high temperatures.[27] The decrease in sodium content in the surface layer did not cause this increase. Since we performed the water treatments at R.T., our results were in direct correlation to those obtained by Jonasova et al.[17]. SEM micrographs in Figure 3.4 show that the rate of apatite formation is similar on substrates with different Na content. XRD results (Fig. 3.1) confirm that the substrate surface

consists of rutile after water treatment at RT, instead of anatase as formed by Uchida et al.[27] after water treatment at 80°C

In studies performed by Jonasova et al.[17] and Uchida et al.[27], cracks were persistently present in all the biomimetically deposited coatings. These findings show that the presence of different sodium content in the surface layer prior to soaking in SBF solution does not play a role in the formation of cracks in the apatitic calcium phosphate layer. Rather, it indicates that the phases present on the alkali treated layer are more important parameters than sodium content for producing crack-free apatitic calcium phosphate coatings.

It is important to emphasize that the SEM micrographs (Fig. 3.4) in this present study show significant differences in terms of crack formation on the apatitic calcium phosphate layer. Cracks were observed on the calcium phosphate layer deposited on the substrate containing 8.25 wt. % Na (Fig. 3.4a and 4b) whereas none were observed after soaking in SBF on the substrate previously containing 3.6 wt. % Na (Fig. 3.4c and 4d). The substrate surfaces both before and after water treatment, contains sodium titanate and rutile. No other phase (eg. anatase) was detected by the XRD. Since we rule out the possibility of the sodium contents affecting the crack formation, we can conclude that carbonate must play an important role in crack formation. The role of carbonates in forming cracks initially becomes visible just after the alkali treatment. The SEM micrograph in Figure 3.3a shows the NaOH-treated substrate without water treatment and also demonstrates a multitude of cracks on the sodium titanate surface. This is possibly due to the presence of (a) water, as these substrates are hydrated in nature, and (b) carbonates, as the FTIR pattern in Figure 3.2b confirms their presence. Significant differences are observed in the SEM micrographs after water treatment as no cracks are seen on the sodium titanate layer (Fig. 3.3b). The FTIR pattern in Figure 3.2c shows that the substrate is hydrated in nature and has no carbonate bands present. Thus, the presence of cracks in the alkali treated substrates occurring while drying is due to possible loss of carbonates as CO_2 to the air. Since no carbonates were present in the water treated Ti6Al4V strips, no cracks were observed on the sodium titanate layer.

These substrates with/without cracks and with/without carbonates are soaked in SBF solution. During the final drying step, coatings with underlying carbonated titanate phase end up cracking because the carbonates are released from them. These cracks substantially increase the likelihood of delamination, thereby decreasing the implant's bonding ability to natural bones. Thus, water soaking step is expected to improve the performance of coated Ti (or alloy) impants.

3.5 Conclusions

This paper presents results leading to the cause of crack formation in biomimetically coated Ti6Al4V strips. By performing carefully planned experiments, it was found that carbonates are present in the sodium titanate layer formed during the pre-treatment of the substrates. These carbonates during drying tend to evaporate from the underlying surface layer as CO_2 and thus, results in the formation of deep cracks. Successful removal of carbonates from this surface layer was performed by incorporating a water soaking treatment prior to SBF soaking. Once the carbonates are removed, cracks cannot form during any subsequent drying step. This paper suggests a step in the protocol, which should be incorporated into the biomimetic coating process of titanium and related alloy substrates, to obtain crack-free coatings.

3.6 References

1. W.-Q. Yan, T. Nakamura, K. Kawanabe, S. Nishigochi, M. Oka, T. Kokubo. Apatite layer-coated titanium for use as bone bonding implants. *Biomaterials* **18** (1997) 1185-1190.

2. W.-Q. Yan, T. Nakamura, M. Kobayashi, H.-M. Kim, F. Miyaji, T. Kokubo. Bonding of chemically treated titanium implants to bone. *J. Biomed Mater Res* **37** (1997) 267-275.

3. P. Li, I. Kangasniemi, K. de Groot, T. Kokubo. Bone-like hydroxyapatite induction by a gel-derived titania on a titanium substrate. *J Am Ceram Soc* **77** (1994) 1307-1312.

4. T. Kokubo, F. Miyaji, H.-M. Kim, T. Nakamura. Spontaneous formation of bone-like apatite layer on chemically treated titanium metals. *J Am Ceram Soc* **79** (1996) 1127-1129.

5. H.-M. Kim, F. Miyaji, T. Kokubo, T. Nakamura. Apatite forming ability of alkali-treated Ti metal in body environment. *J Ceram Soc Jpn* **105** (1997) 111-116.

6. A.C. Tas, S.B. Bhaduri. Rapid coating of Ti6Al4V at room temperature with a calcium phosphate solution similar to 10× simulated body fluid. *J Mater Res* **19** (2004) 2742-2749.

7. H. Takadama, H.-M. Kim, T. Kokubo, T. Nakamura. TEM-EDX study of mechanism of bonelike apatite formation on bioactive titanium metal in simulated body fluid. *J Biomed Mater Res* **57** (2001) 441-448.

8. S. Jalota, S.B. Bhaduri, A.C. Tas. Effect of carbonate content and buffer used in SBF solutions on calcium phosphate formation on Ti6Al4V. *J Mater Sci Mater M* **17** (2006) 697-707.

9. T. Kokubo. Surface chemistry of bioactive glass-ceramics. *J Non-Cryst Solids* **120** (1990) 138-151.

10. A. Oyane, K. Onuma, A. Ito, H.-M. Kim, T. Kokubo, T. Nakamura. Formation and growth of clusters in conventional and new kinds of simulated body fluids. *J Biomed Mater Res A* **64** (2003) 339-348.

11. H.-M. Kim, K. Kishimoto, F. Miyaji, T. Kokubo, T. Yao, Y. Suetsugu, J. Tanaka, T. Nakamura. Composition and structure of apatite formed on organic polymer in simulated body fluid with a high content of carbonate ion. *J Mater Sci Mater M* **11** (2000) 421-426.

12. D. Bayraktar, A.C. Tas. Chemical preparation of carbonated calcium hydroxyapatite powders at 37°C in urea-containing synthetic body fluids. *J Eur Ceram Soc* **19** (1999) 2573-2579.

13. A.C. Tas. Synthesis of biomimetic Ca-hydroxyapatite powders at 37°C in synthetic body fluids. *Biomaterials* **21** (2000) 1429-1438.

14. H.-M. Kim, H. Takadama, F. Miyaji, T. Kokubo, S. Nishiguchi, T. Nakamura. Formation of bioactive functionally graded structure on Ti6Al4V alloy by chemical surface treatment. *J Mater Sci Mater M* **11** (2000) 555-559.

15. F. Barrere, C.A. van Blitterswijk, K. De Groot, P. Layrolle. Influence of ionic strength and carbonate on the Ca-P coating formation from SBF X 5 solution. *Biomaterials* **23** (2002) 1921-1930.

16. M. Wei, H.-M. Kim, T. Kokubo, J.H. Evans. Optimizing the bioactivity of alkaline-treated titanium alloy. *Mater Sci Eng C* **20** (2002) 125-134.

17. L. Jonasova, F.A. Muller, A. Helebrant, J. Strnad, P. Greil. Hydroxyapatite formation on alkali-treated titanium with different content of Na+ in the surface. *Biomaterials* **23** (2002) 3095-3101.

18. S. Nishiguchi, S. Fujibayashi, H.-M. Kim, T. Kokubo, T. Nakamura. Biology of alkali- and heat-treated titanium implants. *J Biomed Mater Res A* **67** (2003) 26-35 (2003).

19. T. Kokubo, H.-M. Kim, M. Kawashita, T. Nakamura. Bioactive metals: preparation and properties. *J Mater Sci Mater M* **15** (2004) 99-107.

20. L. Jonasova, F.A. Muller, A. Helebrant, J. Strnad, P. Greil. Biomimetic apatite formation on chemically treated titanium. *Biomaterials* **25** (2004) 1187-1194.

21. P. Habibovic, F. Barrère, C. A. van Blitterswijk, K. de Groot, and P. Layrolle. Biomimetic hydroxyapatite coating on metal implants. *J Am Ceram Soc* **85** (2002) 517-522.

22. S. Bharati, M.K. Sinha, D. Basu. Hydroxyapatite coating by biomimetic method on titanium alloy using concentrated SBF. *Bull Mater Sci* **28** (2005) 617-621.

23. X. Yin, M.J. Stott. Biological calcium phosphates and Posner's cluster. *J Chem Phys* **118** (2003) 3717-3723.

24. K. Onuma, A. Ito. Cluster growth model for hydroxyapatite. *Chem Mater* **10** (1998) 3346-3351.

25. G. Treboux, P. Layrolle, N. Kanzaki, K. Onuma, A. Ito. Existence of Posner's cluster in vacuum. *J Phys Chem A* **104** (2000) 5111-5114.

26. J. M. Gomez-Vega, E. Saiz, A. P. Tomsia, T. Oku, K. Suganuma, G. W. Marshall, S. J. Marshall. Novel Bioactive Functionally Graded Coatings on Ti6Al4V. *Adv Mater* **12** (2000) 894-498.

27. M. Uchida, H.-M. Kim, T. Kokubo, S. Fujibayashi, T. Nakamura. Effect of water treatment on the apatite-forming ability of NaOH-treated titanium metal. *J Biomed Mater Res* **63** (2002) 522-530.

CHAPTER 4

IN VITRO TESTING OF CALCIUM PHOSPHATE (HA, TCP, AND BIPHASIC HA-TCP) WHISKERS

Abstract

Calcium phosphate [single-phase hydroxyapatite (HA, $Ca_{10}(PO_4)_6(OH)_2$), single-phase tricalcium phosphate (β-TCP, $Ca_3(PO_4)_2$), and biphasic HA-TCP] whiskers were formed by starting with aqueous solutions containing $NaNO_3$, HNO_3, $Ca(NO_3)_2{\cdot}4H_2O$ and KH_2PO_4 (with or without urea). These solutions were irradiated in a household microwave oven for 5 min. As-recovered precursors were then simply stirred in water at room temperature for 1 hour to obtain the whiskers of the desired calcium phosphate (CaP) bioceramics. Bioactivity and biocompatibility of these whiskers were evaluated, respectively, *in vitro* by (1) soaking those in synthetic body fluid (SBF) solutions at 37°C for one week, and (2) performing cell attachment and total protein assay tests on the as-formed whiskers by using a mouse osteoblast cell line (*7F2*). β-TCP, HA and HA-TCP biphasic whiskers were all found to possess a notable apatite-inducing ability when soaked in SBF. SBF-soaked whiskers of high nanoroughness formed a biomimetic CaP nanotexture. Although the osteoblast viability and protein concentrations were found to be the highest on the HA whiskers, cells were attached and proliferated on all the whiskers. These bioactive whiskers are suitable to use as osteoconductive fillers in biopolymer-based hard tissue scaffolds especially in craniofacial and maxillofacial applications.

(This work is published in *J Biomed Mater Res A* **78** (2006) 481–490)

4.1. Introduction

It is known that whiskers or fibers of many materials can be synthesized; however, the preparation of non-toxic and biocompatible whiskers still remains as an important task. Asbestos whiskers, for instance, which have been used for so many decades are now known to be biohazardous and extremely carcinogenic.[1] Toxicity and carcinogenic properties of SiC whiskers is well known.[2-4] Therefore, it is important to explore other whiskers that are more biocompatible. Human body only uses the carbonated, alkali (Na^+ and K^+) and alkaline earth (Mg^{2+}) ion-doped, apatitic calcium phosphate as the sole inorganic, "ceramic" phase, when and where it needs to exploit the load-bearing ability of such strong materials. Therefore, whiskers of carbonated, apatitic calcium phosphates (CaP) are expected to be non-toxic and perfectly compatible with the human body.[5-14] CaP whiskers were synthesized until now with the aim of using them as possible strengthening additives for the calcium phosphate (e.g., HA: $Ca_{10}(PO_4)_6(OH)_2$) bioceramics. Within this context, reinforcement by whiskers has been regarded as a means of raising the fracture toughness of single-phase HA from <1 to 2-12 $MPa{\cdot}m^{1/2}$.[15-17] We have recently reported[18] a novel procedure which allowed to synthesize short whiskers of either single-phase HA, single-phase TCP or biphasic HA-TCP.

Yoshimura and coworkers[1,7,9,11] laid the foundation for the hydrothermal synthesis of hydroxyapatite whiskers and also for their use in reinforcing calcium phosphate bioceramics.[19] These hydrothermal whisker synthesis procedures, which required aqueous solutions to be heated to 160–200°C in autoclaves, are not suitable (owing to the increased solubility and/or hydrolysis of β-TCP phase under such conditions) for the production of β-TCP or biphasic β-TCP-HA whiskers. [20] Molten salt synthesis techniques, on the other hand, are suitable for the synthesis of monodisperse β-TCP or biphasic whiskers.[10]

To the best of our knowledge, none of the previously synthesized calcium phosphate whiskers has been *in vitro* tested by using the osteoblast cell lines. However, until now the osteoblast attachment and proliferation have been reported only on SiC whiskers, which were used to reinforce calcium phosphate

self-setting cements, bioceramics or polymers.[21-24] The apatite-inducing ability of CaP whiskers,[5-14, 18] when soaked in synthetic body fluid (SBF) solutions,[25-27] was also not studied or reported yet.

The present paper reports the *in vitro* testing of HA, TCP and biphasic HA-TCP whiskers[18] by (1) soaking them in replenished SBF solutions for one week at 37°C, and (2) performing live/dead cytotoxicity counts, protein assay and cell attachment tests by using mouse osteoblasts (7F2).

4.2 Experimental Procedure

4.2.1 ***Sample Preparation.*** The details of calcium phosphate whisker preparation have been given elsewhere.[18] Briefly, aqueous solutions containing dissolved $NaNO_3$, $Ca(NO_3)_2{\cdot}4H_2O$, KH_2PO_4, concentrated HNO_3, and urea (all reagent-grade, Fisher Chemicals, Fairlawn, NJ) were prepared in 10 mL of deionized water in 30 mL-capacity Pyrex® beakers, as shown in Table 4.1. The first chemical added to the beakers was NaNO3, while the last one was urea. Small aliquots of concentrated HNO3 were added to dissolve back any colloidal precipitates that might have formed following the addition of $Ca(NO_3)_2.4H_2O$ and KH_2PO_4 into the $NaNO_3$ solution. For each case shown in Table 4.1, clear-transparent solutions were thus obtained. Sample beakers were then placed onto 10 x 10 x 1 cm^3 alumina insulating fiberboards and covered with an upside down 250 mL-capacity glass beaker. To proceed with the synthesis process, the above-mentioned sample assemblies were placed into a household microwave (MW) oven (Sunbeam, max. power 600 W, 2.45 GHz, Boca Raton, FL) for only 5 min. The MW oven was operated at its maximum power setting. At the end of 5 min of MW heating, the sample beakers reached a temperature of about 500 to 550°C and were slowly cooled to room temperature (RT), in the MW oven, during the next 20 min.

The substance in the sample beaker was then placed into 500 mL of deionized water at RT [(22 ± 1)°C] and stirred with a Teflon-coated magnetic fish on a stirrer at around 300 rpm for 1 h, immediately followed by filtration (No. 42 filter paper, Whatman Int., Maidstone, England) in a vacuum-assisted Buechner

Table 4.1 Sample preparation for HA, TCP, and HA-TCP whiskers[18]

Sample	$NaNO_3$ (g)	$Ca(NO_3)_2 \cdot 4H_2O$ (g)	KH_2PO_4 (g)	15.69 M HNO_3 (mL)	Urea (g)	Ca/P
HA	5.00	1.00	0.345	0.10	1.75	1.67
TCP	5.00	1.00	0.384	0.10	—	1.50
Biphasic	5.00	1.00	0.345	0.10	0.075	1.67

funnel and washing with 2 L of water. The possible influence of varying the stirring rates on whisker synthesis was not studied. At the end of filtration the effluent solutions were transparent and free of whiskers. Samples were dried overnight at 80°C in air.

4.2.2 ***Apatite-inducing ability test.*** Apatite-inducing ability of CaP whiskers were tested by soaking those in a synthetic body fluid (SBF) solution. The details of preparing these solutions were previously given elsewhere.[26] Briefly, the SBF solution we used was a *tris*/HCl-buffered, 27.0 mM HCO_3^- ion-containing solution with the ion concentrations as given in Section 3.2.2 Table 3.1.

The distinctive characteristic of SBF solutions utilized in this study was that they had the same carbonate ion concentration with that of human blood plasma. *In vitro* tests were performed in 100 mL-capacity glass bottles, which contained two grams of HA, TCP or biphasic HA-TCP whiskers and 90 mL of SBF solution. Sealed bottles were kept in an oven at 37±1°C for one week. However, after every 48 hours, the used SBF solution was replenished with a fresh one. Recovered samples (after 1 week) were washed with an ample supply of deionized water, followed by drying at 37°C for 48 hours in air.

4.2.3 ***In vitro cell culture.*** 7F2 mouse osteoblast cells (CRL-12557, American Type Culture Collection, Rockville, MD) were grown on 75 cm^2 culture flasks at 37ºC and 5% CO_2 in alpha-minimum essential medium (MEM) with 2 mM 1-glutamine and 1mM sodium pyruvate, without ribonucleosides and deoxyribonucleosides, augmented by 10% fetal bovine serum (FBS). [28] The culture medium was changed every other day until the cells reached a confluence of 90-95%, as determined visually by using an inverted optical microscope. The

cells were then passaged using trypsin (2.5g/L) EDTA (25mM) solution (Sigma-Aldrich). The obtained cells were then seeded at a concentration of 10,000 cell/well on approximately 6 mm (diameter) x 6 mm (in height) cylindrical samples for various assays. A sintered Al_2O_3 disc was used as the control sample. Cell viability assessment was performed after 72 hours and total protein amount measurements were done after 7 days in a 96-well cell culture plate. The medium was replenished after the first day, and then on every 48 hours during the course of the experiments. After the prescribed time period for each test, substrates were rinsed with phosphate-buffered saline (PBS) solution to remove any non-adherent cells. For statistics, all experiments were performed in triplicate, where n=3. Analysis of variance was performed using the Tukey-Kramer multiple comparisons test.

After 72 hours, live/dead cells were counted on the samples. The unattached cells were collected by trypsinization with 0.5 mL/well trypsin-EDTA solution and were incubated for 10 min. The cells were collected in a conical tube, 1 mL of media was added and centrifuged for 5 min at 1000 rpm. The pellet formed at the base was resuspended in 1 mL media. Finally, trypan blue was added and the cells were counted under an optical microscope. Only cells that stain blue were deemed necrotic because of plasma membrane damage.

The total protein assay was measured using BCA™ Protein Assay Kit (Pierce Biotechnology, Rockford, IL). A working reagent (WR) was prepared by mixing 50 parts of BCA™ Reagent A with 1 part of BCA™ Reagent B. A 200 µL aliquot of the above-mentioned WR was added to each well and thoroughly mixed. Following mixing, the cell culture plate was covered and incubated at 37ºC for 30 min. The absorbance at 562 nm was measured with a spectrophotometer at room temperature. A standard curve was prepared by plotting the average blank-corrected 562 nm measurement for BSA standard versus its concentration in µg/mL. Protein concentration of each sample was then determined by using this standard curve.

Osteoblast attachment and proliferation on the samples were examined by using FESEM. Prior to FESEM investigations, cells were fixed by using 3.5%

glutaraldehyde. The cells were dehydrated with increasing concentrations of ethanol (50%, 75%, 90% and 100%) for 10 minutes each. Critical drying was performed according to the previously published procedures. [20] Samples were sputter-coated with Pt prior to the FESEM imaging at 5 kV.

All cell culture experiments were performed in triplicate and the data were expressed as the mean of three experiments. Statistical analyses were performed using SPSS 8.0 software (Chicago, IL). Fisher's Least Significant Difference (LSD) test was used at a confidence level of 95%, therefore, *p* values _0.05 were considered significant.

4.2.4 ***Characterization*****.** Samples were characterized by powder x-ray diffraction (XRD) (XDS 2000, Scintag, Sunnyvale, CA), Fourier-transform infrared spectroscopy (FTIR) (Nicolet 550, Thermo-Nicolet, Woburn, MA), field-emission scanning electron microscopy (FESEM) (S-4700, Hitachi, Tokyo, Japan), and inductively-coupled plasma atomic emission spectroscopy (ICP-AES) (61E, Thermo-Jarrell Ash, Woburn, MA) analysis.

4.3 Results and Discussion

Figures 4.1a and b display the SEM morphology of the starting β-TCP (whitlockite) whiskers used in this study. The morphology of HA and biphasic HA-TCP whiskers were the same as reported previously.[18] The biphasic whiskers initially contained 60% TCP and 40% HA, prior to the SBF-soaking. Inductively-coupled plasma analyses of the starting whiskers of HA, TCP and biphasic HA-TCP revealed that they contain around 1.5 wt% Na and 250 ppm K. With such a presence of alkali ions, it becomes impossible to name these whiskers as fully stoichiometric HA or TCP. The mineralized portion of human bones is not consisting of pure $Ca_{10}(PO_4)_6(OH)_2$, it contains elements like Na^+, K^+, and Mg^{2+} up to the significant level of 1.3 wt%.[15] Bone mineral is also rich in carbonate ions, i.e., 5.8 wt% of its total weight.[15]

The SEM photomicrographs of Figure 4.2 depicted the unique morphology of TCP, HA-TCP, and HA whiskers after being soaked in the SBF solution at 37°C for one week. All of the SBF-soaked whiskers comprised

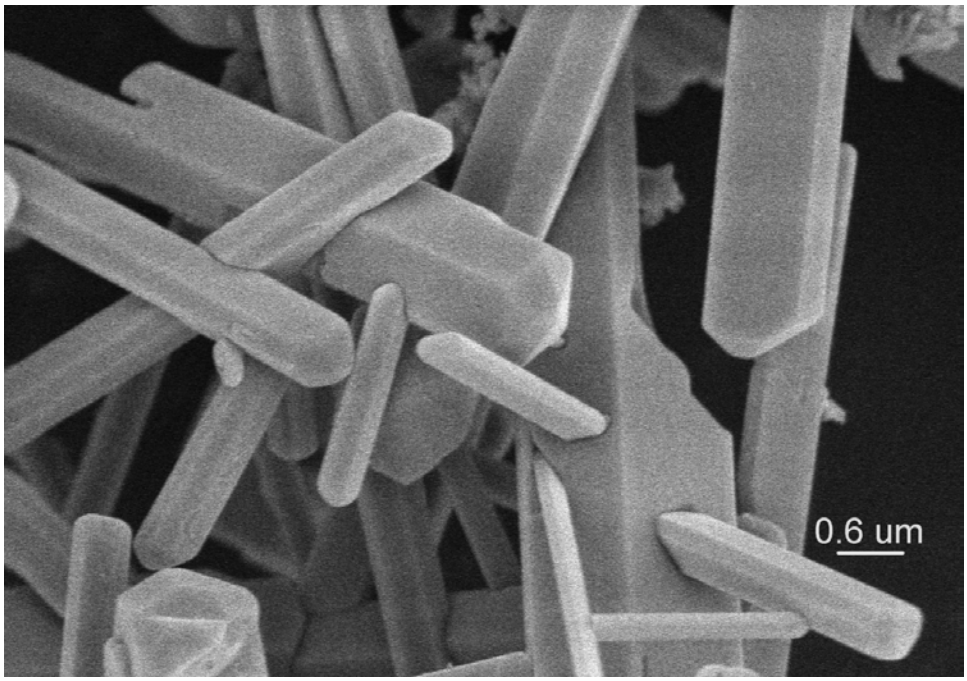

(*a*)

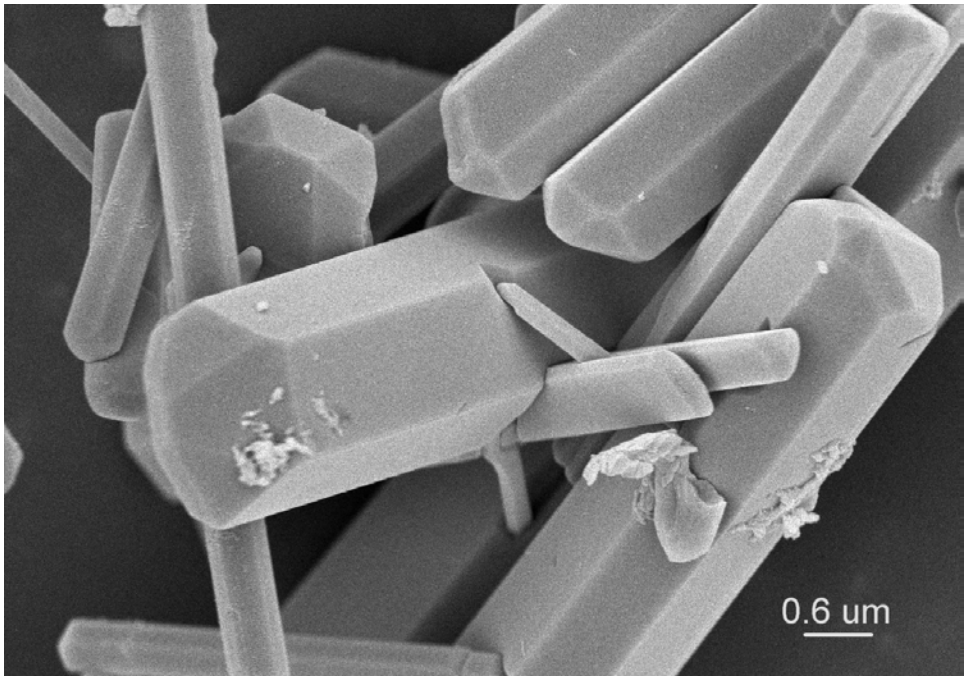

(*b*)

Fig. 4.1 FESEM photomicrographs of β-TCP whiskers

surfaces covered with carbonated apatitic calcium phosphates with a nanoscale roughness. To the best of our knowledge, CaP whiskers (of initial composition of either TCP, biphasic HA-TCP, or HA) with such a morphology have never been synthesized and reported. We hereby propose to name this morphology as the "biomimetic (*SBF-grown*) CaP nanotexture." The same surface texture appears whenever and wherever one uses an SBF solution to grow calcium phosphates regardless of the substrate used. Biomimetic CaPs grown in an SBF solution on Ti6Al4V strips or the CaP precipitates formed in SBF solutions always had the same nanotexture.[30]

The morphology of TCP whiskers (Fig. 4.2b) soaked in SBF was significantly different than that of HA whiskers (Fig. 4.2f), which has underwent exactly the same treatment. TCP samples exhibited a finer, more intimately interwoven surface, whereas in the case of HA the texture was much coarser. The BET surface areas of all *samples* are reported in Table 4.2. The highest experimental surface area value measured for the SBFsoaked TCP whiskers corresponded very well with the highest nano-roughness / nano-texture visually observed for these samples (compare Fig. 4.2b with Figs. 2d and 2f).

Powder X-ray diffraction and FT-IR data for the SBF-soaked whiskers are given in Figures 4.3 and 4.4, respectively. Prior to collecting these XRD and FT-IR data, the SBF-soaked whiskers (2 g in each SBF-soaking bottle) were ground into a fine powder by using an agate mortar and a pestle. The XRD and FT-IR data presented in Figures 4.3 and 4.4, therefore, were not limited only to the surfaces of the whiskers. According to XRD data, TCP whiskers almost completely transformed into apatitic calcium phosphates after one week of soaking in the synthetic body fluid (Fig. 4.3). Since SBF solutions can only form apatitic CaP (but not TCP), neat HA whiskers soaked in SBF solutions again yielded characteristic HA patterns (Fig. 4.3). On the other hand, XRD peaks for crystalline β-TCP were still visible in the SBF-soaked biphasic HA-TCP samples.

FT-IR data of Figure 4.4 revealed the presence of CO_3^{2-} (1480-1420 and 873 cm^{-1}) and HPO_4^{2-} groups (870, 1133 and 1210 cm^{-1}) in all the SBF-soaked samples.[31] Most of the time it may become somewhat difficult to distinguish

Table 4.2 BET Surface Areas of Sample

Sample	Surface Area (m^2/g)[a]
Neat HA	8.7 ± 0.4
Neat biphasic HA-TCP	4.4 ± 0.2
Neat TCP	3.1 ± 0.2
SBF-soaked HA	45.0 ± 1.6
SBF-soaked biphasic HA-TCP	56.9 ± 2.1
SBF-soaked TCP	112.2 ± 2.5

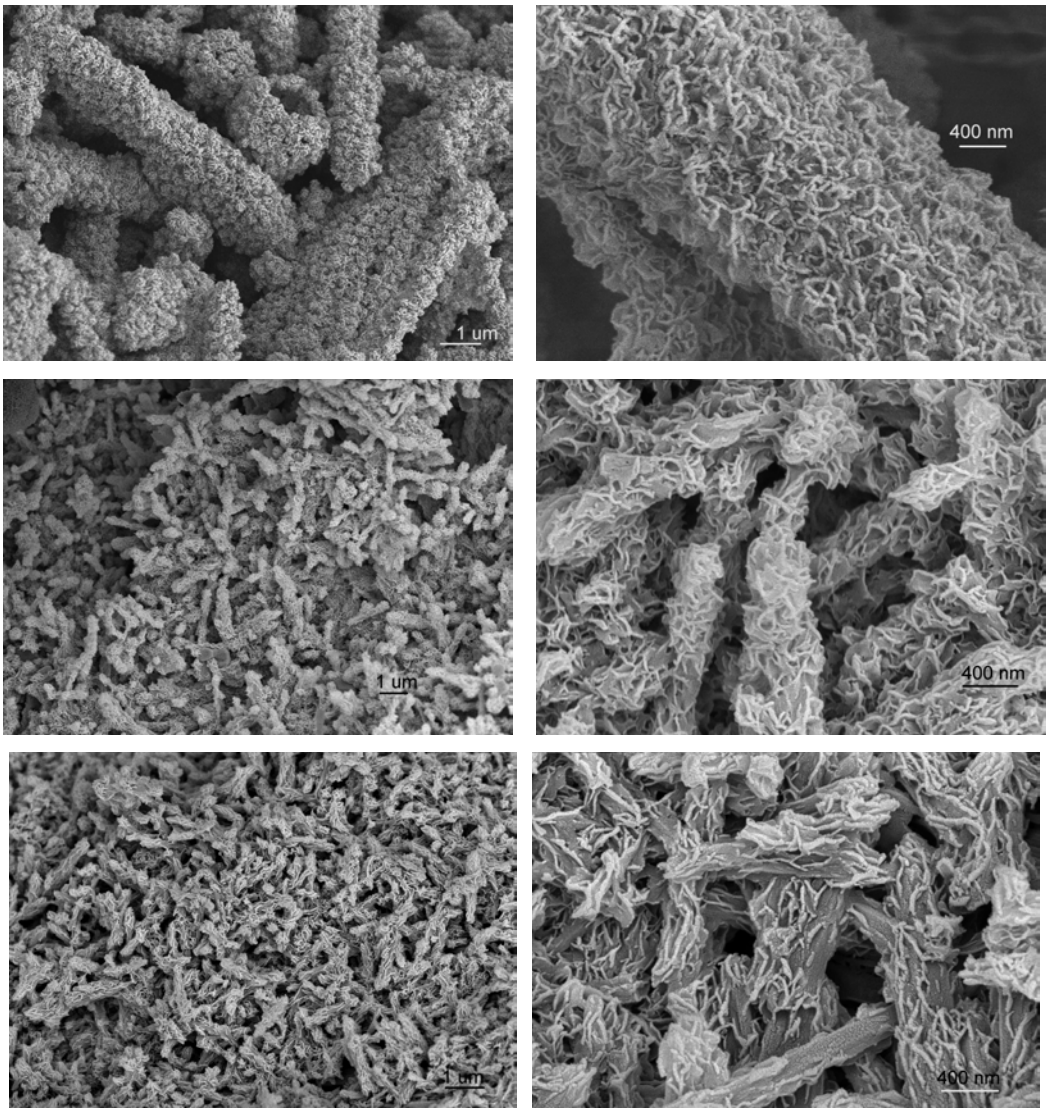

Fig. 4.2 FESEM photomicrographs of SBF-soaked whiskers, *(a)* & (*b*): β-TCP whiskers; (*c*) & (*d*): biphasic HA-TCP whiskers; (*e*) & (*f*): HA whiskers

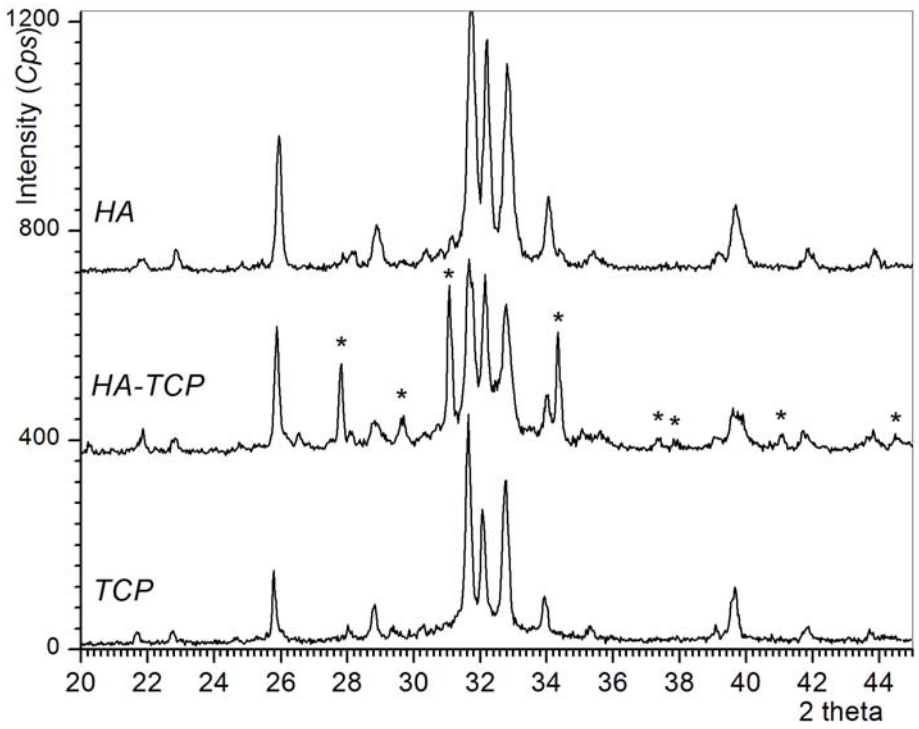

Fig. 4.3 XRD traces of SBF-soaked whiskers (* denotes TCP peaks)

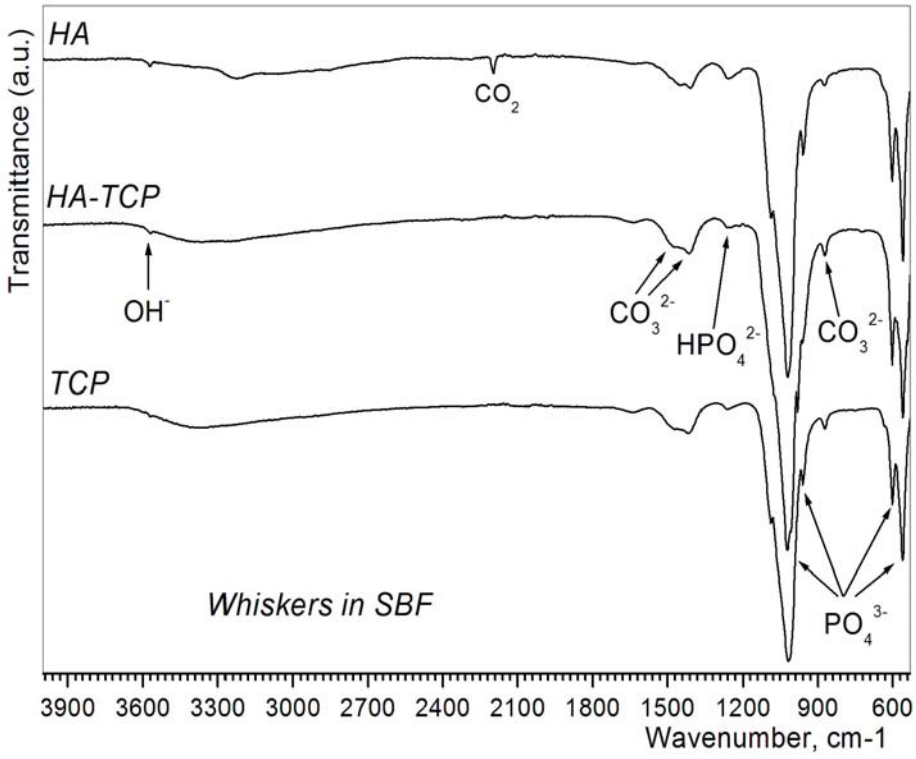

Fig. 4.4 FTIR traces of SBF-soaked whiskers

between the resembling FT-IR spectra of β-TCP and HA, and for this purpose the FT-IR trace of single phase β-TCP (99%, Fluka) powders is presented here in Figure 4.5. For β-TCP, there were no absorption bands present over the range 4000 and 1300 cm^{-1}. It is visible from Figure 4.5 that there are at least 25 absorption bands in the characteristic FT-IR trace of pure β-TCP samples

Relying on the experimental solubility values of some of the calcium phosphate phases reported by Tang *et al*. [32], it is seen that the dissolution rate of β-TCP (i.e., $1.26x10^{-4}$ mol/m^{-2} min^{-1}) in an aqueous solution at a pH of about 6 is about 89 times greater than that of carbonated apatite, $1.42x10^{-6}$ mol/m^{-2} min^{-1}. According to this, it is not difficult to assume that the whiskers of TCP of this study would dissolve in the SBF solution (in 1 week, at 37°C) at a much faster rate than those of HA. The dissolution of TCP in aqueous solutions can be described by the following reaction:

$$3Ca_3(PO_4)_2\,(s) + H_2O \rightarrow 9Ca^{2+}(aq) + HPO_4^{2-}(aq) + 5PO_4^{3-}(aq) + OH^-(aq) \quad (1).$$

During the dissolution of β-TCP, the above aqueous ions combine to form what is known as calcium-deficient hydroxyapatite (CDHA), $Ca_9(OH)(HPO_4)(PO_4)_5$.[33] CDHA can also incorporate CO_3^{2-} ions, and it lacks one Ca^{2+} and one OH^- in the unit cell of its crystal structure. CDHA yields the same XRD pattern with that of stoichiometric hydroxyapatite, HA.

The bottom XRD trace shown in Figure 4.3, thus, belonged to the newly formed CDHA on and along the initial TCP whiskers, until their total consumption during the process, and this pattern was extremely difficult to differentiate from that of HA. The original TCP whiskers, in a sense, behaved like a "guiding scaffold" for the formation or regeneration of biomimetic CaP with a unique rod-like morphology. The detection of HPO_4^{2-} bands in the FTIR data of Figure 4.4 also confirmed the formation of carbonated CDHA after soaking the whiskers in SBF.[34] Such non-stoichiometric, carbonated apatitic calcium phosphates can readily accommodate a Ca/P molar ratio between 1.67 and 1.33 (i.e., octacalcium phosphate, OCP, $Ca_8H_2(PO_4)_6{\cdot}5H_2O$). OCP is an acidic calcium

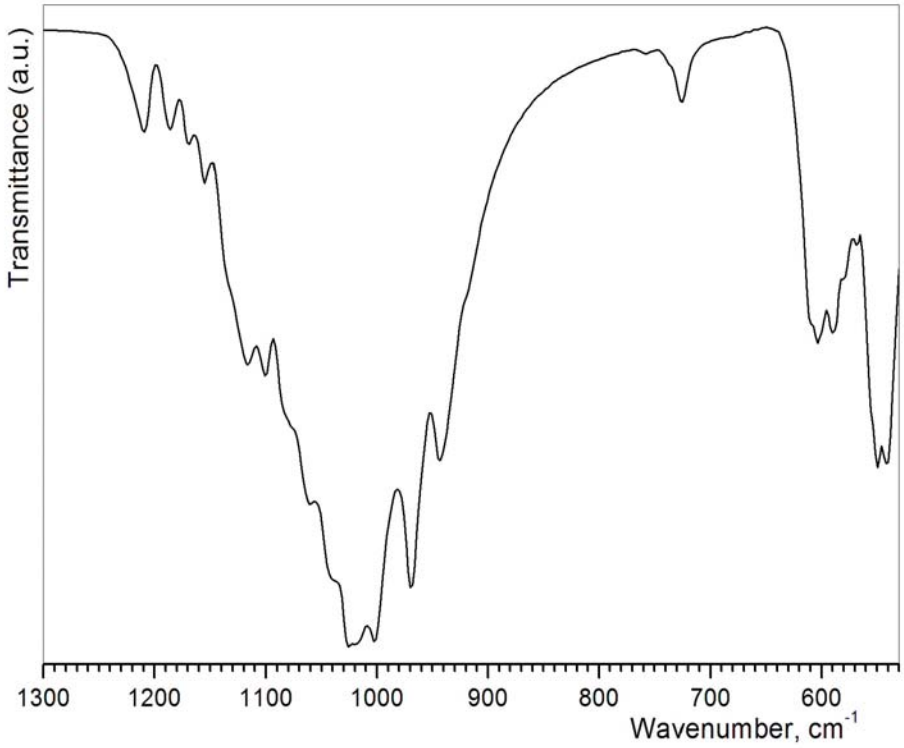

Fig. 4.5 FTIR trace of pure β-TCP powders

phosphate salt, and the formation of it in neutral aqueous solutions of pH 7.4 (such as SBF) is extremely difficult, if not impossible. The strongest XRD reflection for the OCP phase is to be detected at *d*-spacing = 18.703 Å, however, the XRD data of the SBF-soaked whiskers of this study did not exhibit this peak.

SBF solutions are supersaturated with respect to apatitic calcium phosphate nucleation due to their high Ca/P molar ratio of 2.5, and therefore, even when they are optically transparent, they contain calcium phosphate clusters with sizes around 10 Å. [35] These CaP clusters were first described by Betts and Posner et al.[36] to have the $Ca_9(PO_4)_6$ stoichiometry, and are now known as Posner clusters. These clusters present in the SBF solutions aggregate to produce the biomimetic CaP nanotexture, while filling the intercluster spaces with water and bicarbonate molecules. Dorozhkina and Dorozhkin[37] quantitatively confirmed the carbonated nature of such clusters when they reached the micron-size range.

Dissolution of β-TCP provided the SBF solution, at the dissolution interface, with the aqueous ions given in equation (1), and the presence of these ions triggered the hexagonal packing of Posner clusters[35] of the SBF to form carbonated, nano-textured, apatitic calcium phosphates on the whiskers [Figs. 4.2a and b). When HA was present as a phase in those whiskers (since it had a significantly lower solubility in comparison to β-TCP), the supply of those ions to the solution was slowed down. This was why the XRD traces (Fig. 4.3) of biphasic HA-TCP still contained peaks of β-TCP. In the case of pure HA whiskers (Figs. 4.2e and f), the formation of the biomimetic CaP nanotexture was much more incomplete as compared to those of β-TCP whiskers (Figs. 4.2a and b), due to their almost two order of magnitude lower solubility. As expected, biphasic HA-TCP whiskers had taken an intermediate place in between the pure TCP and pure HA samples, in terms of forming that interlocking, intermingling biomimetic CaP nanotexture.

The characteristic surface morphology of the neatwhisker cylinders (6 mm x 6 mm) on which the osteoblast cells were cultured is given in the SEM micrograph of Figure 4.6. As a result of the pressing action, whiskers formed a porous compact while maintaining their individual shapes. Mouse osteoblast cells

(7F2) cultured on whisker samples (as is, not soaked in SBF) exhibited differences in terms of the number of attached cells and protein concentration, as presented in Figures 4.7a & b. The number of attached cells and the measured protein concentrations were found to yield the highest values for HA whiskers.

The results of the Fisher's least significant difference (LSD) test are shown in Table 4.3. LSD test is basically a student's *t* test using a pooled error variance, and is suitable for making pair-wise comparisons among a set of *t* population means. In Table 4.3, *p* values less than 0.05 indicated that there was a statistically meaningful and reliable difference. In other words, the cell attachment and protein concentrations registered for the Al2O3 control samples were statistically different than those of all the CaPs of this study.

At the significance level of 0.05, when TCP was compared with HA in terms of cell attachment and total protein concentration, the *p* values for both LSD tests came out to be less than 0.05 (as shown in Table 4.3). Therefore, we are 95% confident that there is a difference in cell viability and total protein concentration between HA and TCP whisker compacts. However, it was not possible to detect any statistical difference between HA-TCP and TCP or HA-TCP and HA in terms of number of cells attached and protein concentration.

Osteoblast attachment and proliferation on the surfaces of whisker samples was monitored by SEM, and given in Figures 4.8a through f. Osteoblasts were attached to the surfaces of all the whisker samples tested here, however, the high-magnification pictures showed significant differences in osteoblast proliferation.

Osteoblast behavior is sensitive to the biochemical and topographical features (i.e., chemical and physical microarchitecture) of their substrate. The ideal and most preferred surface used by osteoblasts in vivo is the osteoclast resorption pits.[38] The cell attachment and the protein assay histograms given in Figures 4.7a and 4.7b clearly showed that the CaP whiskers always performed better than the control samples of sintered, dense Al_2O_3. Mouse osteoblasts were able to easily differentiate between the chemical compositions of the CaP whiskers. In other words, osteoblasts favored whiskers of hydroxyapatite (HA) those of over β-TCP

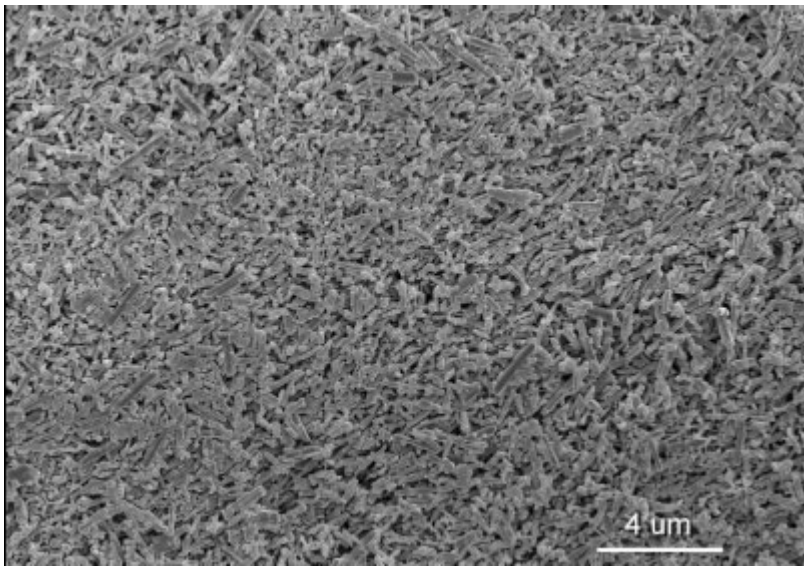

Fig. 4.6 FESEM micrograph of the surface of whisker cylinders used in cell culture tests.

Table 4.3 *p* Values for the Number of Cells Attached and Protein Concentration

Test		Control	HA	HA-TCP	TCP
No. of Cells Attached	Control	-	0.001*	0.006*	0.019*
	HA	0.001*	-	0.143	0.041*
	HA-TCP	0.006*	0.143	-	0.441
	TCP	0.019*	0.041*	0.441	-
Total Protein Conc.	Control	-	0	0*	0*
	HA	0*	-	0.159	0.019*
	HA-TCP	0*	0.159	-	0.202
	TCP	0*	0.019*	0.202	-

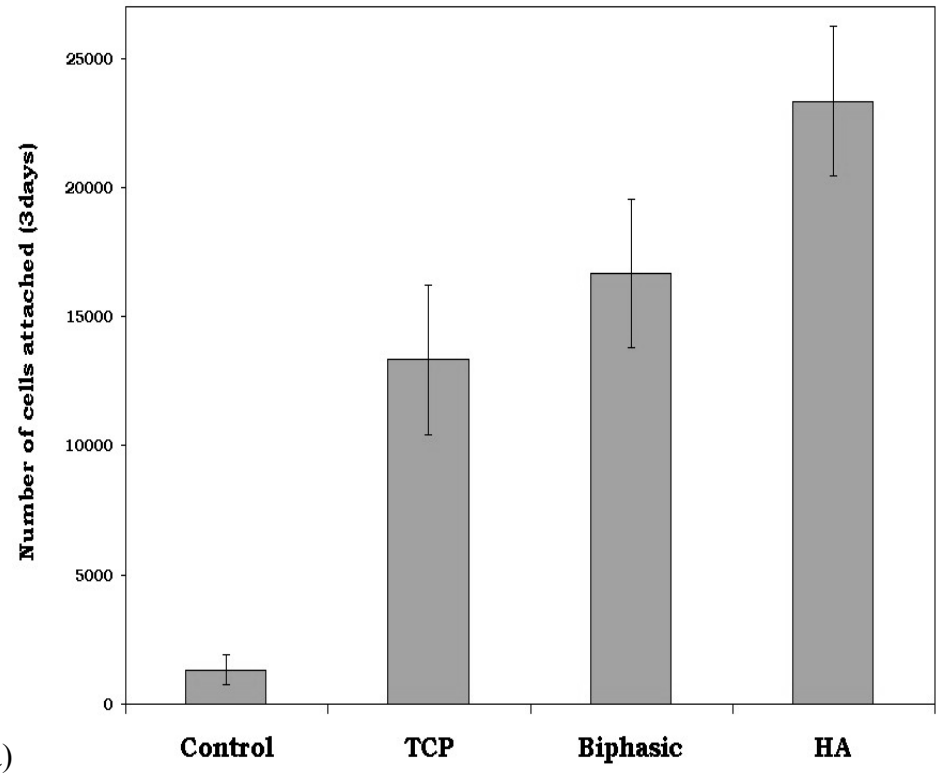

(a)

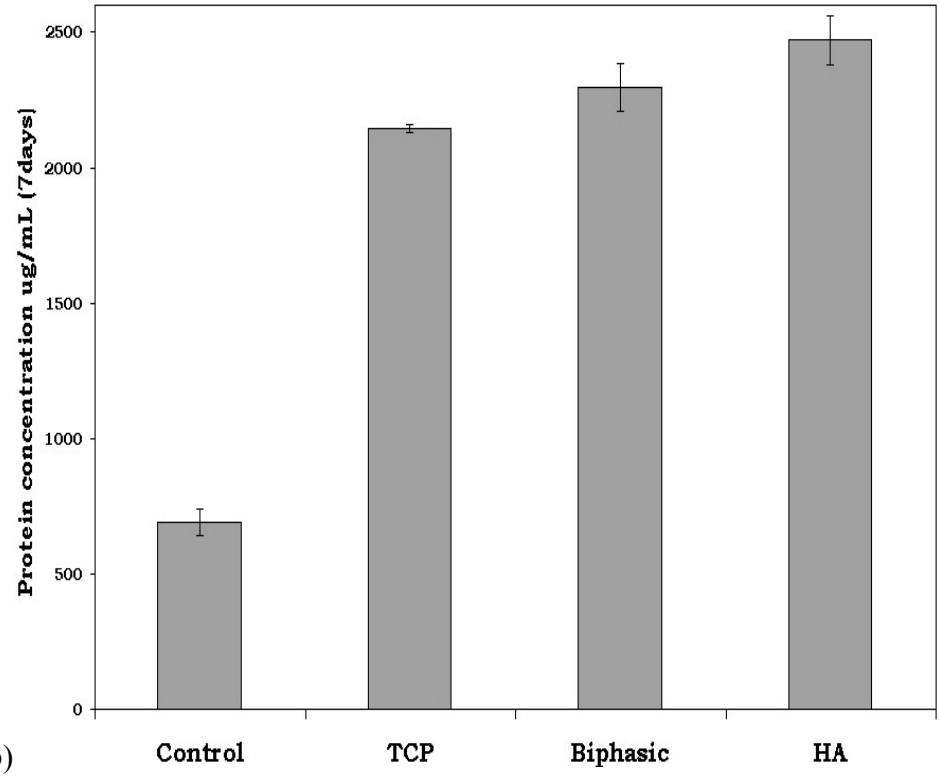

(b)

Fig. 4.7 (a) Number of attached cells on whiskers (*control*: Al_2O_3) and (b) Protein assays for whiskers (*control*: Al_2O_3)

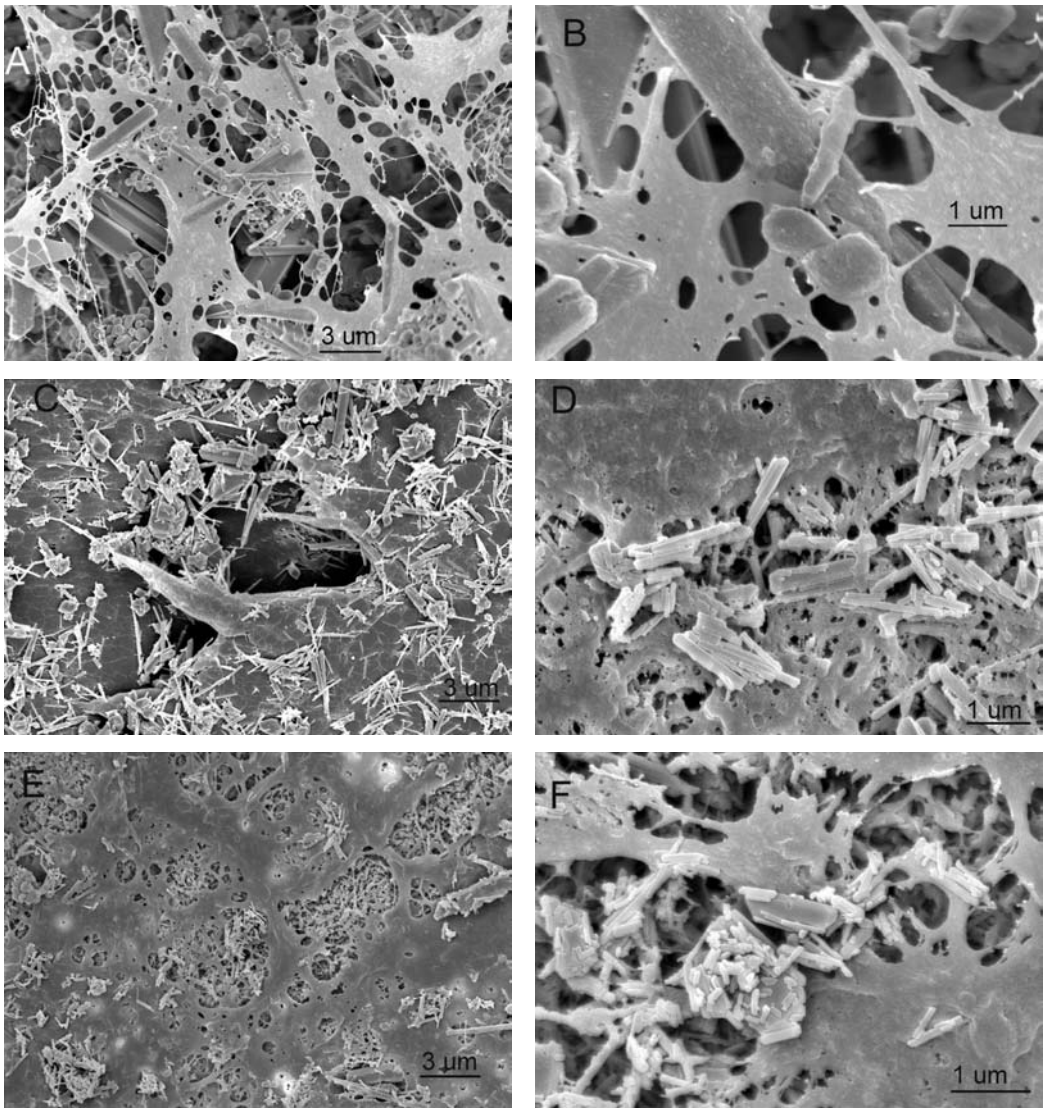

Fig. 4.8 FESEM photomicrographs of osteoblast proliferation on whiskers, (*a*) & (*b*): β-TCP whiskers; (*c*) & (*d*): biphasic HA-TCP whiskers; (*e*) & (*f*): HA whiskers

or biphasic HA-TCP. It is a well-known fact that the surface chemistry of a material determines the initial *in vitro* interactions of proteins, such as fibronectin with integrin cell-binding domains, which in turn regulate the cell adhesion process. Osteoblast response to the CaP surfaces of this study can be regarded as the sum of their ability to attach, proliferate, and differentiate. In the attachment stage, osteoblast filopodia explore the substrate topography for areas to which a greater surface area of the cell can adhere. These filopodia are used in sensing the substrate, and they extend over significant distances to find areas appropriate for attachment.[39] All of the FESEM micrographs of Figure 4.8 revealed the readily extension of those filopodia.

On whisker surfaces, cells were flattened and spread with clear actin fibers associated with vinculin adhesion plaques (Fig. 4.8). For instance, the FESEM micrograph of Figures 4.8a and b, recorded on the surfaces of β-TCP whiskers, clearly showed the actin cytoskeleton and the stress fibers. On the other hand, the micrographs of Fig. 4.8d and f displayed the vinculin adhesion plaque formation on the biphasic HA-TCP and HA whiskers, respectively.

Cells are known to produce fewer adhesion plaques while still in the process of migration than once permanently settled in place.[40] Sun et al.[41] exposed cells to calcium phosphate particles and reported that HA particles (100 nm) or β-TCP particles (100 nm) inhibited the growth of primary mouse osteoblasts, while causing an increase in their expression of alkaline phosphatase.[42] In addition, Pioletti et al.[43] observed a decrease in growth, viability, and synthesis of extracellular matrix (ECM) in primary mouse osteoblasts that were exposed to β-TCP particles (1–10 μm) or $CaHPO_4 \cdot 2H_2O$ particles (1–10 μm). A 90% decrease in viability was reported by Pioletti et al.[43] when evaluated using a Live-Dead assay similar to what we have used in this study. Our results with the β-TCP whiskers also confirmed the findings of Pioletti et al.[43] The bone depositing cells, i.e., osteoblasts, always prefer more basic surfaces to attach and proliferate, and this was also confirmed in the present study. The basicity of the whiskers increased in going from β-TCP (neutral pH) to HA (pH> 9). The pH values of as-synthesized whiskers were measured, at 37°C, by inserting a pH electrode into

suspensions prepared by adding 1 g of whiskers into 5 mL deionized water, and after keeping the whiskers in these for 15 min.

CaP particles and other bioactive materials have been used as fillers in polymer-based bone cements to improve their mechanical properties.[44-47] Besides calcium phosphates, SiC whiskers were also used as fillers, for instance, to reinforce Bis-GMA-based dental resins to extend their use to large load-bearing restorations.[20] The SiC whiskers possessed a high structural perfection resulting in superior strength values. While plain whiskers did not significantly strengthen the resin matrix, nano-silica attachment (on the whiskers) was reported[48] to roughen the whisker surfaces and enhanced whisker retention in the matrix, resulting in strong composites with substantially increased strength and toughness. Nevertheless, even calcium carbide "ceramic" particles are not resorbable *in vivo*, and their cytotoxicity behavior, in case they go into the bloodstream of a patient and possibly end up in kidneys and/or liver are not known at all.[49]

The SBF-soaked β-TCP, biphasic HA-TCP, and HA whiskers reported in this study have a very high nanoscale surface roughness, and they are fully biocompatible with the human body. These novel whisker scaffolds will speak to the hypotheses recently developed by Webster et al.[28,29] on the extraordinary bioactivity behavior observed on the surfaces of otherwise bioinert materials, such as Al_2O_3, ZrO_2, or metallic alloys, when they possess some degree of nanoscale roughness. Our research on the incorporation of these SBF-soaked whiskers having a "biomimetic CaP nanotexture" into biopolymers, such as cross-linked gelatin or alginates, is in progress, which we plan to report in due time. These biopolymer-CaP composites will be utilized in craniofacial and maxillofacial surgery.

4.4. Conclusions

1. Whiskers of bioactive β-TCP, biphasic HA-TCP and HA have been synthesized by using a simple microwave-assisted molten salt synthesis procedure.[18] This procedure readily allowed for the *on demand* synthesis of any of these whiskers.

2. When soaked in synthetic body fluid (SBF) solutions for 1 week at 37°C, all of the whiskers were found to form carbonated, apatitic calcium phosphates, while still retaining their whisker form.
3. After SBF-soaking a unique "biomimetic CaP nanotexture" was observed on the surfaces, which imparted to the whiskers a nanoscale surface roughness.
4. *In vitro* cell culture tests performed with the mouse osteoblasts (7F2) on the whiskers showed increasing cell attachment and protein concentration rates in the following order: HA > biphasic HA-TCP > β-TCP.

4.5 References

1. M. Yoshimura, H. Suda, K. Okamoto, and K. Ioku. Hydrothermal synthesis of biocompatible whiskers. *J. Mater. Sci*. **29** (1994) 3399-3402.

2. P. Romundstad, A. Andersen, T. Haldorsen. Cancer incidence among workers in the Norwegian silicon carbide industry. *Am J Epidemiol* **153** (2001) 978-986.

3. G.L. Vaughan, S.A. Trently. The toxicity of silicon carbide whiskers. A review. *J Environ Sci Health* A **31** (1996) 2033-2054.

4. N.F. Johnson, F.F. Hahn. Induction of mesothelioma after intrapleural inoculation of F344 rats with silicon carbide whiskers or continuous ceramic filaments. *Occup Environ Med* **53** (1996) 813-816.

5. D. B. Warheit. A review of some biophysical factors and their potential roles in the development of fiber toxicity. *Regul Toxicol Pharmacol* **20** (1994) S113-S120.

6. T. Kasuga, T. Inoue, K. Tsuji, Y. Ota, Y. Abe. Preparation of porous ceramics with calcium metaphosphate fiber skeleton for biomedical use. *J Am Ceram Soc* **78** (1995) 245-247.

7. W. Suchanek, H. Suda, M. Yashima, M. Kakihana, M. Yoshimura. Biocompatible whiskers with controlled morphology and stoichiometry,'' *J Mater Res* **10** (1995) 521-529.

8. P. K. Kundu, T. S. Waghode, D. Bahadur, D. Datta. Cell culture approach to biocompatibility evaluation of unconventionally prepared hydroxyapatite. *Med Biol Eng Comput* **36** (1998) 654-658.

9. W. Suchanek, M. Yoshimura. Preparation of fibrous, porous hydroxyapatite ceramics from hydroxyapatite whiskers. *J Am Ceram Soc* **81** (1998) 765-767.

10. A. C. Tas. Molten salt synthesis of calcium hydroxyapatite whiskers. *J Am Ceram Soc* **84** (2001) 295-300.

11. S. Jinawath, D. Pongkao, W. Suchanek, and M. Yoshimura. Hydrothermal synthesis of monetite and hydroxyapatite from monocalcium phosphate monohydrate. *Int J Inorg Mater* **3** (2001) 997-1001.

12. H. C. Park, D. J. Baek, Y. M. Park, S. Y. Yoon, R. Stevens. Thermal stability of hydroxyapatite whiskers derived from the hydrolysis of α-TCP. *J Mater Sci* **39** (2004) 2531-2534.

13. T. Iizuka, A. Nozuma. Effects of the buffer solutions on the growth of hydroxyapatite whiskers. *J Ceram Soc Jpn* **107** (1999) 442-448.

14. T. Toyama, A. Oshima, T. Yasue. Hydrothermal synthesis of hydroxyapatite whisker from amorphous calcium phosphate and the effect of carboxylic acid. *J Ceram Soc Jpn* **109** (2001) 232-237.

15. L. L. Hench. Bioceramics: From Concept to Clinic. *J Am Ceram Soc* **74**, 1487-1510 (1991).

16. Y.N. Yeni, C.U. Brown, T.L. Norman. Influence of bone composition and apparent density on fracture toughness of the human femur and tibia. *Bone* **22** (1998) 79-84.

17. J.B. Phelps, G.B. Hubbard, X. Wang, C.M. Agrawal. Microstructural heterogeneity and the fracture toughness of bone. *J Biomed Mater Res* **51** (2000) 735-741

18. S. Jalota, A. C. Tas, S. B. Bhaduri. Microwave-assisted synthesis of calcium phosphate nanowhiskers. *J Mater Res* **19** (2004) 1876-1881.

19. W. Suchanek, M. Yashima, M. Kakihana, M. Yoshimura. Processing and mechanical properties of hydroxyapatite reinforced with hydroxyapatite whiskers. *Biomaterials* **17** (1996) 1715-1723.

20. M. Aizawa, A.E. Porter, S.M. Best, W. Bonfield. Ultrastructural observation of single-crystal apatite fibers. *Biomaterials* **26** (2005) 3427-3433.

21. H. H. K. Xu, D. T. Smith, and C. G. Simon. Strong and bioactive composites containing nano-silica-fused whiskers for bone repair. *Biomaterials*. **25**, 4615 (2004).

22. H.H.K. Xu. Long-term water-ageing of whisker-reinforced polymer-matrix composites. *J Dent Res* **82** (2003) 48-52.

23. H.H.K. Xu, J.B. Quinn. Whisker-reinforced bioactive composites containing calcium phosphate cement fillers: Effects of filler ratio and surface treatments on mechanical properties. *J Biomed Mater Res* **57** (2001) 165-174.

24. K. Park, S. Sundaresan, T. Vasilos, and C. Sung. SiC whisker-reinforced and C fiber-reinforced calcium phosphate composites. *J Mater Res* **9** (1994) 2476-2479.

25. T. Kokubo. Surface chemistry of bioactive glass-ceramics. *J Non-Cryst Solids* **120** 138-151.

26. D. Bayraktar, A. C. Tas. Chemical preparation of carbonated calcium hydroxyapatite powders at 37°C in urea-containing synthetic body fluids. *J Eur Ceram Soc* **19** (1999) 2573-2579.

27. A. Oyane, H.-M. Kim, T. Furuya, T. Kokubo, T. Miyazaki, T. Nakamura. Preparation and assessment of revised simulated body fluids. *J Biomed Mater Res A* **65** (2003) 188-195.

28. T. J. Webster, R. W. Siegel, R. Bizios. Osteoblast adhesion on nanophase ceramics. *Biomaterials* **20** (1999) 1221-1227.

29. T. J. Webster, J. U. Ejiofor. Increased osteoblast adhesion on nanophase metals: Ti, Ti6Al4V, CoCrMo. *Biomaterials* **25** (2004) 4731-4739.

30. A. C. Tas, S. B. Bhaduri. Rapid coating of Ti6Al4V at RT with a calcium phosphate solution similar to 10x simulated body fluid. *J Mater Res* **19** (2004) 2742-2749.

31. M. Tamai, M. Nakamura, T. Isshiki, K. Nishio, H. Endoh, A. Nakahira. A metastable phase in thermal decomposition of Ca-deficient hydroxyapatite. *J Mater Sci Mater M* **14** (2003) 617-622.

32. R. Tang, M. Hass, W. Wu, S. Gulde, G. H. Nancollas. Constant composition dissolution of mixed phases II. Selective dissolution of calcium phosphates. *J Coll Int Sci* **260** (2003) 379-384.

33. Y.B. Li, X.D. Zhang, K. de Groot. Hydrolysis and phase transition of alpha-tricalcium phosphate. *Biomaterials* **18** (1997) 737-741.

34. T. Kokubo, T. Himeno, H. M. Kim, M. Kawashita, T. Nakamura. Process of bonelike apatite formation on sintered hydroxyapatite in serum-containing SBF. *Key Eng Mater* **254-2** (2004) 139-142.

35. K. Onuma, A. Ito. Cluster growth model for hydroxyapatite. *Chem Mater* **10** (1998) 3346-3351.

36. F. Betts, A. S. Posner. A structural model for amorphous calcium phosphate. *Trans Am Cryst Assoc* 10 (1974) 73-84.

37. E. I. Dorozhkina, S. V. Dorozhkin. Structure and properties of the precipitates formed from condensed solutions of the revised simulated body fluid. *J Biomed Mater Res A* **67** (2003) 578-581.

38. B. D. Boyan, Z. Schwartz, C. H. Lohmann, V. L. Sylvia, D. L. Cochran, D. D. D. Dean, J. E. Puzas. Pretreatment of bone with osteoclasts affects phenotypic expression of osteoblast-like cells. *J Orthop Res* **4** (2003) 638-647.

39. S. M. Rea, R. A. Brooks, A. Schneider, S. M. Best, W. Bonfield. Osteoblast-like cell response to bioactive composites surface-topography and composition effects. *J Biomed Mater Res* **70** (2004) 250-261.

40. M. J. Dalby, L. Di Silvio, G. W. Davies, W. Bonfield. Surface topography and HA filler volume effect on primary human osteoblast *in vitro*. *J Mater Sci Mater M* **12** (2000) 805-810.

41. J. S. Sun, Y. H. Tsuang, C. J. Liao, H. C. Liu, Y. S. Hang and F. H. Lin. The effects of calcium phosphate particles on the growth of osteoblasts. *J Biomed Mater Res* **37** (1997) 324-334.

42. C. G. Simon, W. F. Guthrie and F. W. Wang. Cell seeding into calcium phosphate cement. *J Biomed Mater Res A* **68** (2004) 628-639.

43. D. P. Pioletti, H. Takei, T. Lin, P. V. Landuyt, Q. J. Ma, S. Y. Kwon and K. L. P. Sung. The effects of calcium phosphate cement particles on osteoblast functions. *Biomaterials* **21** (2000) 1103-1114.

44. A. M. P. Dupraz, J. R. de Wijn, S. A. T. van de Meer, and K. de Groot. Characterization of silane-treated hydroxyapatite powders for use as filler in biodegradable composites. *J Biomed Mater Res* **30** (1996) 231-238.

45. Y. E. Greish and P. W. Brown. Characterization of bioactive glass-reinforced HAP-polymer composites. *J Biomed Mater Res* **52** (2000) 687-694.

46. E. J. Harper, M. Braden, and W. Bonfield. Mechanical properties of hydroxyapatite reinforced poly(ethylmethacrylate) bone cement after immersion in a physiological solution influence of a silane coupling agent. *J Mater Sci Mater M* **11** (2000) 491-497.

47. C. G. Simon, C. A. Khatri, S. A. Wight, F. W. Wang. Preliminary report on the biocompatibility of a moldable, resorbable, composite bone graft consisting of calcium phosphate cement and poly(lactide-co-glycolide) microspheres. *J Orthop Res* **20** (2002) 473-482.

48. H. H. K. Xu, T. A. Martin, J. M. Antonucci, F. C. Eichmiller. Ceramic whisker reinforcement of dental composite resins. *J Dent Res* **78** (1999) 706-712.

49. H. Kjuus, A. Andersen, S. Langard. Incidence of cancer among workers producing calcium carbide. *Br J Ind Med* **43** (1986) 237-242.

CHAPTER 5

A NEW RHENANITE (β-$NaCaPO_4$) AND HYDROXYAPATITE BIPHASIC BIOMATERIAL FOR SKELETAL REPAIR

Abstract

Biphasic β-rhenanite (β-$NaCaPO_4$)–hydroxyapatite ($Ca_{10}(PO_4)_6(OH)_2$) biomaterials were prepared by using a one-pot, solution-based synthesis procedure at the physiological pH of 7.4, followed by low-temperature (300–600°C) calcination in air for 6 h. Calcination was for the sole purpose of crystallization. An aqueous solution of $Ca(NO_3)_2.4H_2O$ was rapidly added to a solution of Na_2HPO_4 and $NaHCO_3$, followed by immediate removal of gel-like, poorly-crystallized precursor precipitates from the mother liquors of pH 7.4. Freeze-dried precursors were found to be nanosize with an average particle size of 45 nm and a surface area of 128m^2/g. Upon calcination in air, precursor powders crystallized into biphasic (60% HA–40% rhenanite) biomaterials, while retaining their submicron particle sizes and high surface areas. β-rhenanite is a high solubility sodium calcium phosphate phase. Samples were characterized by XRD, FTIR, SEM, TEM, ICP-AES, TG, DTA, DSC, and surface area measurements.

(This work is published in *J Biomed Mater Res Part B* **80** (2007) 304–316)

5.1. Introduction

In orthopedic, oral and maxillofacial surgery, a variety of synthetic bone grafts have been used to fill skeletal defects originating from tumor resection, trauma, or infection.[1–3] Synthetic calcium phosphates, such as calcium hydroxyapatite [HA; $Ca_{10}(PO_4)_6(OH)_2$], β-tricalcium phosphate [β-TCP; β - $Ca_3(PO_4)_2$] and biphasic mixtures of these two have found use as bone substitutes.[4–6] HA or β-TCP implants exhibit relatively good tissue compatibility, and new bone is formed directly on the implants with no fibrous encapsulation.[7] However, sintered and well-crystallized HA ceramics usually demonstrated minimal *in vivo* resorption, with resorption times lagging the new bone formation rates.[8–12] Kilian et al. [13] showed that nonsintered HA could even be phagocytized and dissolved by macrophages and osteoclasts, while sintered ceramics were not degraded and remained at the site of implantation for years following the surgery. β-TCP, on the other hand, has a significantly high solubility[14,15] and typically fades away from the defect site even before the completion of new bone formation. An ideal skeletal repair implant should readily take part in the bone remodeling processes, and also allow for the direct anchorage by the bony tissues surrounding it (osteoconduction).[16] If the skeletal repair implant itself causes the *in situ* formation of the mineral part of the bone tissues (osteoinduction) rich in carbonated, apatitic calcium phosphates,[17] while it is continuously resorbing (*in vivo* osseointegration), this could be its most affirmative contribution to the defect site.[18–21] Therefore, efforts in the direction of developing calcium phosphate-based bone substitutes of higher *in vivo* resorbability and osteoinductive/osteoconductive capabilities are still needed.

In stark contrast to sintered HA ceramics,[10,11] calcium phosphate (CaP) self-setting cement formulations, which intentionally employed poorly-crystallized apatite as their major powder component, were shown[22–24] to have significant *in vivo* resorbability (i.e., with resorption rates in excess of 98% in 26 weeks following the implantation in the case of, for instance, α-BSM™, Etex, Cambridge, MA). These cements rapidly took part in the bone remodeling processes by going through phagocytosis under the action of macrophages and

osteoclasts.[22] Besides these special orthopedic cements, such high resorption rates with calcium phosphates have only been encountered when the tested (*in vivo*) materials comprised nanoapatites.[25]

Bone is a connective tissue with extracellular substance consisting of a carbonated, apatitic calcium phosphate nanosize mineral dispersed in what is essentially a hydrated collagen matrix. The mineral portion comprises two intimately mixed calcium phosphate phases; (i) noncrystalline or amorphous calcium phosphate and (ii) a poorly-crystallized apatitic calcium phosphate. In the formation of bone mineral, the amorphous phase is laid down first by the bone-depositing cells, i.e., osteoblasts, and subsequently a significant portion of this is then converted in the physiological environment to the carbonated, Na-, K-, and Mg-doped, Ca-deficient bioapatite during the *in vivo* maturation of bones.[26] The presence of the noncrystalline calcium phosphate phase in bones has been detected even by the very first electron microscope studies.[27] The earlier work of Posner and coworkers[28–35] set the foundation for the synthesis and characterization of amorphous or poorly-crystallized calcium phosphate powders. The cytoplasmic calcium phosphate mineral was found to have a structure built up of close-packed ion clusters of about 10 Å similar to those of $Ca_9(PO_4)_6$ present in synthetic amorphous calcium phosphates. Short-range order existed in these amorphous clusters (i.e., Posner clusters) but no long-range order was detected as crystalline hydroxyapatites have.[35] The work of Eanes and coworkers[36–43] and Rey and coworkers[24,44–52] on the preparation of poorly-crystallized calcium phosphates should also be cited in this context.

β-Rhenanite (β-$NaCaPO_4$) is an alkali calcium orthophosphate, which was recently shown to support cellular proliferation together with expression of osteogenic markers at a level higher than β-TCP,[53] and $NaCaPO_4$ was, therefore, suggested to possess a higher potency to enhance osteogenesis than β-TCP. Ramselaar and coworkers[54–57] were the first to investigate the biodegradation rate of $NaCaPO_4$ implants in direct comparison to HA and β-TCP from six weeks to three months *in vivo*. Knabe et al.[58] noted the remarkably high solubility (1.0 g per liter of H_2O at pH 7.54) of $NaCaPO_4$ samples in a comparative set of *in vitro*

rat bone marrow cell culture tests performed on a number of calcium phosphates. Suchanek et al.[59] discovered the formation of $NaCaPO_4$ interphase layers of high biocompatibility during the hot pressing of hydroxyapatite and bioactive glass powders together. Glass ceramics which contained $NaCaPO_4$ as the crystalline phase were also reported to be bioactive.[60–62]

On the other hand, "Rhenania process" is a well-known procedure mostly used in the fertilizer industry to obtain a soluble phosphate material.[63] In this process, the natural mineral of hydroxyapatite is mixed with Na_2CO_3 and SiO_2 whereas the molar ratio of Na_2CO_3/P_2O_5 fixed at 1.0. SiO_2 is added to prevent the occurrence of free CaO in the sintered product. These powder mixtures are then ground together and calcined in a rotary kiln at about 1000–1200°C for about few hours. Rhenanite, $NaCaPO_4$, of high solubility, has been the major phase in the final product of the Rhenania process.[63] As could be expected, $NaCaPO_4$ received such a high-temperature treatment has a rather low surface area, low surface reactivity, and larger powder particles.

Resorbable, granular bone graft substitutes based on NaCaPO4 formulations have already been commercialized and marketed for the orthopedic surgeons.[64,65] Self-setting cements based on $NaCaPO_4$ are also available for the repair of bone defects.[66] Nevertheless, the powders of such products have been produced by high-temperature (>1100°C) processes.[64]

The motivation for the present study stems from our interest in developing a robust synthesis route for the manufacture of biphasic nanopowders of $NaCaPO_4$ and carbonated, apatitic calcium phosphate using temperatures less than 700°C. Specifically, the apatitic calcium phosphate powders are known to lose their carbonate ions when and if a temperature higher than 700°C was used.[67] The soluble component of these biphasic mixtures (i.e., $NaCaPO_4$), under the *in vivo* action of osteoclasts, is assumed to supply Ca^{2+} ions, as well as hydrogenated phosphate ions, to the surrounding tissues upon implantation. Such materials can, therefore, be expected to act like an osteoinductive stimulant in the body.

Therefore, our experimental approach to that end was framed around the following straightforward supposition: "amorphous or poorly-crystallized calcium

phosphate powders are known to consist of nanoparticles of apatitic calcium phosphates,[24] and if those powders were synthesized at the physiological pH in the presence of a rather significant amount of Na^+ ions, then upon calcining those powders over the temperature range of 300–600°C, the resultant material should be a biphasic powder mixture of $NaCaPO_4$ and apatitic calcium phosphate with a high surface area." This work, to the best of the knowledge of authors, reports for the first time the aqueous preparation of nanosize calcium phosphate precursor powders, which are able to readily transform into biphasic powder mixtures of β-$NaCaPO_4$ and carbonated hydroxyapatite upon low-temperature calcination.

5.2. Experimental Procedure

5.2.1 ***Synthesis of Calcium Phosphate Powder Samples.*** The synthesis method used to form the Na-containing poorly-crystallized apatitic calcium phosphate powders simply consisted of preparing two solutions, and the procedure adapted here was inspired by the work of Lee et al.[68] Solution-A was prepared as follows; 86.4 g Na_2HPO_4 (disodium hydrogen phosphate, >99%, Fisher Scientific, Fairlawn, NJ) was dissolved in 1.2 L of deionized water, followed by the addition of 60.0 g $NaHCO_3$ (sodium hydrogen carbonate or sodium bicarbonate, >99%, Fisher), which resulted in a clear solution with a pH of about 9 at RT (22 ± 1°C). Solution-B was prepared by dissolving 70.0 g of $Ca(NO_3)_2.4H_2O$ (calcium nitrate tetrahydrate, >99%, Fisher) in 500 mL of deionized water. Solution-B was then rapidly added into solution-A under constant stirring (at 250 rpm, with a 5 cm long, Tefloncoated magnetic fish) at room temperature. The pH of the resultant milky suspension (with a nominal Ca/P molar ratio of 0.49) was then rapidly raised to around 7.4, i.e., the physiological pH value, by adding 3 – 5 mL of concentrated NaOH solution. The solids were immediately filtered by using a filter paper (No. 42, Whatman International, Maidstone, UK) placed in a vacuum-suction porcelain Buechner funnel assembly, and washed with 4 L of deionized water. Upon filtering and washing the precipitates in the funnel one obtains a gel-like calcium phosphate precipitate body (i.e., CaP gel). Some portion of the recovered gels was placed in a glass Petri dish and dried at 37°C for 72 h in static

air in a drying oven, while the remainder of the sample was first frozen at -80°C for 2 h, and then lyophilized in a vacuum chamber (Freezone® 4.5, Labconco, Kansas City, MO) kept at 5 x 10^{-2} mbar at RT overnight. The above-mentioned synthesis recipe has been repeated six times, and the reproducibility in the composition of precursor powders was checked by consecutive triplicate chemical analyses.

To test the influence of solution pH on the phase composition of the resultant precipitates, in a number of experiments the pH of Solution-A was first decreased to 4.2 at room temperature, under vigorous stirring, by slowly adding aliquots of concentrated HNO_3 (69.2%, Fisher Scientific, Fair Lawn, NJ). The pH value of Solution-B was also reduced to 4.2 by adding HNO_3, followed by adding Solution-B into Solution-A rapidly, as described above. The precipitates were then immediately filtered out of the mother liquor in a fashion similar to that mentioned above.

CaP powders obtained at pH 7.4 placed in clean aluminum oxide crucibles or boats were calcined in a static air atmosphere in an electrically-heated muffle furnace (5°C/min heating and cooling rates) over the temperature range of 300–600°C, with 6 h of soak time at the peak temperatures. Calcined samples were lightly ground (only for few minutes) in an agate mortar by using an agate pestle. To test the sinterability of these rhenanite–HA biphasic samples, we have uniaxially pressed (5000 kg/cm^2) eight pellets (each 1.5 mm thick) out of the 600°C-calcined biphasic powders. These pellets were then separately heated in an electrical resistance, chamber furnace to 1000°C at the rate of 5°C/min, held at that temperature for 6 h, and then cooled back to room temperature within the furnace either at the rate of 5°C/min or 1°C/min.

5.2.2 ***Powder Characterization*.** Samples were characterized, at all stages, by powder X-ray diffraction (XRD Model XDS 2000, Scintag, Sunnyvale, CA), scanning electron microscopy (SEM, Model S-4700, Hitachi, Tokyo, Japan), transmission electron microscopy (TEM, Model HD200, Hitachi), Fourier-transform infrared spectroscopy (FTIR, Model Nicolet 550, Thermo-Nicolet, Woburn, MA), inductively-coupled plasma atomic emission spectroscopy (ICP-

AES, Model 61E, Thermo Jarrell Ash, Woburn, MA), thermogravimetry (TG/DTA, Model 851e, Mettler-Toledo, Columbus, OH) and differential scanning calorimetry (DSC, Model SDT 2960, TA Instruments, New Castle, DE) analyses, and surface area measurements (Model ASAP 2020, Micromeritics, Norcross, GA).

Powder samples for XRD analyses were first ground in an agate mortar using an agate pestle and then sprinkled onto ethanol-damped single crystal quartz sample holders as a thin and flat layer, followed by tapping to remove the excess of powder. The X-ray diffractometer was operated at 40 kV and 30 mA with monochromated Cu Kα radiation. XRD data were collected in the step mode over the 2θ range of 3°–50°, with a scanning speed corresponding to 0.01° per minute. FTIR samples were first ground in a mortar, in a manner similar to that used in the preparation of XRD samples, and then placed onto the diamond ATR holder of the FTIR spectrometer. This spectrometer was equipped with an Endurance Foundation Series single-bounce diamond ATR (50° incidence angle), and 32 scans were performed at a resolution of 4 cm^{-1}. Powder samples examined with the scanning electron microscope (SEM) were sputter-coated with a thin Pt layer, just prior to imaging, to improve the conductivity of samples. For the transmission electron microscope (TEM) investigations, small aliquots of respective powder samples were first dispersed in pure ethanol, and then few drops of those suspensions were dried on the sample holder grids. The BET surface area of powder samples was determined by applying the standard Brunnauer–Emmet–Teller method to the nitrogen adsorption isotherm obtained at -196°C using the Micromeritics ASAP 2020 instrument. Powder samples used in the ICP-AES analyses were first dissolved in nitric acid prior to measurements. For carbon analyses, 200 mg of powder samples was combusted at around 1200°C in oxygen atmosphere by using a C analyzer (Model Vario Macro, Elementar, Mt. Laurel, NJ). In this process, carbonaceous moieties were converted into CO_2, and after catalytic post-oxidation, drying, and cleaning of carrier gas, all carbon oxides are reduced to molecular carbon over a reducing agent and transported by the carrier gas to the thermoconductivity cell for the final quantitative determination of

carbon content. Carbon content was then reported by the computer of the instrument as wt % C present in the samples. We converted the measured C contents into CO_3 percentages. Thermogravimetric analyses (TGA) of the CaP gel (or powder) samples were performed in Pt crucibles in a static air atmosphere with a heating rate of 5°C/min from RT to 800°C. Water content of the precursor powders were directly deduced from the TGA traces. DTA and DSC runs were also performed in Pt crucibles in flowing air atmosphere with a heating rate of 5°C/min, and Al_2O_3 powder was used as the reference sample in these experiments.

5.3 Results and Discussion

The synthesis procedure described in Synthesis of Calcium Phosphate Powder Samples was able to produce apatitic calcium phosphate powders when the synthesis solution pH was maintained at 7.4. The results and data given below are all for pH 7.4 samples, unless otherwise noted. XRD data for 37°C- and freeze-dried CaP gels were given in the comparative chart of Figure 5.1a. Both traces were characteristic of poorly-crystallized CaP powders,[24,46–52] although drying at 37°C seemed to cause a slight increase in the overall crystallinity with respect to freeze drying. In freeze drying, the water initially present was gradually sublimed, whereas in 37°C drying that water present at the end of the washing step helped the crystallization to proceed at a low rate. Freeze-dried powders were found to be fluffier with respect to those dried at 37°C, therefore, after the preliminary experiments all of the powders obtained by aqueous synthesis procedure were freeze-dried. Surface area measurements also confirmed this observation, and the BET surface area of freeze-dried powders was 128 ± 5, whereas that of the powders dried at 37°C for 72 h was 62 ± 3 m^2/g.

Adult human bones yield XRD data very similar to those given in Figure 5.1a.[69,70] If the syntheses were to be carried out under refrigeration, e.g., at around 4°C, the XRD charts obtained would consist of, more or less, X-ray amorphous traces.[68] The hydrated nature of CaP gel samples dried at 37°C were also confirmed by the wide water bands displayed in their FTIR spectra given in

Figure 5.1b. On the other hand, in the FTIR spectra of freeze-dried samples, the intensities of those water bands have been significantly reduced (Fig. 5.1b). Therefore, drying at 37°C did not completely eliminate the water present in those precipitated precursor gels. The symmetric and antisymmetric stretching of the PO_4^{-3} group were observed at 1097, 1043, 964, 604, and 565 cm^{-1}. Bands of CO_3^{2-} ions were observed at 1470–1420 and 875 cm^{-1}. The very weak IR band at around 919 cm^{-1} and again the weak shoulder at around 1297–1310 cm^{-1} were attributed to the smaller presence of HPO_4^{2-} ions.[71] HPO_4^{2-} ions do also have a band at 874 cm^{-1}, which partially overlaps with that of CO_3^{2-} ions rendering the distinction between HPO_4^{2-} and CO_3^{2-} ions more difficult. In contrast to our findings, Wu et al.[45] previously noted that unique HPO_4^{2-} group present in the human bone mineral was not seen in synthetic CaP samples produced under conditions similar to those of this study. The synthesis procedure adopted and used in this study was, therefore, able to produce a hydrated and carbonated CaP gel precursors, which contained a trace amount of protonated orthophosphate ions similar to the human fetal bones (Fig. 5.1b). The ICP-AES and C analyses results are given in Table 5.1. Analyses were performed in triplicate on all the samples. Freeze-dried CaP gel precursors gave the following medians: Ca: 21.27 ± 0.02%; P: 13.27 ± 0.01% and Na: 9.10 ± 0.01 wt %, which corresponded to a molar Ca/P ratio of 1.239 (Table 5.1), and a molar (Na+Ca)/P ratio of 2.163 in these powders. It is not so surprising that even if one started with a nominal precipitation solution Ca/P molar ratio of around 0.5, the precipitates formed at or near the physiological pH would still be Ca-deficient apatitic CaP. C analyses proved that the precursor powders were carbonated, and the carbonate content decreased with an increase in the calcinations temperature, while the Ca/P molar ratio and the Na content remained almost the same.

When the pH values of the same precipitation solutions were fixed at around 4.2, then the formed powders only consisted of the brushite phase (DCPD, $CaHPO_4.2H_2O$), whose XRD and FTIR data are not shown here to save space. The size and shape of those brushite crystals were also perfectly the same as mentioned elsewhere.[72] The SEM morphology of the freeze-dried powders was

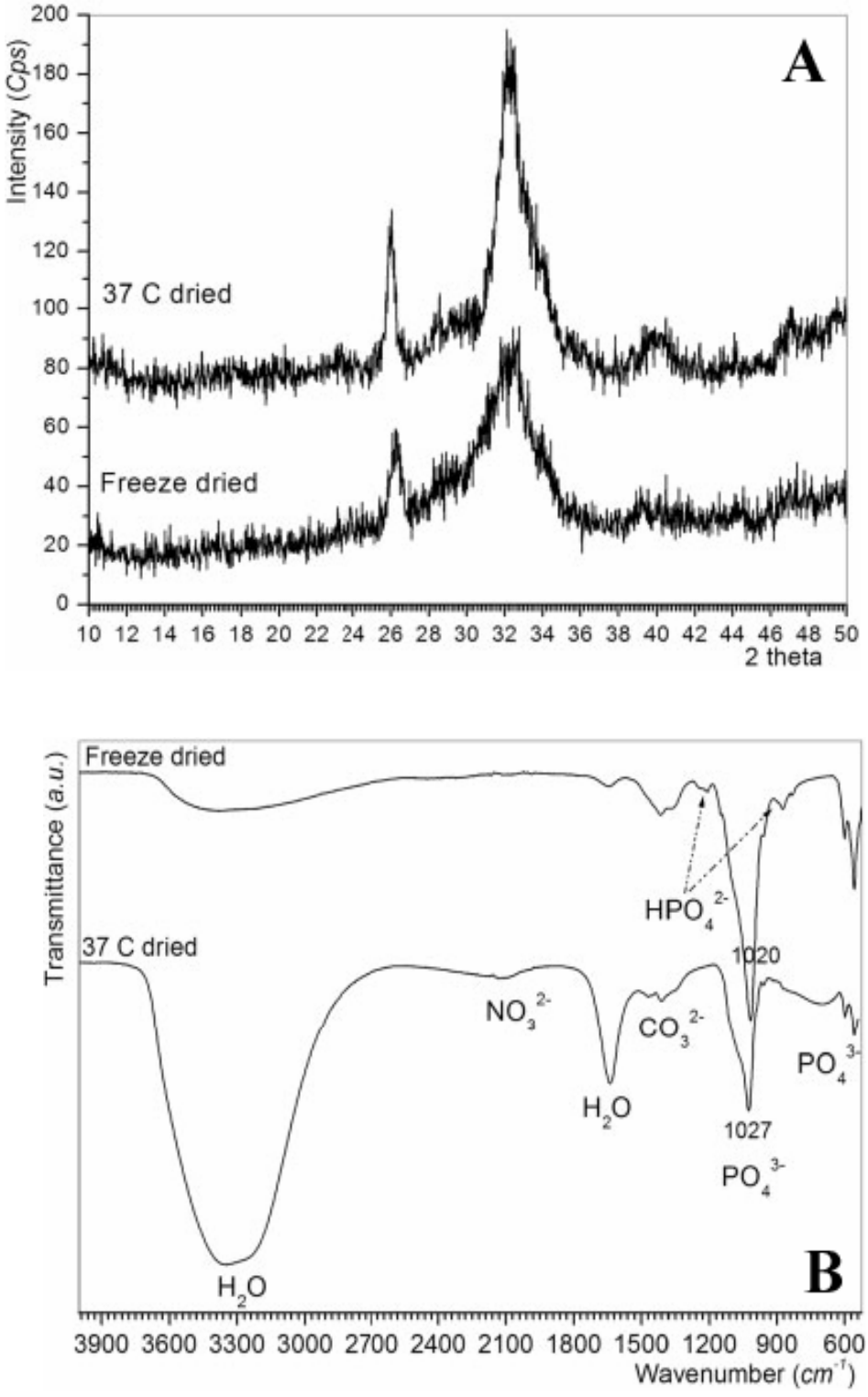

Fig. 5.1 (a) XRD traces and (b) FTIR traces of 37°C-heated and freeze-dried CaP gel precursors

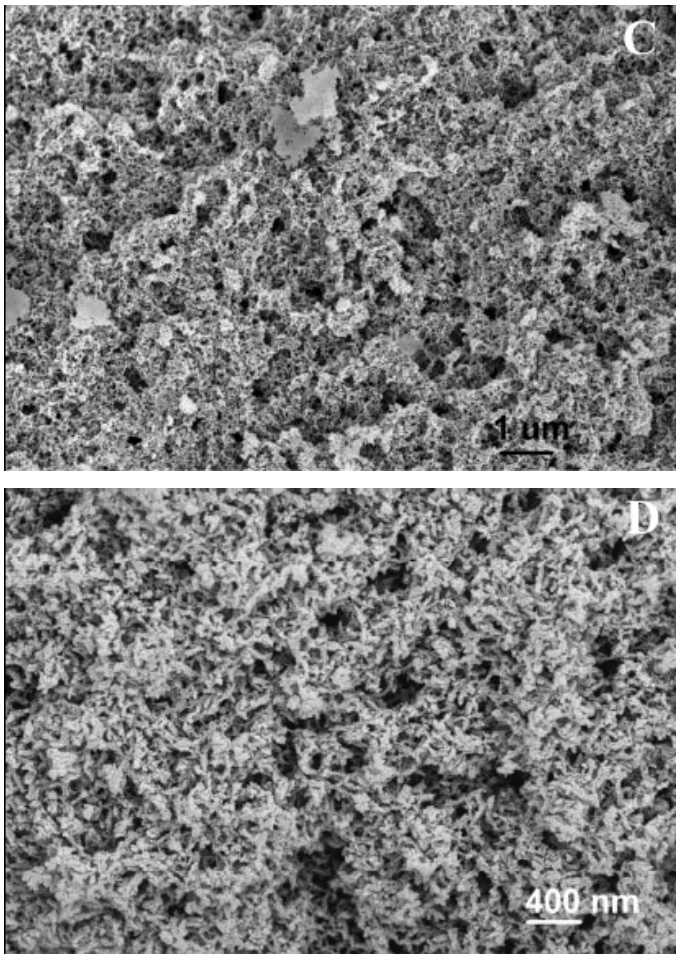

Fig. 5.1 (c) & (d) SEM micrographs of freeze-dried CaP gel precursors at two different magnifications

Table 5.1 Results of ICP-AES and C Analyses (in wt %, average of 3 runs)

	Sample					
	Ca	**P**	**Ca/P (molar)**	**Na**	**C**	**CO_3**
Freeze-dried	21.27	13.27	1.239	9.10	0.82	4.10
300°C	28.93	17.99	1.243	8.98	0.58	2.90
400°C	28.49	18.06	1.219	9.02	0.39	1.95
500°C	28.36	17.88	1.226	9.35	0.32	1.60
600°C	29.17	18.30	1.232	9.16	0.21	1.05
1000°C	28.64	18.04	1.227	9.09	0.01	0.05

shown, at two different magnifications, in Figures 5.1c and d. The bright-field TEM photomicrographs given in Figures 5.2a and b depicted the nanostructure of the same powders. It should be noted that the selected-area electron diffraction inset of Figure 5.2b proved the nanocrystalline nature of those powders. TG/DTA/DSC analyses of the freeze-dried CaP precursors (Fig. 5.2c) indicated that upon heating to 155–160°C the samples first lost around 7.5% of their initial weight. This corresponded to the adsorbed water. Therefore, the water content of the precursor powders was deduced to be around 7 to 7.5%. With continued heating to 415°C, another gradual weight loss of about 2.5% was observed, and this was probably due to the volatilization of the remnants of nitrate ions. Characteristic IR bands for nitrate ions were to be found at 1440–1300 and 1070–1030 cm^{-1},[73] but in the IR spectra of Figure 5.1b it was quite difficult to identify those nitrate bands because of severe overlapping with the phosphate and carbonate bands over the same range. However, the weak bands at around 2200–2030 cm^{-1} in Figure 5.1b can be ascribed to the nitrates.[74] Further heating at above 415°C, up to 650°C, displayed the removal of carbonate ions that was accompanied with a weight decrease of around 5 wt %, bringing up the total weight loss to 15%. The temperature when one reached constant weight was 640°C (Fig. 5.2c).

β-Rhenanite, i.e., β-$NaCaPO_4$, phase in these gel precursors started to crystallize upon low-temperature calcination of the samples over the temperature range of 300–600°C. Especially, the DSC spectrum given in Figure 5.2c showed that there were two exothermic events taking place over the temperature range of 440–570°C. The starting points of these exothermic events were indicated with arrows in Figure 5.2c. It should be noted that DSC is a dynamic process taking place at a heating rate of 5°C/min, and under isothermal heatings the starting points of those exothermic events would be slightly lower than those indicated by the TG/DTA/DSC spectra. XRD spectra of Figure 5.3a showed the crystallization of $NaCaPO_4$ in a matrix of apatitic calcium phosphate. β-$NaCaPO_4$ (sometimes it may also be written as $CaNaPO_4$) has an orthorhombic (space group Pnam62) unit cell with the lattice parameters of a = 6.797, b = 9.165, and c =

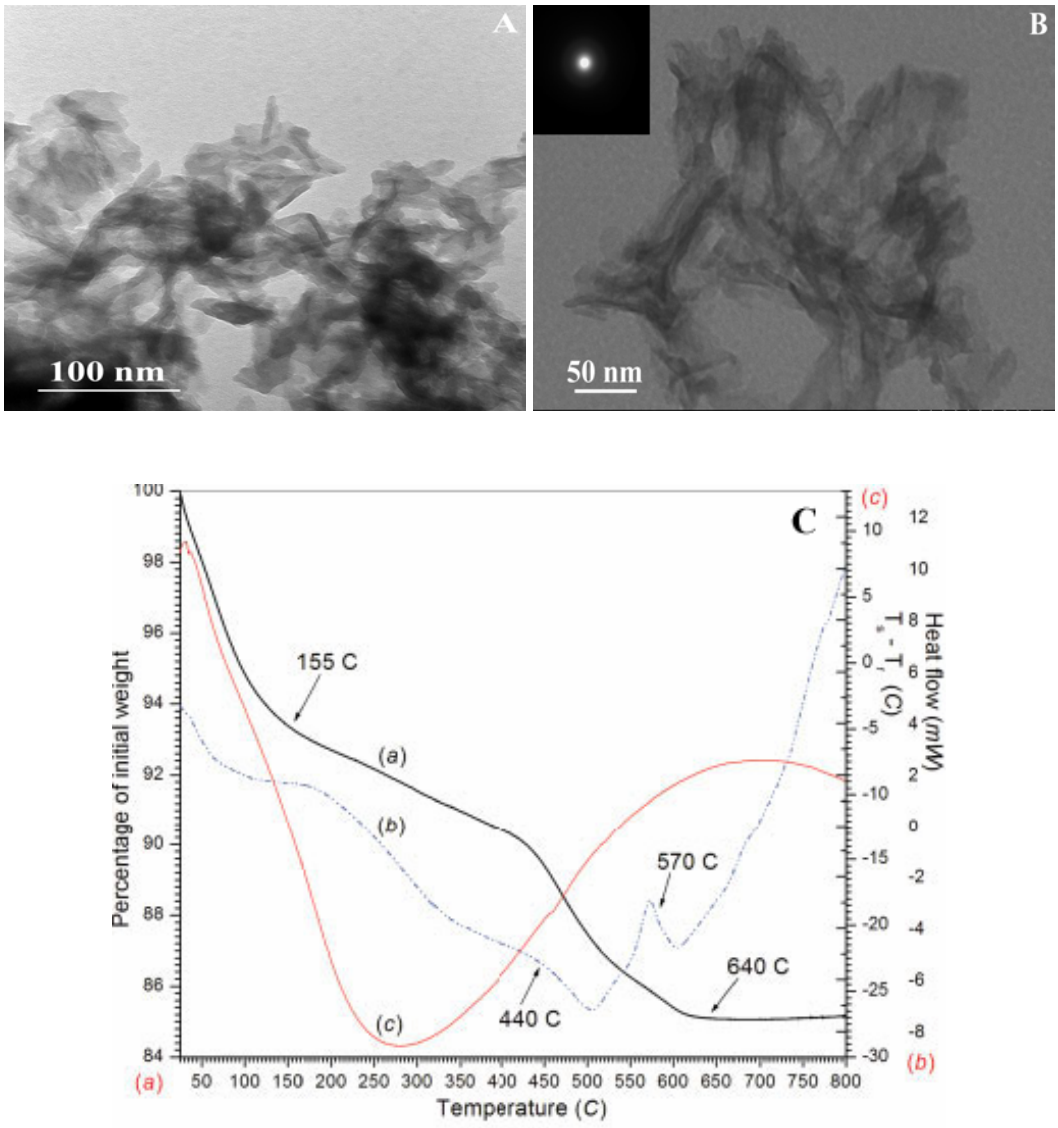

Fig. 5.2 (a) & (b) TEM micrographs of freeze-dried CaP gel precursors and (c) shows TG/DTA/DSC spectra of freeze-dried CaP gel precursors - *(a)* TG, *(b)* DSC, and *(c)* DTA spectra.

5.406 Å.[75] This phase (which will transform into α-$NaCaPO_4$ at 650°C) is also isostructural with β-K_2SO_4. The most straightforward way of synthesizing phase-pure $NaCaPO_4$ powders can be the solid state reactive firing of the powder mixtures (in a 1:2:2 molar ratio) of Na_2CO_3, $CaCO_3$, and $(NH_4)_2HPO_4$ at 900–950°C.[75] However, such a synthesis route (which involves the formation of liquid phases upon melting of first $(NH_4)_2HPO_4$ and then Na_2CO_3) will not be able to yield nanosize, therefore, high surface area and high surface reactivity powders.[76] The peaks denoted by * (and their respective *hkl* reflections) were those of β-$NaCaPO_4$, and the 2θ positions of such peaks were in close agreement with those given in ICDD PDF 29–1193. Upon heating at 600°C, CaP gel precursors of this study crystallized about 40 ± 3% β-$NaCaPO_4$. This value was calculated from the data of Figure 5.3a by using the relative intensity ratio of the most intense peak of hydroxyapatite (at 31.78° 2θ) to that of $NaCaPO_4$ (at 32.59° 2θ). The samples heated at 600°C for 6 h can therefore be named as 40% $NaCaPO_4$–60% HA biphasic biomaterials.

FTIR traces of the same calcined samples were depicted in Figure 5.3b. CaP precursors calcined even at the low temperature of 300°C were able to exhibit the characteristic OH^- stretching vibration at 3572 cm^{-1}, and this band became more pronounced with the increase in calcination temperature at or above 500°C. The OH^- bending vibration was also recorded at 634 cm^{-1}.[77] These bands proved that the freeze-dried apatitic calcium phosphate phase (which lacked the OH vibrations) present in the gel precursors completely converted into hydroxyapatite upon calcination. Precipitated apatitic calcium phosphate precursors need the humidity in the calcination atmosphere to transform into Ca–hydroxyapatite upon heating.[78–82] The relative humidity in our laboratories was at around 65–70% during those calcination runs. Characteristic FTIR spectrum of pure β-$NaCaPO_4$ was previously given by Driessens et al.[55] The orthophosphate stretching bands for the 500°C-calcined samples were observed at 603 (ν_4), 962 (ν_1), 1020, and 1089 (ν_3) cm^{-1}, which were contributed both by crystalline β-rhenanite and apatitic calcium phosphate.[77] The absence of the P─O─P

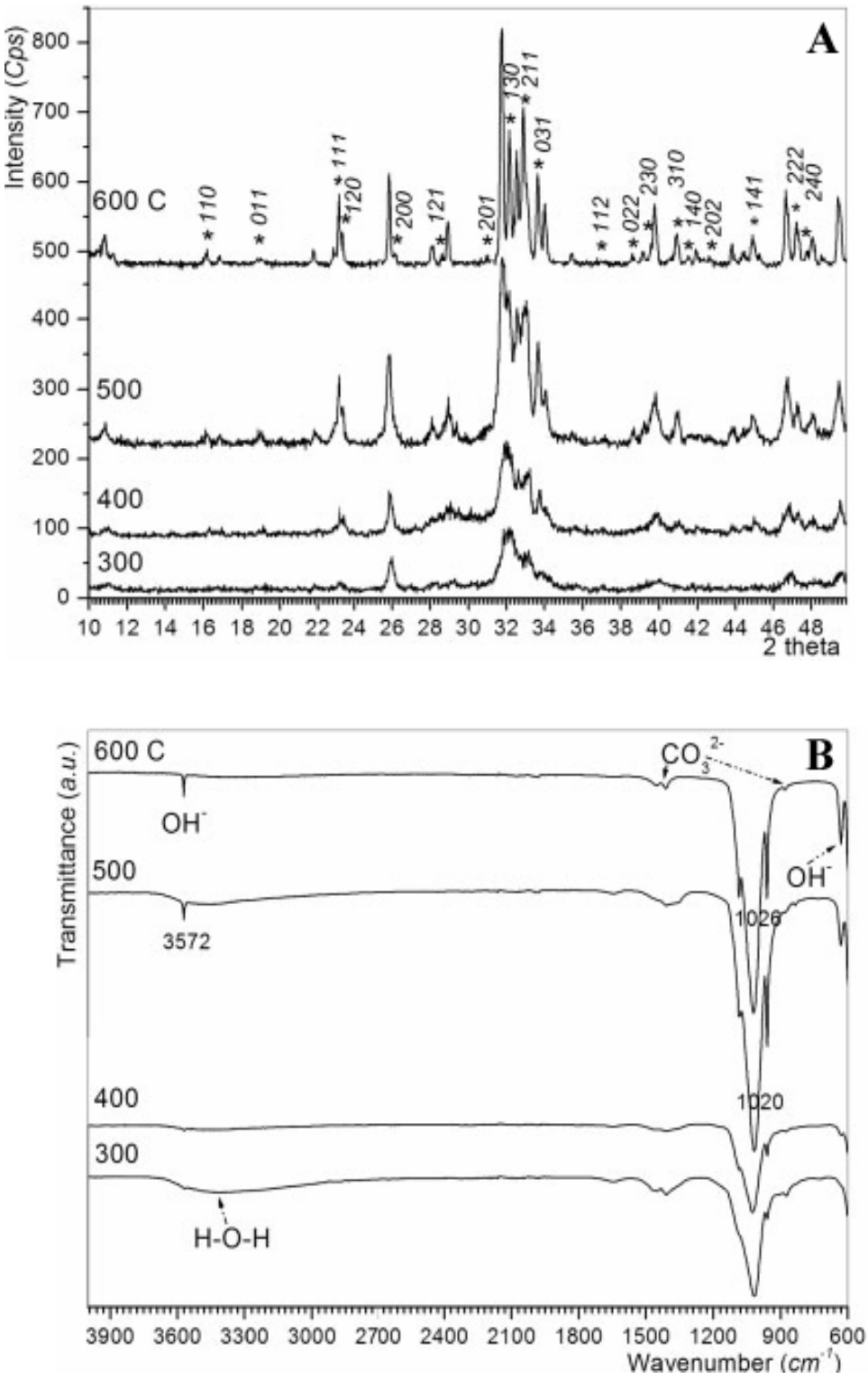

Fig. 5.3 (a) XRD spectra of CaP gel precursors heated in air from 300°C to 600°C (* and the respective *hkl* indices denote the reflections of β-NaCaPO4, all the other peaks belong to HA); (b) FTIR traces of CaP gel precursors heated in air for 6 h from 300°C to 600°C

vibrational mode of pyrophosphates at 740 cm^{-1} (Fig. 5.3b) proved that the calcined samples did not contain any traces of $Ca_2P_2O_7$.[77] If the amount of HPO_4^{2-} ions in the precursor powders were significant, then their conversion into pyrophosphate would have been inevitable through the reaction $2HPO_4^{2-} \rightarrow 3P_2O_7^{4-} + H_2O$, which takes place at 600°C.[31] Moreover, Loong et al.[83] definitively demonstrated the lack or significant deficiency of OH^- ions occupying crystallographic sites in the Ca-deficient, non-stoichiometric apatitic crystals of rat and bovine bones by using inelastic neutron-scattering spectroscopy.

It is known that an IR band at 1020 cm^{-1} can be attributed to the v_3 vibration of PO_4^{3-} in non-stoichiometric or Ca-deficient and/or carbonated apatitic calcium phosphates; however, a band recorded at 1030 cm^{-1} is pinpointing to the v_3 vibration of PO_4^{3-} in stoichiometric hydroxyapatite.[84] Therefore, the relative ratios of 1020/1030 bands in the FTIR spectra could provide a measure of mineral crystallinity and maturity in bone minerals or apatitic-looking calcium phosphates.[77,85] While the samples calcined at 300°C or 500°C were displaying that orthophosphate v_3 vibration at 1020 cm^{-1}, the same vibration was found to shift to 1026 cm^{-1} in the 600°C-calcined sample (Fig. 5.3b). This can be ascribed to the transition from non-stoichiometric to stoichiometric apatite together with the crystallization of β-$NaCaPO_4$ phase. On the other hand, it is interesting to note here that for the gel precursor samples dried at 37°C the same v_3 vibration was recorded at 1027 cm^{-1}, whereas the freeze-dried samples had it at 1020 cm^{-1}, as shown in the IR traces of Figure 5.1b. This means that drying those gel precursors at 37°C for 72 h may have a positive effect on the progress of crystallization or so-called "maturation."

Variations in the grain size and morphology of the rhenanite-hydroxyapatite biphasic powders, as a function of increasing calcination temperature, were monitored by the SEM micrographs given in Figure 5.4. The cracked-like grain/particle surfaces seen especially in the high magnification micrographs of Figure 5.4 are the artifacts created by the Pt-coating layer. Grain sizes directly measured from the SEM micrographs, as well as the respective surface areas of these powders, is given in Table 5.2.

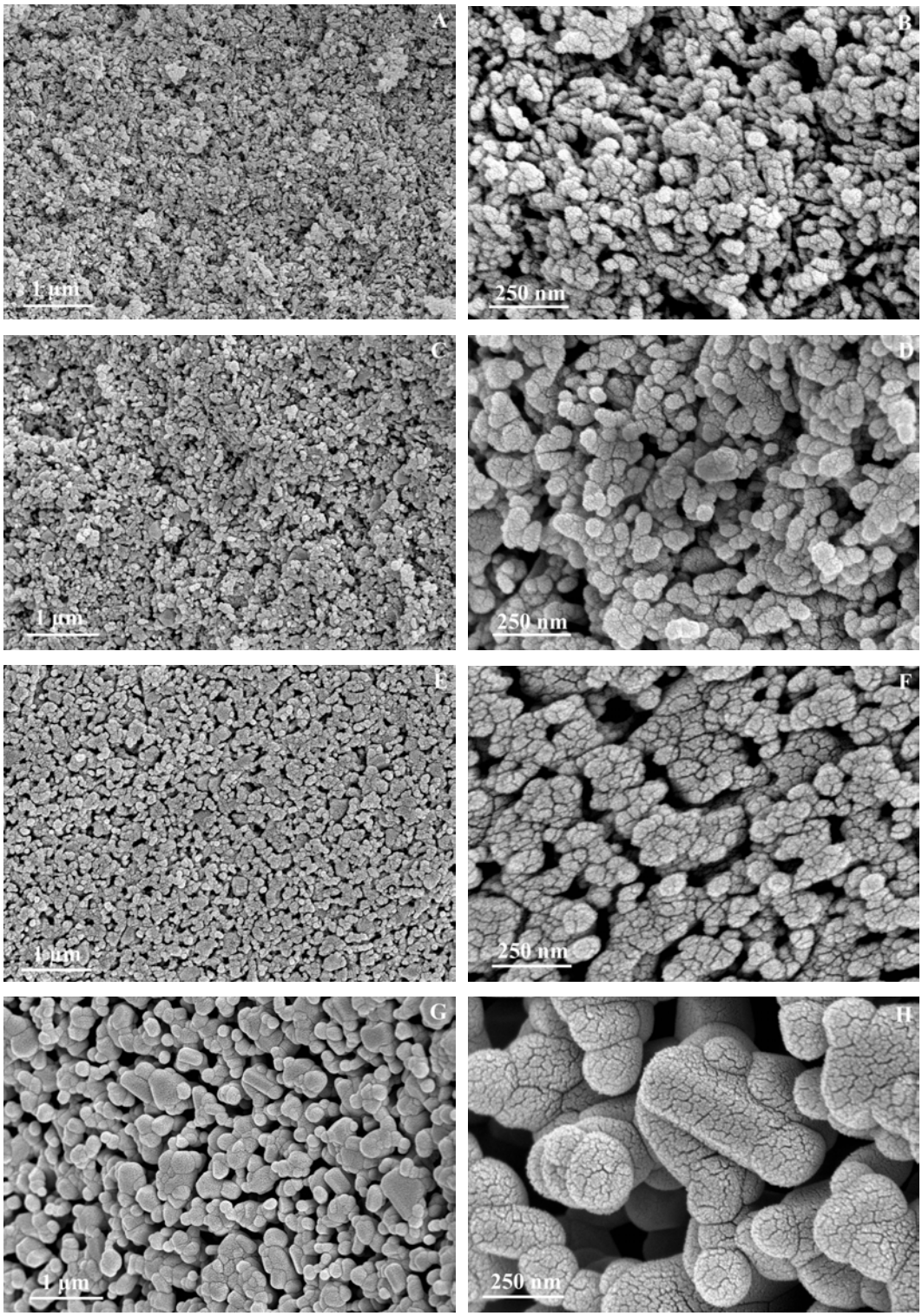

Fig. 5.4 SEM morphology of freeze-dried CaP gel precursors heated: (a) & (b) at 300°C; (c) & (d) at 400°C; (e) & (f) at 500°C; and (g) & (h) at 600°C (two different magnifications are reported)

Table 5.2 Grain Sizes and Surface Areas of Powders

Sample	Grain Size (nm)	Surface area (m^2/g)
Freeze-dried	45 ± 10	128 ± 5
300°C	60 ± 10	79 ± 4
400°C	100 ± 10	70 ± 5
500°C	150 ± 10	53 ± 3
600°C	300 ± 70	34 ± 3

Even after light calcination at temperatures from 300 to 600°C, these materials retained their initially small grain sizes still in the nano- or submicron-range. These surface area data were quite comparable to those reported by Somrani et al.[51] in a study on the thermal evolution of poorly-crystalline apatitic calcium phosphate powders produced by using Ca-nitrate tetrahydrate and diammonium hydrogen phosphate as the starting water soluble reagents, in the absence of any Na ions in their precipitation solutions. Apatitic calcium phosphate samples of Somrani et al.[51] decomposed into crystalline tricalcium phosphate upon calcination. Freeze-dried samples of the current study consisted of (as shown in the micrographs of Figs. 5.1 and 5.2) particles (or moieties) having a needlelike morphology with average dimensions of 10 (thickness) and 70 (length) nanometer. These are very well within the size range of bone apatite crystals, which were documented by using electron microscopy for more than 5 decades ago.[27,86] Johansen and Parks[87] reported that bone apatite crystallites were platelike in shape with dimensions 400 x 200–350 x 25–50 Å. Upon calcination of the samples of this study, those initially plate- or needle-like, longitudinal moeities present in the freeze-dried powders (Figs. 5.1 and 5.2) tended to form more or less equiaxed or globular grains (Fig. 5.4). Such a tendency of nanosize globule formation upon heating can also be taken as a sign of those moieties (Fig. 5.2) actually being comprised of very much smaller particles. Indeed, early studies by

Molnar[88,89] suggested that bone crystals are composed of chains of microcrystals fused in an end-to-end relationship. An X-ray diffraction study by Posner et al.[90] reported that the largest dimension of the bone apatite crystals was about 100 Å, and those apatitic crystallites should be regarded as a mosaic of microcrystals rather than as a continuously uniform, single crystal.[31] The sodium-doped calcium phosphate gel precursors of this study [enthused by the work of Refs. 24, 48, 68] consisted of poorly-crystallized apatitic microcrystals very similar in dimensions and appearance to those of bone mineral.

Nakahira et al.,[91] in a study of testing the applied magnetic field on the bioactivity of hydroxyapatite, reported the formation of $NaCaPO_4$ as a second phase in 10% $NaHCO_3$- mixed hydroxyapatite bioceramic samples upon sintering those at 1000°C. These authors blended the hydroxyapatite and $NaHCO_3$ (at 10% level) powders by using a conventional ball-mill, followed by compaction, cold isostatic pressing, and sintering. Nakahira et al.[91] also tested the bioactivity of those 1000°C-sintered samples by soaking them, at 37°C, in SBF (simulated/synthetic body fluid[92,93]) solutions from 4 to 7 days. It is quite interesting to note here that, under the identical SBF soaking conditions, according to Nakahira et al.,[91] while the pure hydroxyapatite samples (with no magnetic field application) were not showing any bonelike CaP deposits on their surfaces, $NaCaPO_4$-containing samples were covered with a high abundance of such deposits. This was again attributed to the higher bioactivity of $NaCaPO_4$ phase than that of pure hydroxyapatite.[91,94] Although we did not include an SBF-soaking study in this manuscript, the strong evidence brought upon by the work of Nakahira et al.[91] was considered to be sufficient to ascertain the bioactivity (in SBF solutions) of such $NaCaPO_4$-containing hydroxyapatite bioceramics. Moreover, the presence of Na ions that weaken the bond between Ca^{2+} and PO_4^{3-} in the crystal surface accounts for the high dissolution rate of β-$NaCaPO_4$. If the surface of a bioceramic sample inserted in an SBF solution exhibits such a significant ionic level dissolution phenomenon, then the Ca^{2+} and HPO_4^{2-} ions to be abundant on these surfaces will further trigger the aggregation, and the consequent surface segregation, of Posner's clusters found in those solutions.[95]

The $NaCaPO_4$–HA biphasic powders of this study sintered well even after heating them at the low temperature of 1000°C for 6 h in air as pressed pellets. The SEM photomicrographs given in Figure 5.5a and 5b (insets showed a higher magnification view) depicted the surface of the well-densified pellets heated at 1000°C for 6 hours after cooling at the rate of 5°C/min and 1°C/min, respectively. It is interesting to note that even the chemically synthesized, submicron HA-TCP biphasic powders do not show a densification rate (even after heating those at 1200°C) as high as the samples of this study.[96] Cooling rate was found to have a pronounced effect on the $NaCaPO_4$–HA biphasic samples though. Samples cooled at the rate of 5°C/min (Fig. 5.5a) showed a larger number of both inter- and intra-granular cracks, when the cooling rate was decreased to 1°C/min (Fig. 5.5b) those cracks were reduced. The mismatch between the coefficients of thermal expansion of $NaCaPO_4$ and HA phases might be responsible for the formation of those cracks. Pellets sintered at 1000°C still had the same biphasic nature (i.e., 60% HA - 40% $NaCaPO_4$) and their XRD spectra were in strong resemblance to those given in Figure 5.3a for the 600°C-calcined powder sample. Sintering the biphasic samples at 1000°C for 6 hours did not destroy the original phase constitution. However, as expected, the FTIR spectra of the 1000°C-sintered pellets did not exhibit the carbonate bands. Carbonate ions in apatitic calcium phosphate structures cannot easily persist at temperatures greater than 700–750°C. Nevertheless, a more detailed study of the sintering behavior of these biphasic powders, with the aim of forming dense, carbonate ion-free ceramics of low surface area, over the temperature range of >1000–1300°C was out of the scope of this study.

β-$NaCaPO_4$ phase was recently reported by El-Ghannam[61] to form upon the calcination (180–800°C) of a new class of SiO_2–$CaHPO_4.2H_2O$ physically-mixed powder blends initially wetted by rather concentrated NaOH solutions. *In vivo* studies performed by El-Ghannam[61] found that these materials were superior to Bioglass® in terms of protein absorption, enhancement of bone generation, and overall resorption. Gong et al.[60] reported that crystalline β-rhenanite in contact

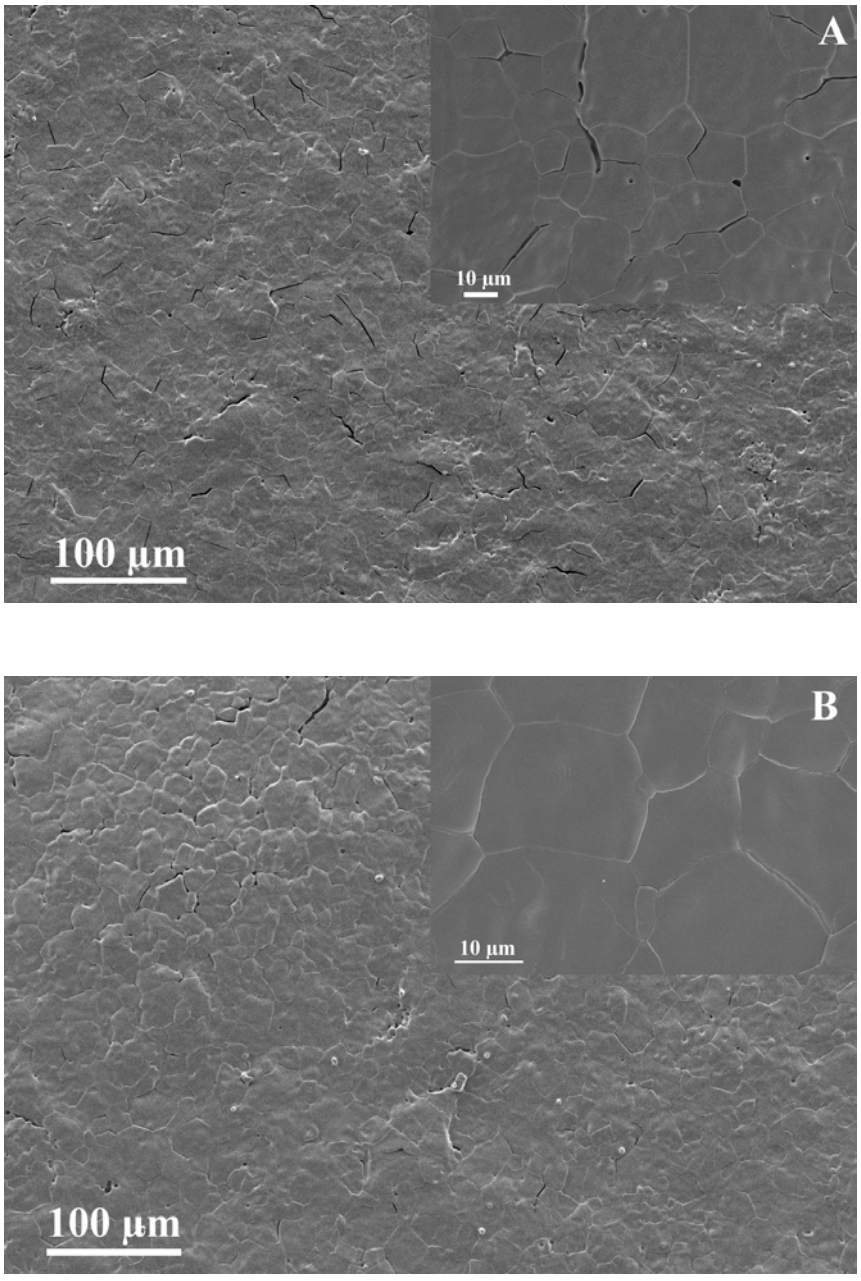

Fig. 5.5 600°C-calcined biphasic powders sintered at 1000°C for 6 h and cooled at the rate of (a) 5°C/min and (b) 1°C/min

with SBF solutions may act as a nucleation precursor for the formation of apatitic calcium phosphates with respect to the following reaction:

$$3NaCaPO_4 + 2Ca^{2+} + H_2O \rightarrow 3Ca_5(PO_4)_3OH + 3Na^+ + H^+ \quad (1)$$

Kangasniemi et al.[97] prepared _-rhenanite powders by sintering stoichiometric mixtures of $CaHPO_4$ and Na_2CO_3 at 1300°C, followed by sieving the ground sintered chunks to a size below 45 μm, and used those later as crystalline additives (from 20 to 30 wt %) in their experimental bioactive glass compositions. The same authors were then reported in a separate study[98] the dissolution behavior of crystalline β-rhenanite- or crystalline HA-containing bioactive glasses soaked in SBF from 5 h to 6 days. Kangasniemi et al.[98] concluded that the β-rhenanite-containing composites had a very positive effect on the rate of apatitic CaP layer formation on the surfaces of samples soaked in SBF.

The earlier but quite comprehensive work of Ramselaar et al.[54–56] should be taken as a good reference for the strong potential of β-rhenanite in developing resorbable or osteoinductive calcium phosphate bioceramics. The *in vivo* canine studies performed by Ramselaar et al.[56] demonstrated that statistically more bone deposition occurred on β-rhenanite particles than on hydroxyapatite particles.

This study showed that by simple calcination of a poorlycrystallized, Na-containing calcium phosphate gel precursor synthesized at the physiological pH it will be possible to form biphasic biomaterials consisting of a high solubility β-$NaCaPO_4$ and less soluble nanosize hydroxyapatite. Since the starting material is a gel precursor, it can be easily shaped (for instance, by extrusion, injection molding or solid freeform fabrication techniques) into any desired three-dimensional form before the full crystallization of the phases to take place during the final calcination step. The initial viscosity of such gels can be readily adjusted prior to the form fabrication. We have also observed that these gels can even be stored in ordinary zip-lock, air-tight nylon bags for more than a year (under refrigeration at 4°C), without resulting in any detectable changes in their XRD

and FTIR patterns. Moreover, leachable porogen phases or particulates (such as, NaCl, ammonium carbonate, ammonium acetate, ice crystals, etc.) may also be incorporated into these gels for forming porous bodies at the end of the fabrication processes. The only delicate step in the use of such preformed gels for forming 3D shapes would be the careful drying in a relative humidity controlled environment that should avoid the formation of drying cracks due to the rapid removal of entrapped water.

The osteoinductive character reported[99–101] for the biphasic β-TCP (40%) and HA (60%) biomaterials may also be expected for the β-rhenanite-HA materials of this study. Finally, to validate the above speculation and the clinical usefulness of the β-rhenanite + HA biphasic biomaterials of this work *in vivo* studies must be performed, which we plan to report in a follow-up study.

5.4 Conclusions

Sodium-doped calcium phosphate precursors were produced at room temperature by using a robust aqueous synthesis procedure involving the use of Na_2HPO_4, $NaHCO_3$, and $Ca(NO_3)_2.4H_2O$. The precursors formed at the physiological pH of 7.4 were in the form of a gel. Upon freeze-drying, these precursor gels were found to consist of poorly-crystallized, nanosize apatitic calcium phosphates with a surface area in excess of 120 m^2/g. Calcination of these samples in a static air atmosphere over the temperature range of 400–600°C for 6 h led to the production of β-rhenanite and hydroxyapatite biphasic biomaterials. Calcined powder samples had surface areas over the range 30 to 80 m^2/g, and consisted of nanosize grains.

5.5. References

1. J.P. Schmitz, J.O. Hollinger. The critical size defect as an experimental model for craniomandibulofacial nonunions. Clin Orthop **205** (1986) 299-308.

2. M.J. Yaszemski, R.G. Payne, W.C. Hayes, R. Langer, A.C. Mikos. Evolution of bone transplantation: Molecular, cellular and tissue strategies to engineer human bone. *Biomaterials* **17** (1996) 175-185.

3. M. Jarcho. Calcium phosphate ceramics as hard tissue prosthetics. *Clin Orthop* **157** (1981) 259 –278.

4. C.R. Nunes, S.J. Simske, R. Sachdeva, L.M. Wolford. Long-term ingrowth and apposition of porous hydroxylapatite implants. *J Biomed Mater Res* **36** (1997) 560-563.

5. R.W. Nicholas, T.A. Lange. Granular tricalcium phosphate grafting of cavitary lesions in human bone. *Clin Orthop* **306** (1994) 197–203.

6. J.C. Elliott. Structure and Chemistry of the Apatites and Other Calcium Orthophosphates. Amsterdam: Elsevier; 1994.

7. M. Spector. Anorganic bovine bone and ceramic analogs of bone mineral as implants to facilitate bone regeneration. *Clin Plast Surg* **21** (1994) 437-444.

8. D.S. Metsger, T.D. Driskell, J.R. Paulsrud. Tricalcium phosphate ceramic - A resorbable bone implant: Review and current status. *J Am Dent Assoc* **105** (1982) 1035-1038.

9. J.P. Schmitz, J.O. Hollinger JO, S.B. Milam. Reconstruction of bone using calcium phosphate bone cements: A critical review. *J Oral Maxillofac Surg* **57** (1999) 1122-1126.

10. S. Joschek, B. Nies, R. Krotz, A. Goepferich. Chemical and physicochemical characterization of porous hydroxyapatite ceramics made of natural bone. *Biomaterials* **21** (2000) 1645–1658.

11. K.A. Hing, S.M. Best, K.E. Tanner, W. Bonfield, P.A. Revell. Mediation of bone ingrowth in porous hydroxyapatite bone graft substitutes. *J Biomed Mater Res* A **68** (2004) 187–200.

12. S. Kamakura, Y. Sasano, T. Shimizu, K. Hatori, O. Suzuki, M. Kagayama, K. Motegi. Implanted octacalcium phosphate is more resorbable than β-tricalcium phosphate and hydroxyapatite. *J Biomed Mater Res* **59** (2002) 29-34.

13. O. Kilian, S. Wenisch, C. Heiss, U. Horas, E. Dingeldein, R. Schnettler. Einfluss von Ostim kombiniert mit autologen thrombozytaeren Wachstumsfaktoren. Biomaterialien **3** (2002) 126-132.

14. R. Tang, M. Hass, W. Wu, S. Gulde, G.H. Nancollas. Constant composition dissolution of mixed phases. II. Selective dissolution of calcium phosphates. *J Colloid Interface Sci* **260** (2003) 379-384.

15. S.H. Kwon, Y.K. Jun, S.H. Hong, H.E. Kim. Synthesis and dissolution behavior of β-TCP and HA/β-TCP composite powders. *J Eur Ceram Soc* **23** (2003) 1039-1045.

16. A. Hoshikawa, N. Fukui, A. Fukuda, T. Sawamura, M. Hattori, K. Nakamura, H. Oda. Quantitative analysis of the resorption and osteoconduction process of a calcium phosphate cement and its mechanical effect for screw fixation. *Biomaterials* **24** (2003) 4967-4975.

17. H.P. Yuan, Z.J. Yang, Y.B. Li, X.D. Zhang, J.D. De Bruijn, K. De Groot. Osteoinduction by calcium phosphate biomaterials. *J Mater Sci Mater M* **9** (1998) 723-726.

18. E. Goyenvalle, N.J.M. Guyen, E. Aguado, N. Passuti, G. Daculsi. Bilayered calcium phosphate coating to promote osseointegration of a femoral stem prosthesis. *J Mater Sci Mater M* **14** (2003) 219-227.

19. M. Szpalski, R. Gunzburg. Applications of calcium phosphate-based cancellous bone void fillers in trauma surgery. *Orthopedics* **25** (2002) S601–S609.

20. W.F. Neuman, M.W. Neuman. The Chemical Dynamics of Bone Mineral. Chicago: Chicago University Press; 1958.

21. A.C. Tas. Participation of calcium phosphate bone substitutes in the bone remodeling process: Influence of materials chemistry and porosity. *Key Eng Mater* **264 –268** (2004) 1969 –1972.

22. S. Wenisch, J.P. Stahl, U. Horas, C. Heiss, O. Kilian, K. Trinkaus, A. Hild, R. Schnettler. *In vivo* mechanisms of hydroxyapatite ceramic degradation by osteoclasts: Fine structural microscopy.*J Biomed Mater Res A* **67** (2003) 713-718.

23. F.W. Bloemers, T.J. Blockhuis, P. Patka, F.C. Bakker, B.W. Wippermann, H.J.T.M. Haarman. Autologous bone versus calcium–phosphate ceramics in treatment of experimental bone defects. *J Biomed Mater Res B* **66** (2003) 526-531.

24. D. Knaack, M.E.P. Goad, M. Aiolova, C. Rey, A. Tofighi, P. Chakravarthy, D.D. Lee. Resorbable calcium phosphate bone substitute. *J Biomed Mater Res* **43** (1998) 399-409.

25. C.M. Muller-Mai, S.I. Stupp, C. Voigt, U. Gross. Nanoapatite and organoapatite implants in bone: Histology and ultrastructure of the interface. *J Biomed Mater Res* **29** (1995) 9-18.

26. E.D. Eanes, J.D. Termine, A.S. Posner AS. Amorphous calcium phosphate in skeletal tissues. *Clin Orthop Relat Res* **53** (1967) 223-235.

27. R.A. Robinson, M.L. Watson. Collagen-crystal relationships in bone as seen in the electron microscope. III. Crystals and collagen morphology as a function of age. *Ann N Y Acad Sci* **60** (1955) 596-628.

28. A.S. Posner, S.R. Stephenson. Crystallographic investigation of tricalcium phosphate hydrate. *J Dent Res* **31** (1952) 371-382.

29. J.M. Stutman, E.R. Lippincott, A.S. Posner. Hydrogen bonding in the calcium phosphates. *Nature* **193** (1962) 368-370.

30. J.D. Termine, A.S. Posner. Amorphous/crystalline interrelationships in bone mineral. *Calcif Tissue Res* **1** (1967) 8-23.

31. A.S. Posner AS. Crystal chemistry of bone mineral. *Physiol Rev* **49** (1969) 760-792.

32. N.C. Blumenthal, J.M. Holmes, A.S. Posner. Effect of preparation conditions on the properties and transformation of amorphous calcium phosphate. *Mater Res Bull* **7** (1972) 1181-1190.

33. A.L. Boskey, A.S. Posner. Magnesium stabilization of amorphous calcium phosphate: A kinetic study. *Mater Res Bull* **9** (1974) 907-916.

34. N.C. Blumenthal, F. Betts, A.S. Posner. Effect of carbonate and biological macromolecules on formation and properties of hydroxyapatite. *Calcif Tissue Res* **18** (1975) 81-90.

35. F. Betts, N.C. Blumenthal, A.S. Posner, G.L. Becker, A.L. Lehninger. Atomic structure of intracellular amorphous calcium phosphate deposits. *Proc Natl Acad Sci USA* **72** (1975) 2088-2090.

36. U. Nylen, E.D. Eanes, J.D. Termine. Molecular and ultrastructural studies of noncrystalline calcium phosphates. *Calcif Tissue Res* **9** (1972) 95-108.

37. D.J. Greenfield, E.D. Eanes. Formation chemistry of amorphous calcium phosphates from carbonate-containing solutions. *Calcif Tissue Res* **9** (1972) 152-162.

38. J.D. Termine, E.D. Eanes. Comparative chemistry of amorphous and apatitic calcium phosphate preparations. *Calcif Tissue Res* **10** (1972) 171-197.

39. E.D. Eanes, J.D. Termine, M.U. Nylen. Electron microscopic study of the formation of amorphous calcium phosphate and its transformation to crystalline apatite. *Calcif Tissue Res* **12** (1973) 143-158.

40. D.J. Greenfield, J.D. Termine, E.D. Eanes. Chemical study of apatites prepared by hydrolysis of amorphous calcium phosphates in carbonate-containing aqueous solutions. *Calcif Tissue Res* **14** (1974) 131-138.

41. E.D. Eanes. The interaction of supersaturated calcium phosphate solutions with apatitic substrates. *Calcif Tissue Res* **20** (1976) 75-89.

42. E.D. Eanes, J.L. Meyer. The maturation of crystalline calcium phosphates in aqueous solutions at physiologic pH. *Calcif Tissue Res* **23** (1977) 259-269.

43. D. Skrtic, J.M. Antonucci, E.D. Eanes, N. Eidelman. Dental composites based on hybrid and surface-modified amorphous calcium phosphates. *Biomaterials* **25** (2004) 1141-1150.

44. C. Rey, K. Beshah, R. Griffin, M.J. Glimcher. Structural studies of the mineral phase of calcifying cartilage. *J Bone Miner Res* **6** (1991) 515-525.

45. Y.T. Wu, M.J. Glimcher, C. Rey, J.L. Ackerman. A unique protonated phosphate group in bone-mineral not present in synthetic calcium phosphates—Identification by P-31 solid-state NMR spectroscopy. *J Mol Biol* **244** (1994) 423-435.

46. C. Rey, A. Hina, A. Tofighi, M.J. Glimcher. Maturation of poorly crystalline apatites: Chemical and structural aspects *in vivo* and *in vitro*. *Cells Mater* **5** (1995) 345-356.

47. S. Quizat, A. Barroug, A. Legrouri, C. Rey. Adsorption of bovine serum albumin on poorly crystalline apatite: Influence of maturation. *Mater Res Bull* **34** (1999) 2279-2289.

48. A. Tofighi, S. Mounic, P. Chakravarthy, C. Rey, D. Lee. Setting reactions involved in injectable cements based on amorphous calcium phosphate. *Key Eng Mater* **192-1** (2000) 769-772.

49. L. Benaziz, A. Barroug, A. Legrouri, C. Rey, A. Lebugle. Adsorption of *o*-phospho-L-serine and L-serine onto poorly crystalline apatite. *J Colloid Interf Sci* **238** (2001) 48-53.

50. H.M. Kim, Y.S. Kim, K.M. Woo, S.J. Park, C. Rey, Y. Kim, J.K. Kim, J.S. Ko. Dissolution of poorly crystalline apatite crystals by osteoclasts determined on artificial thin-film apatite. *J Biomed Mater Res* **56** (2001) 250-256.

51. S. Somrani, C. Rey, M. Jemal. Thermal evolution of amorphous tricalcium phosphate. *J Mater Chem* **13** (2003) 888-892.

52. S. Cazalbou, C. Combes, D. Eichert, C. Rey, M.J. Glimcher. Poorly crystalline apatites: Evolution and maturation *in vitro* and *in vivo*. *J Bone Miner Metab* **22** (2004) 310-317.

53. C. Knabe, G. Berger, R. Gildenhaar, C.R. Howlett, B. Markovic, H. Zreiqat. The functional expression of human bone-derived cells grown on rapidly resorbable calcium phosphate ceramics. *Biomaterials* **25** (2004) 335–344.

54. M.M.A. Ramselaar, F.C.M. Driessens, W. Kalk, J.R. de Wijn, P.J. van Mullem. Biodegradation of four calcium phosphate ceramics; in vivo rates and tissue interactions. *J Mater Sci Mater M* **2** (1991) 63–70.

55. F.C.M. Driessens, M.M.A. Ramselaar, H.G. Schaeken, A.L.H. Stols, P.J. van Mullem. Chemical reactions of calcium phosphate implants after implantation in vivo. *J Mater Sci Mater M* **3** (1992) 413-417.

56. M.M.A. Ramselaar, P.J. van Mullem, W. Kalk, J.R. de Wijn, A.L.H. Stols, F.C.M. Driessens. *In vivo* reactions to particulate rhenanite and particulate hydroxylapatite after implantation in tooth sockets. *J Mater Sci Mater M* **4** (1993) 311-317.

57. O. Bermudez, M.G. Boltong, F.C.M. Driessens, M.P. Ginebra, E. Fernandez, J.A. Planell. Chloride- and alkali-containing calcium phosphates as basic materials to prepare calcium phosphate cements. *Biomaterials* **15** (1994) 1019-1023.

58. C. Knabe, R. Gildenhaar, G. Berger, W. Ostapowicz, R. Fitzner, R.J. Radlanski, U. Gross. Morphological evaluation of osteoblasts cultured on different calcium phosphate ceramics. *Biomaterials* **18** (1997) 1339-1347.

59. W. Suchanek, M. Yashima, M. Kakihana, M. Yoshimura. β-rhenanite (β-$NaCaPO_4$) as weak interphase for hydroxyapatite ceramics. *J Eur Ceram Soc* **18** (1998) 1923-1929.

60. Gong W, Abdelouas A, Lutze W. Porous bioactive glass and glass-ceramics made by reaction sintering under pressure. *J Biomed Mater Res* **54** (2001) 320-327.

61. A.R. El-Ghannam. Advanced bioceramic composite for bone tissue engineering: Design principles and structure– bioactivity relationship. *J Biomed Mater Res A* **69** (2004) 490-501.

62. E. Apel, W. Holand, V. Rheinberger V. Bioactive rhenanite glass ceramic. US Pat. Appl. No. 2004/0167006 A1.

63. F.P. Glasser, R.P. Gunawardane. Fertilizer material from apatite. US Pat. No. 4,363,650, December 14, 1982.

64. OsteoStim® resorbable bone graft substitute. EBI L.P., Parsippany, NJ, 2006. Available at: www.ebimedical.com/products.

65. B. Eppley, S. Stal, L. Hollier, M. Kumar. Compartmentalized bone regeneration of cranial defects with biodegradable barriers—Effects of calcium sodium phosphate surface coatings on LactoSorb. *J Craniofac Surg* **13** (2002) 681-686.

66. Biomet, Inc. Calcigen™-NaP bone void filler. Biomet, Inc., Warsaw, IN, 2006.

67. A.C. Tas. Synthesis of biomimetic Ca-hydroxyapatite powders at 37°C in synthetic body fluids. *Biomaterials* **21** (2000) 1429-1438.

68. D.D. Lee, C. Rey, M. Aiolova, A. Tofighi. Bioresorbable ceramic composites. US Pat. No. 6,331,312, December 18, 2001.

69. J.C. Hiller, T.J.U. Thompson, M.P. Evison, A.T. Chamberlain, T.J. Wess. Bone mineral change during experimental heating: An X-ray scattering investigation. *Biomaterials* **24** (2003) 5091-5097.

70. K.D. Rogers, P. Daniels. An X-ray diffraction study of the effects of heat treatment on bone mineral microstructure. *Biomaterials* **23** (2002) 2577-2585.

71. E.D. Spoerke, S.I. Stupp. Synthesis of a poly(L-lysine)-calcium phosphate hybrid on titanium surfaces for enhanced bioactivity. *Biomaterials* **26** (2005) 5120-5129.

72. A.C. Tas, S.B. Bhaduri. Chemical processing of $CaHPO_4.2H_2O$: Its conversion to hydroxyapatite. *J Am Ceram Soc* **87** (2004) 2195-2200.

73. A.C. Tas, P.J. Majewski, F. Aldinger. Chemical preparation of pure and strontium- and/or magnesium-doped lanthanum gallate powders. *J Am Ceram Soc* **83** (2000) 2954-2960.

74. A.C. Tas. Combustion synthesis of calcium phosphate bioceramic powders. *J Eur Ceram Soc* **20** (2000) 2389-2394.

75. ICDD PDF No. 29–1193. The International Centre for Diffraction Data. Newtown Square, PA.

76. Y. Doi, Y. Shimizu, Y. Moriwaki, M. Aga, H. Iwanaga, T. Shibutani, K. Yamamoto, Y. Iwayama. Development of a new calcium phosphate cement that contains sodium calcium phosphate. *Biomaterials* **22** (2001) 847-854.

77. N. Pleshka, A. Boskey, R. Mendelsohn. Novel infrared spectroscopic method or determination of crystallinity of hydroxyapatite minerals. *Biophys J* **60** (1991) 786-793.

78. H.E.L. Madsen, G. Thodvadarson. Precipitation of calcium phosphate from moderately acid solutions. *J Cryst Growth* **66** (1984) 369-376.

79. W.P. Inskeep, J.C. Silvertooth. Kinetics of hydroxyapatite precipitation at pH 7.4 to 8.4. *Geochim Chosmochim Acta* **52** (1988) 1883-1893.

80. E. Ebrahimpour, M. Johnson, C.F. Richardson, G.H. Nancollas. The characterization of HA precipitation. *J Colloid Interface Sci* **159** (1993) 158-163.

81. J. Zhou, X. Zhang, J. Chen, S. Zeng, K. de Groot. High temperature characteristics of synthetic hydroxyapatite. *J Mater Sci Mater M* **4** (1993) 83-85.

82. R.Z. LeGeros, J.P. LeGeros. Dense hydroxyapatite. In: Hench LL, Wilson J, editors. An Introduction to Bioceramics. London: World Scientific; 1993. pp 144, 145.

83. C.K. Loong, C. Rey, L.T. Kuhn, C. Combes, Y. Wu, S.H. Chen, M.J. Glimcher. Evidence of hydroxyl-ion deficiency in bone apatites: An inelastic neutron-scattering study. *Bone* **26** (2000) 599-602.

84. C. Rey, M. Shimizu, B. Collins, M.J. Glimcher. Resolution-enhanced Fourier transform infrared spectroscopy study of the environment of phosphate ion in the early deposits of a solid phase of calcium phosphate in bone and enamel and their evolution with age: 2. Investigations in the ν_3PO_4 domain. *Calcif Tissue Int* **49** (1991) 383-388.

85. S.Y. Lin, K.H. Chen, M.J. Li, W.T. Cheng, S.L. Wang. Evidence of octacalcium phosphate and type-B carbonated apatites deposited on the surface of explanted acrylic hydrogel intraocular lens. *J Biomed Mater Res B* **70** (2004) 203-208.

86. R.A. Robinson, M.L. Watson. Collagen-crystal relationships in bone as seen in the electron microscope. *Anat Rec* **114** (1952) 383-410.

87. E. Johansen, H.F. Parks. Electron microscopic observations on the three-dimensional morphology of apatite crystallites of human dentine and bone. *J Biophys Biochem Cytol* **7** (1960) 743-746.

88. Z. Molnar. Additional observations on bone crystal dimensions. *Clin Orthop* **17** (1960) 38-42.

89. Z. Molnar. Development of the parietal bone of young mice I: Crystals of bone mineral in frozen-dried preparations. *J Ultrastruct Res* **3** (1959) 39-45.

90. A.S. Posner, E.D. Eanes, R.A. Harper, I. Zipkin. X-ray diffraction analysis of the effect of fluoride on human bone apatite. *Arch Oral Biol* **8** (1963) 549-570.

91. A. Nakahira, S. Konishi, F. Nishimura, M. Iwasaka, S. Ueno. Effect of a high magnetic field on the bioactivity of apatite-based biomaterials. *J Appl Phys* **93** (2003) 8513-8515.

92. K. Hata, T. Kokubo, T. Nakamura, T. Yamamuro. Growth of a bonelike apatite layer on a substrate by a biomimetic process. *J Am Ceram Soc* **78** (1995) 1049-1053.

93. D. Bayraktar, A.C. Tas. Chemical preparation of carbonated calcium hydroxyapatite powders at 37°C in urea-containing synthetic body fluids. *J Eur Ceram Soc* **19** (1999) 2573-2579.

94. Y. Doi, T. Koda, N. Wakamatsu, T. Goto, H. Kamemizu, Y. Moriwaki, M. Adachi, Y. Suwa. Influence of carbonate on sintering of apatites. *J Dent Res* **72** (1993) 1279-1284.

95. A.C. Tas, S.B. Bhaduri. Rapid coating of Ti6Al4V at room temperature with a calcium phosphate solution similar to 10x simulated body fluid. *J Mater Res* **19** (2004) 2742-2749.

96. N. Kivrak, A.C. Tas. Synthesis of calcium hydroxyapatite-tricalcium phosphate (HA-TCP) composite bioceramic powders and their sintering behavior. *J Am Ceram Soc* **81** (1998) 2245-2252.

97. I.M.O. Kangasniemi, K. de Groot, J.G.M. Becht JGM, A.U. Yli-Urpo. Preparation of dense hydroxylapatite or rhenanite containing bioactive glass composites. *J Biomed Mater Res* **26** (1992) 663-674.

98. Kangasniemi IMO, Vedel E, de Blick-Hogerworst J, Yli-Urpo AU, de Groot K. Dissolution and scanning electron microscopic studies of Ca, P particle-containing bioactive glasses. *J Biomed Mater Res* **27** (1993) 1225-1233.

99. H. Yuan, M. van Den Doel, S. Li, C.A. van Blitterswijk, K. de Groot, J.D. de Bruijn. A comparison of the osteoinductive potential of two calcium phosphate ceramics implanted intramuscularly in goats. *J Mater Sci Mater M* **13** (2002) 1271-1275.

100. K. Kurashina, H. Kurita, Q. Wu, A. Ohtsuka, H. Kobayashi. Ectopic osteogenesis with biphasic ceramics of hydroxyapatite and tricalcium phosphate in rabbits. *Biomaterials* **23** (2002) 407-412.

101. D. Le Nihouannen, G. Daculsi, A. Saffarzadeh, O. Gauthier, S. Delplace, P. Pilet, P. Layrolle. Ectopic bone formation by microporous calcium phosphate ceramic particles in sheep muscles. *Bone* **36** (2005) 1086-1093.

CHAPTER 6

PREPARATION OF Zn-DOPED β-TRICALCIUM PHOSPHATE (β-$Ca_3(PO_4)_2$) BIOCERAMICS

Abstract

Pure β-tricalcium phosphate (β-TCP) and Zn-doped (600, 2900, 4100, 7000, 9300 and 10100 ppm) β-TCP samples were prepared by using a wet chemical/coprecipitation synthesis technique, followed by calcination at 1000°C in air. Precursor powders of the coprecipitation process were Ca-deficient nanoapatites (i.e., Ca/P molar ratio varying from 1.49 to 1.51) with needlelike but agglomerated particles of 30 nm thickness. *In vitro* culture tests performed by mouse osteoblast-like cells showed that the samples doped with 2900 to 4100 ppm Zn showed the highest cell viability (via Live/Dead counts), and with a further increase in the Zn-content towards 1 wt% the number of dead cells in the well plates started to increase. Alkaline phosphatase (ALP) activity peaked for the β-TCP sample doped with 4100 pm Zn. The sample surface roughness, measured by non-contact profilometry, was also found to have an effect on the Live/Dead cell counts, and the highest cell viability encountered in this study corresponded to the surface with the least roughness.

(This work is published in *Mater Sci Eng C* **27** (2007) 394–401)

6.1. Introduction

The mineralized portion of human bones and teeth essentially consists of nanosize and imperfect crystals of Ca-deficient, carbonated and alkali- and alkaline earth-doped biological apatites.[1] Bone apatites do not contain the β-tricalcium phosphate (β-TCP: β-$Ca_3(PO_4)_2$) phase. However, Mg-doped whitlockite, which can form in aqueous environments and structurally related to β-TCP, was found in human dental calculus[2] and in carious lesions[3,4]. Human bone depositing cells, namely the osteoblasts, are not programmed to synthesize the β-TCP phase in their physiological habitat, pH and temperature. β-TCP is a calcium phosphate ceramic of high solubility in comparison to Ca-hydroxyapatite (HA; $Ca_{10}(PO_4)_6(OH)_2$). The solubility activity product (K_{sp}) of β-TCP is $2.51x10^{-30}$,[5, 6] whereas that of HA is $2.34x10^{-59}$ [7]. Owing to its significant solubility and ability of taking part in bone remodeling/turnover processes, β-TCP has become a bone substitute bioceramic in successful clinical use.[8-10] Wiltfang *et al*.[11] reported the *in vivo* resorbability (more than 95%) of β-TCP bioceramics in a minipig-tibia model observed over a period of 86 weeks.

The human nutritional need for zinc is small, but its role in growth and well-being is enormous, starting even before birth.[12] The entire body of a normal human weighing 70 kg may contain 1.4 to 2.3 g of zinc, and the recommended daily allowance of zinc is between 8 and 15 mg. Meats, seafood (especially oysters) and liver are the richest sources of zinc in food; brewer's yeast, milk, egg yolks, popcorn, beans, cocoa, and wheat germ also supply some zinc.[13] Zinc is found in body in small amounts in almost all tissues, however, the bones, teeth, and the pancreas contain slightly higher amounts than others. Human blood plasma contains approximately $1.5x10^{-2}$ mM of zinc.[14] Zinc is an essential trace element in a variety of cellular processes including DNA synthesis, behavioral responses, reproduction and virility, bone formation, bone growth and wound healing.[15] Zinc plays an important role in gene expression and in the regulation of cellular growth and differentiation,[16] since it participates as a co-factor of more than 200 enzymes implied in the metabolism of nucleic acids, carbohydrates and proteins. Approximately 85% of the body store of zinc is found in skeletal

muscles (55%) and bones (30%).[17] The necessity of this trace element for bone growth was demonstrated by the observation that normal bone growth was retarded in animals that are zinc-deficient,[18] and the addition of zinc to these deficient diets resulted in a stimulation of both bone growth and mineralization.[19] Zinc is the only metal to be incorporated in all six enzyme classes of metalloenzymes, with the examples of oxidoreductase, transferase, hydrolase, lyase, isomerase, and ligase activity.[20] Important bone enzymes, including alkaline phosphatase (ALP) and carbonic anhydrase are zinc metalloenzymes, and tartrate-resistant acid phosphatase (TRAP) is strongly inhibited by zinc [21, 22]. In brief, zinc deficiency has been associated with skeletal growth retardation, reduced ALP activity[18], reduced premenopausal bone mass[23] and postmenopausal osteoporosis[24]. Clinical trials have also shown that zinc supplementation inhibits postmenopausal bone loss [25]. Zinc has been implicated in bone formation, mineralization,[26] and the stimulation of ALP activity in calvarial organ cultures,[18, 27] osteoblast-like cell cultures,[28-30] as well as the stimulation of the bone DNA synthesis via the activation of bone DNA polymerase[31]. Zinc deficiency, on the other hand, were recently shown to cause about 300% increase in programmed cell death (or apoptosis) in mice in a variety of kinds of cells[32], and insufficient zinc initiated apoptosis in hepatocytes, glioma, kidney, monocytes, fibroblasts, and testicular cells.

To the best of our knowledge, a thorough investigation on the synthesis of Zn-doped HA and/or TCP bioceramics has a rather short history. Fuierer *et al*.[33] and Bigi *et al*.[34] performed the pioneering studies in this field, which reported the inhibiting effect of zinc on HA crystal growth in aqueous systems. A later report by Bigi *et al*.[35] attempted to synthesize Zn-doped β-TCP bioceramics at Zn dopant levels from 2.5 to 20 mole%, with increments of 2.5 mole% over this range. Bigi *et al*.[35] first prepared single-phase β-TCP ceramics by calcining a stoichiometric powder mixture of $CaHPO_4 \cdot 2H_2O$ and $CaCO_3$ at 1000°C for 15 h. To produce the Zn-doped β-TCP bioceramics, Bigi *et al.*[35] mixed the phase-pure β-TCP powders with those of α-$Zn_3(PO_4)_2$ and calcined the resultant mixtures at 1000°C for 15 h. Bigi *et al*.[35] concluded that the small Zn ion (0.074 nm) readily

replaced the larger Ca ion (0.099 nm) in the β-TCP structure (rhombohedral, space group R*3c*), causing a steady and monotonic decrease in the a-axis of the unit cell from 10.44 to 10.325 Å, while causing a slight decrease in the c-axis length from 37.41 to 37.25 Å, with isomorphic Zn substitution from 2.5 to 20 mol% over the Ca-sites. LeGeros[36, 37] has been the first to report the formation of TCP phase (together with needle-like apatite crystals) in aqueous solutions containing zinc. The last five years have seen a number of publications[38-51] coming from the laboratory of Dr. Atsuo Ito, all concerning with the synthesis and/or *in vitro-in vivo* testing of Zn-containing calcium phosphate ceramics. In some studies of the Ito group, the ZnTCP samples (to be later blended with HA powders) were prepared by the $Ca(OH)_2$-H_3PO_4 neutralization route with the addition of zinc nitrate into those solutions to obtain 10 to 30 mol% Zn doping,[39] while in some studies by Layrolle *et al*.[52] a sol-gel route, which used $Ca(OEt)_2$ (obtained from the reaction of Ca metal shots and ethyl alcohol), H_3PO_4 and Zn-acetate, was employed to synthesize the samples. The Ito group synthesized numerous calcium phosphate samples by doping Zn starting from 600 ppm level up to 10-20 mol%.[48] However, most of the studies of this group were focused more on the *in vivo* and *in vitro* testing of ZnTCP-HA biphasic samples. Therefore, the reports originating from the Ito group which focused only on the testing of Zn-doped β-TCP (i.e., without any HA) [41, 45, 50, 51] are in direct relevance with the present study. However, in these studies the following points can be underlined: (i) their powder samples were produced by using the $Ca(OH)_2$-H_3PO_4-Zn-nitrate synthesis route,[41, 45, 50, 51] (ii) when the authors were adding 12 mol% Zn, their samples were reported to contain the phase of $CaZn_2(PO_4)_2$,[51] (iii) the authors first synthesized 10 mol% ZnTCP powders and then mixed those in a mortar with pure β-TCP powders to obtain 0.28, 2.56, 5.0, 7.47, and 10.5% Zn-containing ZnTCP samples after calcination at 1000°C,[45] (iv) when the authors were preparing the so-called 12 wt% Zn-containing ZnTCP samples, they reported to have the secondary phases of $Ca_{2.7}Zn_{0.3}(PO_4)_2$ and $CaZn_2(PO_4)_2$, [41, 50] (v) the authors never cited the important work of Bigi *et al*.[35] and compared their findings with those reported before, (vi) the authors did not study the low end of

the Zn-doping range. The goals of the present study can be briefly stated as follows; (i) to develop an aqueous co-precipitation process (incorporating a calcination step; at 1000°C) for synthesizing Zn-β-TCP samples with Zn levels ranging from 600 ppm to about 1.0 wt% to eliminate the need for physical mixing of more than one powders to produce Zn-doped calcium phosphate bioceramics, (ii) to characterize the samples by using XRD, FTIR, TGA, ICP-AES, density and surface profilometry measurements, (iii) to test the cytotoxicity and ALP (alkaline phosphatase) activity of the Zn-β-TCP samples (600, 2900, 4100, 7000, 9300 and 10100 ppm Zn) by using rat osteoblast-like cells.

6.2. Experimental Procedure

6.2.1 ***Sample preparation*.** $Ca(NO_3)_2{\cdot}4H_2O$ (>99.5%, Fisher), $NH_4H_2PO_4$ (>99.5%) and $Zn(NO_3)_2{\cdot}6H_2O$ (>99.9%) were the starting chemicals used in powder synthesis. α-$Zn_3(PO_4)_2$ powder (TZP; 99.995%, #13013) was provided by Alfa-Aesar Inc. Briefly, $NH_4H_2PO_4$ was dissolved in deionized water in a glass beaker, and in a separate beaker $Ca(NO_3)_2{\cdot}4H_2O$ and $Zn(NO_3)_2{\cdot}6H_2O$ were dissolved in proper amounts. Ca-Zn-nitrate mixed solution was then added at once into the phosphate solution, the slight turbidity instantly observed was eliminated by adding few drops of concentrated HNO_3 (69 vol%, Fisher) which also brought the solution pH down to 3±0.1 from around 4, and therefore, a clear solution was obtained. This solution was stirred (200 rpm) at 37°C for 2 h to ensure a homogeneous mixture, followed by rapidly adding about 50 mL of a concentrated NH_4OH (29% NH_3, Merck) solution to obtain precipitation and a stable pH value of around 9.2 ±0.2 again at 37°C. The opaque solution was stirred for 1 h. Formed precipitates were filtered (paper No. 42) via a Buechner funnel, washed with 4 L of water, and then dried at 90°C for 12 hours in air in glass dishes. Dried powders, which were free of hard agglomerates, were only lightly ground in an agate mortar by a pestle. Precursor powders were uniaxially pressed (3580 kg/cm^2) into 1.5 mm-thick, 1.27 cm-diameter pellets in steel molds and then calcined in air at 1000°C for 6 h in clean Al_2O_3 boats or crucibles (heating/cooling rate: 3°C/min).

Table 6.1 Powder synthesis procedure

Sample[a] (*ppm Zn*) *Ca/P*	$NH_4H_2PO_4$ *in 225 mL H_2O*	$Ca(NO_3)_2{\cdot}4H_2O$	$Zn(NO_3)_2{\cdot}6H_2O$ *[in 600 mL H_2O]*	ICP-AES results[b] *P (%)*	*Ca(%)*	*Zn (ppm)*
Zn-600	22.4424 g	[69.0483 g	+ 0.2763 g]	22.14	42.85	600	1.496
Zn-2900	22.4424 g	[68.9212 g	+ 0.4362 g]	21.58	42.52	2900	1.513
Zn-4100	22.4424 g	[68.7205 g	+ 0.6900 g]	18.94	36.46	4100	1.488
Zn-7000	22.4424 g	[68.3422 g	+ 0.9651 g]	19.95	38.85	7000	1.505
Zn-9300	22.4424 g	[68.1447 g	+ 1.3140 g]	18.78	36.25	9300	1.492
Zn-10100	22.4424 g	[67.9471 g	+ 1.6631 g]	20.16	38.92	10100	1.493

[a] *ppm Zn in β-TCP, measured by ICP-AES in powder samples calcined at 1000 ℃ for 6 h*
[b] *ICP-AES analyses of powder samples calcined at 1000 ℃ for 6 h*

TZP powders were also pressed into pellets and later calcined in the way as described above. The details of powder syntheses were given in Table 6.1, in which the samples of interest were named according to their experimentally-determined (by ICP-AES) ppm Zn values after calcination.

6.2.2 Characterization. Chemical analyses of powder (both precursor and calcined) samples were performed by ICP-AES (Model 61E, Thermo Electron, Madison, WI). During the ICP-AES analyses, 50 mg portions of powder samples were dissolved in 5 mL of concentrated HNO_3 solution. Surface roughness of the calcined Zn-β-TCP pellets were measured, prior to cell culture tests, by a non-contacting surface profilometer (NT-2000, Wyko, Tucson, AZ) at the magnification of 25 X and over a 164 x 215 μm field of view. In profilometry, R_t was the maximum height minus the minimum height in the field of view, whereas R_z was the average of 5 highest peaks minus the average of 5 lowest valleys. Bulk densities of the calcined pellets (repeated 5X) were measured by using a pycnometer (AccuPyc 1330, Micromeritics, Norcross, GA) with He gas.

For the phase analyses of powder samples an X-ray diffractometer (XRD; XDS 2000, Scintag Corp., Sunnyvale, CA) was used (Cu K_α radiation at 40 kV and 30 mA, with a step size of 0.03° and preset time of 1 s at each step). Samples

were also analyzed by FTIR (Nicolet 550, Thermo-Nicolet, Woburn, MA). Scanning electron microscopy (FE-SEM; S-4700, Hitachi, Tokyo) was used in the secondary electron mode with an acceleration voltage of 5 kV to image the samples.

6.2.3 ***In vitro cell culture tests.*** Statistical sample size (i.e., *n*) was 16 in the entirety of the cell culture tests.7F2 rat osteoblast-like cells (CRL-12557, American Type Culture Collection, Rockville, MD) were grown on 75 cm^2 culture flasks at 37ºC and 50% CO_2 in α-MEM with 2 mM 1-glutamine and 1 mM sodim pyruvate without ribonucleosides and deoxyribonucleosides, augmented by 10% FBS. The culture medium was changed every other day until the cells reached a confluence of 90-95%, as determined visually with an inverted microscope. The cells then were passaged using trypsin (2.5 g/L)/ EDTA (25mM) solution (Sigma-Aldrich Corp., St. Louis, MO, USA). The obtained cells were then seeded at a concentration of 3500 cell/well on 0.14 cm^3 samples for various assays. Cell viability and alkaline phosphatase activity measurements were performed after 72 hours. The cell viability assessment was performed using Live/Dead® Viability/Cytotoxicity Kit (L-3224, Molecular Probes, Eugene, OR). A working solution is prepared by mixing 5µl aliquot of Component A (4 mM calcein AM solution in DMSO) to 10 ml of 4 mM EthD-1 solution (20 µl of the Component B to 10 ml of DPBS). 100 µl of this working solution was added to the cell-containing samples along with 100 µl of cell-containing media. Samples were incubated at room temperature for 30-45 minutes. After the prescribed time period, the fluorescence values were recorded at 494/517 nm for live cells and 528/617 nm for dead cells by using a standard curve obtained by seeding different number of cells in different wells. The alkaline phosphatase (ALP) activity was determined using the ALP concentration and the cell extracted protein concentration. The ALP concentration was calculated using Enzymatic Assay of Phosphatase Alkaline Kit (EC 3.1.3.1, Sigma-Aldrich Corp., St. Louis, MO, USA). A working reagent was prepared by first mixing 2.7 ml of Reagent A (1.0 M Diethanolamine Buffer with 0.50 mM Magnesium Chloride) with 0.30 ml of Reagent B (150 mM p-Nitrophenyl Phosphate Solution (pNPP)) and then mixing

the mixture with 0.10 ml of cell-containing media. 100 µl of this solution was added to each well and thoroughly mixed and incubated at 37ºC for 30 minutes. Following incubation, the absorbance was recorded at 405 nm with the spectrophotometer at room temperature. The standard curve was obtained by plotting the absorbance measured at 405 nm for certain concentration against the concentration in µg/ml. ALP concentration of each sample was then determined using this standard curve and is expressend as µg-pNP/ml. The cell extracted protein concentration was determined in a two-step procedure, first the protein was extracted using M-PER™ Mammalian Protein Extraction reagent and then this extracted protein was measured using BCA™ Protein Assay Kit. The cell samples were lysed by adding 200 µl of M-PER™ Reagent to each well plate and then shaking for 5 minutes. Lysate was collected and transferred to microcentrifuge tubes, followed by centrifuging at 4000g for 10 minutes to pellet the cell debris. Supernatant was transferred to clean tubes for analyzing the protein concentration. To measure the protein amount, a working reagent (WR) was prepared by mixing 50 parts of BCA™ Reagent A with 1 part of BCA™ Reagent B (50:1, Reagent A:B). 200 µl of the above mentioned WR was added to each well and thoroughly mixed. Following mixing, the well plate was covered and incubated at 37ºC for 30 minutes. The absorbance at 562 nm was measured with the spectrophotometer at room temperature. A standard curve was prepared by plotting the average blank-corrected 562 nm measurement for each BSA standard versus its concentration in µg/ml. Cell extracted protein concentration was then determined by using this standard curve and is expressed as µg/ml. The ALP activity was then calculated as follows; ALP Activity = [(µg pNP)/139] / µg(cell extracted protein) = µmoles pNPP/ µg cell protein. Osteoblast attachment/proliferation on the pellets was studied using SEM. Cells were first fixed by using 3.5% glutaraldehyde, and then dehydrated through sequential washings in 50%, 70%, 95% ethanol solutions and 2 times in 100% ethanol. Samples were then critical point-dried, prior to sputter-coating with a thin layer of Pt.

6.3. Results and Discussion

The pure and Zn-doped precursor powders of this study gave the same XRD pattern as shown in Figure 6.1a, which belonged to that of Ca-deficient apatitic calcium phosphate (CDHA: $Ca_9(HPO_4)(PO_4)_5OH$). Yubao *et al*.[53] previously called this phase as apatite-TCP and gave a full account of its crystal structure. Rietveld refinement of the structure of CDHA was performed by Ivanova *et al*.[54] and Tas *et al*.[55]. Gibson *et al*.,[56] on the other hand, studied the thermal transformation of CDHA into β-TCP. FTIR spectra of the precursor powders were given in Figure 6.1b, while the ICP-measured Zn levels (in ppm) were indicated on the diagram. The vibrations indicated in Figure 6.1b with arrows denoted the OH vibrations, whereas the rest indicated the characteristic PO_4^{3-} and CO_3^{2-} vibrations.[56]

It should hereby be noted that there was a difference between the ppm Zn levels achieved in the powders before and after calcination (see Table 6.1). This was believed to be due to the difference(s) in surface adsorbed or in hydroxide-form Zn (i.e., in precursor powders) and the structure-assimilated Zn ions (i.e., after heating). Calcination, and therefore, the solid-state diffusion apparently had a certain effect on the stabilization of the final Zn content of the samples. According to the ICP-AES results of the precursors and the calcined samples, vaporization of Zn was not observed during calcination. TGA traces of the precursors (Fig. 6.1c) showed, from RT to around 500°C, an initial weight loss between 4 to 9%, which corresponded to the loss of surface adsorbed water and probably some residual ammonium and nitrate ions.[54] The unique shoulder observed at around 720°C in Figure 6.1c represented the volatilization of carbonate ions. Carbonated nature of these precursor powders were also detected by their FTIR spectra of Figure 6.1b. It was difficult to find a direct correlation between the TGA weight loss behavior and the Zn-dopant level. The high-magnification SEM micrographs given in Figure 6.1d were recorded directly on the surface of a green pellet prepared from 8700 ppm Zn-containing TCP precursors, and the same morphology was also observed on 600 ppm Zn-containing precursors (data not shown). Micrographs of Figure 6.1d confirmed (as

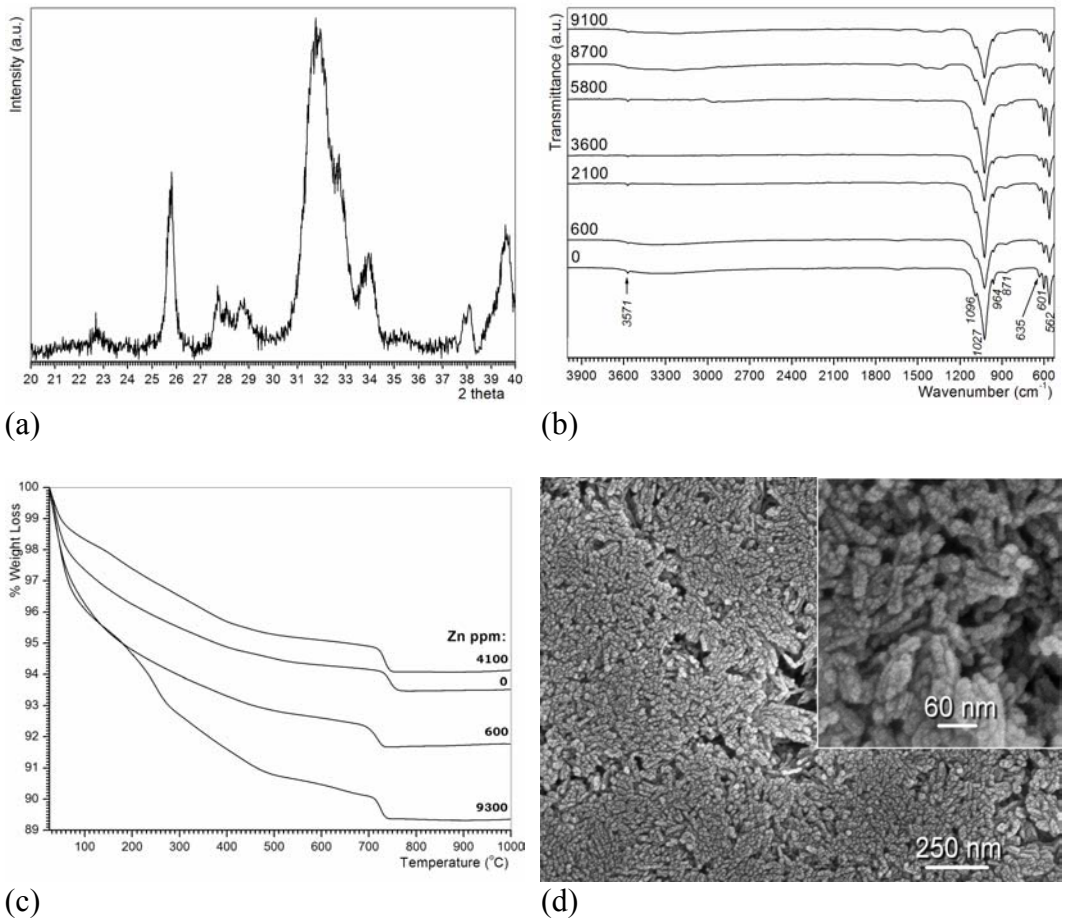

Fig. 6.1 Precursor samples (a) XRD spectra; (b) FTIR spectra; (c) TGA traces; and (d) SEM micrographs (inset shows high magnification).

did Fig. 6.1a) the nanocrystalline nature of these precursors, and the powders consisted of acicular particles of about 100 nm-long and 30 nm-thick. TEM studies are underway. Apparently, uniaxial pressing of those powders into a pellet at 3580 kg/cm^2 forced them to pack closely.

Calcination of the pure and Zn-doped precursor powders at 1000°C resulted in the complete transformation of CDHA into β-TCP and Zn-doped β-TCP. The Zn-content and Ca/P molar ratio of the calcined pellets were depicted in Table 6.1. The XRD (Fig. 6.2a, Zn-content in ppm values were indicated on the traces) and FTIR (Fig. 6.2b) spectra of the calcined samples confirmed the formation of β-TCP. The small extraneous peaks in Figure 6.2a, labeled by asterisks in the traces of 7000 and 9300 ppm Zn-containing samples, corresponded to the very strong 211 reflection of the HA phase. In reproduction runs for the samples these peaks were not observed, but we decided to report here the original data. This probably showed an inherent limitation of our synthesis procedure in producing 100% pure β-TCP.

Calcination of the precursors in an air atmosphere (at uncontrolled relative humidity levels from one experiment to the other) may also be influential on this point of HA formation. Surface profilometry data shown in Figure 6.2c indicated to an interesting decrease in surface roughness at around 2900 and 4100 ppm Zn-content, with increasing or decreasing Zn-dopant level surface roughness increased. The surface morphology of a pure β-TCP calcined pellet was given in Figure 6.2d, grain sizes ranged from 350 nm to 2 μm. However, the grain size distribution in 2900 and 4100 ppm Zn-β-TCP samples were quite different from that of pure β-TCP, as shown in Figures 6.2e and f, respectively. The significant increase in the average grain size of the 4100 ppm Zn-β-TCP sample should also explain for the dip in the surface profilometry results given in Figure 6.2c. The slight decrease in the average grain size in the 10100 ppm Zn-β-TCP sample (Fig. 6.2g) was interesting to note. These data showed that Zn was also an effective dopant in altering the grain boundary area in this new class of β-TCP samples. The progressive Zn doping caused a decrease in the bulk density of the pellets

calcined at 1000°C, as shown in Table 6.2. The density data of Table 6.2 represented densification in excess of 95% of the theoretical density of β-TCP. The 600 ppm Zn-β-TCP sample had the formula $Ca_{2.997}Zn_{0.003}(PO_4)_2$, whereas the formula for the 10100 ppm sample was $Ca_{2.952}Zn_{0.048}(PO_4)_2$. The TZP pellet, which was used as a control in the cell culture tests, showed the polymorphic transformation from the α- (ICDD PDF 29-1390) to the β-form (ICDD PDF 30-1489) upon calcination at 1000°C (XRD and FTIR data not shown). This polymorphic transformation in TZP was known to occur above 942°C.

The results of culture tests with mouse osteoblast-like cells were summarized by the histograms given in Figures 6.3a (Live/Dead cytotoxicity) and 6.3b (ALP activity). Taking into consideration the rather significant length of the error bar on the 2900 ppm Zn sample in Figure 6.3a and the highest ALP activity observed for 4100 ppm Zn sample (Figure 6.3b), it can be stated that the maximum proliferation of the osteoblast-like cells was recorded on the 4100 ppm Zn-β-TCP sample of this study. It will also be interesting to couple this finding with the fact that the minimum surface roughness (Figure 6.2c) and the maximum bulk density (Table 6.2) values of this study were observed for the very same 4100 ppm Zn-β-TCP sample. β-TZP was found to be a perfectly cytotoxic material (Figure 6.3a). It also became apparent that, in comparison to pure β-TCP, the presence of Zn especially at the dopant levels of 2900, 4100 and 7000 ppm significantly increased the osteoblastic activity (Figs. 6.3a and b).[57] This point is in very well agreement with the previous literature cited in Section 2. The attachment and spreading of osteoblasts on various Zn-β-TCP pellets were imaged by SEM and given in Figure 6.4. On pure β-TCP pellets, osteoblasts spread like a thin, electron-translucent membrane so that the underlying grains were still visible (Fig. 6.4a). The erosion of the grain boundaries (Fig. 6.4a) during the cell culture tests may indicate that there might have been a highly soluble amorphous CaP grain boundary phase which dissolved under the alkaline phosphatase

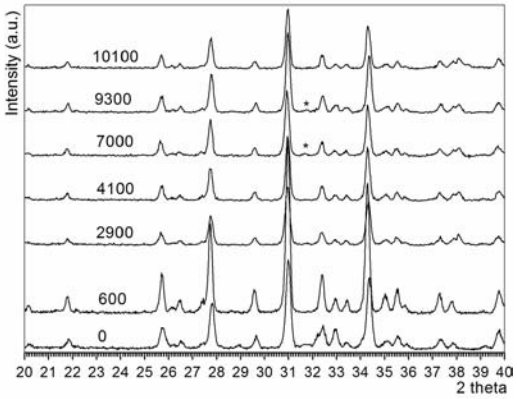

(a)

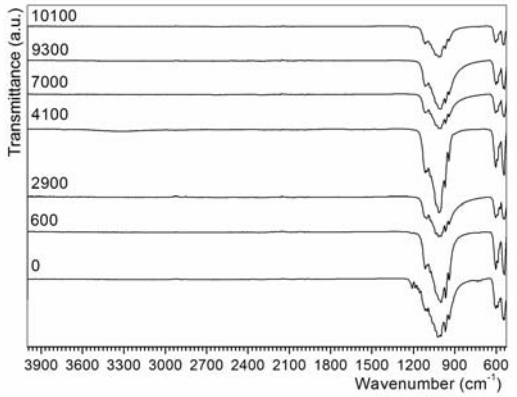

(b)

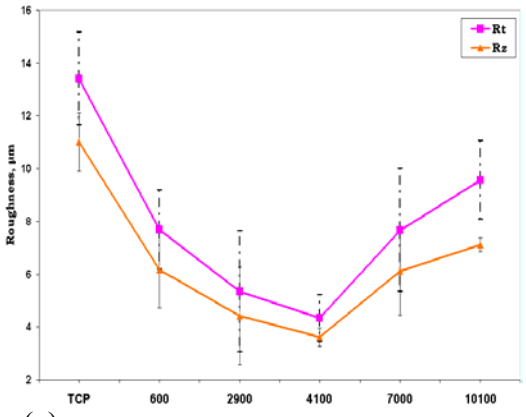

(c)

Fig. 6.2 Calcined samples (a) XRD spectra; (b) FTIR spectra; (c) Surface profilometry.

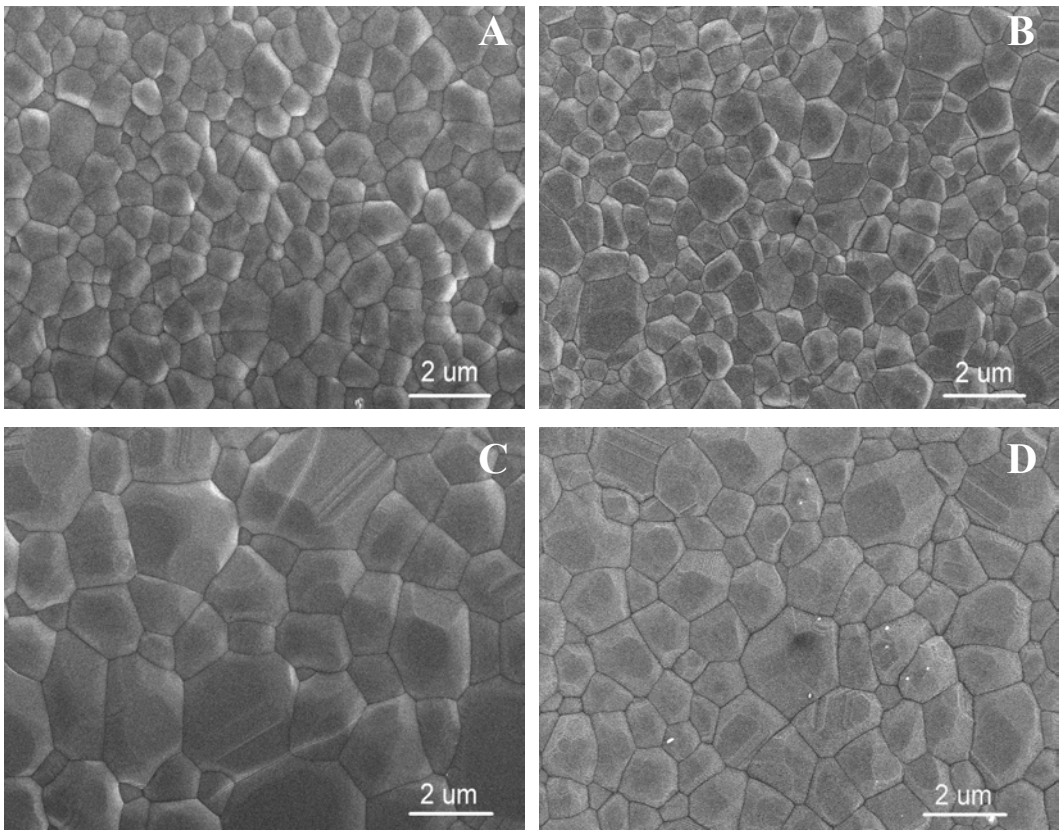

Fig. 6.2 SEM micrographs of calcined samples (d) 0 ppm (pure β-TCP), (e) 2900 ppm, (f) 4100 ppm, and (g) 10100 ppm Zn-βTCP.

Table 6.2 Bulk densities of Zn-doped β-TCP pellets

ppm Zn	*Density (g/cm^3)*	*Std. Deviation*
0	3.049	0.022
600	3.024	0.027
2900	3.028	0.016
4100	3.068	0.028
7000	2.997	0.013
9300	2.992	0.017
10100	2.945	0.021

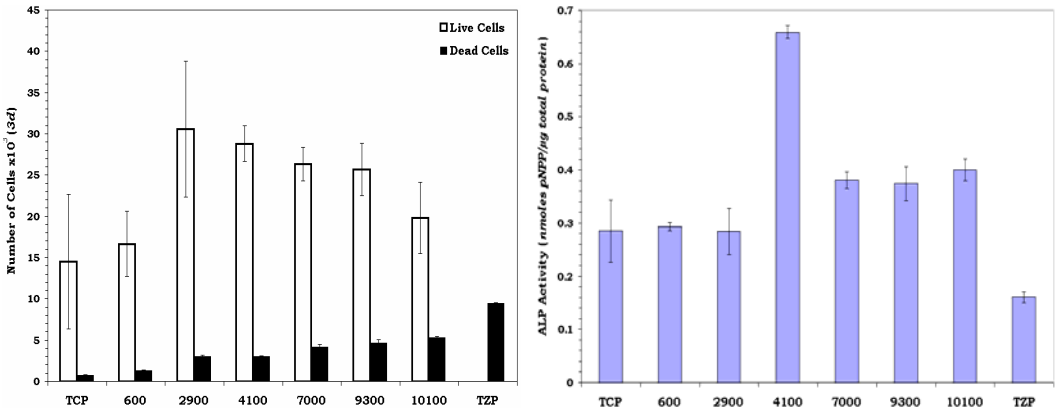

Fig. 6.3 (a) Live/Dead (*cytotoxicity*) data and (b) ALP activity data for Zn- doped β-TCP.

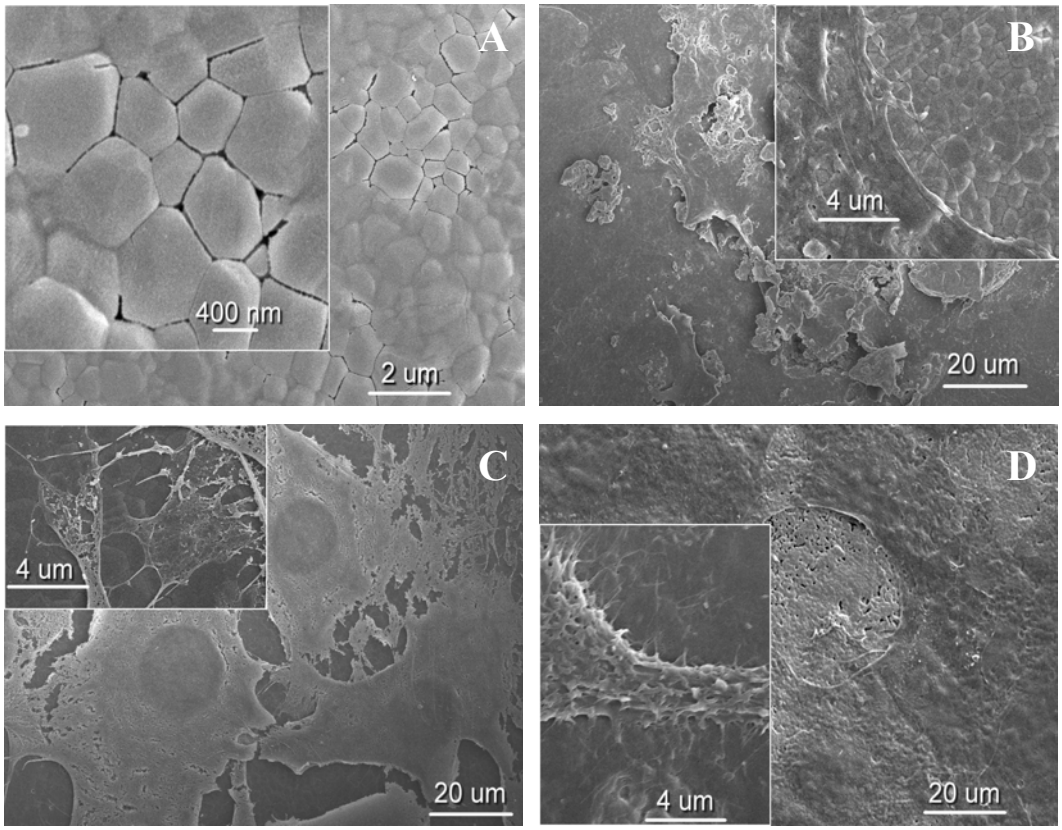

Fig. 6.4 SEM micrographs of osteoblast cells on (a) 0 ppm (pure β-TCP), (b) 2900 ppm, (c) 4100 ppm, and (d) 7000 ppm Zn-β-TCP pellet

enzyme activity. The 2900 ppm Zn-containing sample surfaces (Fig. 6.4b) showed a high degree of osteoblast coverage, and the inset in Figure 6.4b displayed quite a significant degree of cell spreading. The cell nuclei became visible even by the SEM images on 4100 ppm Zn-containing β-TCP samples (Fig. 6.4c). Typically, such imaging of cell nuclei could be achieved by using fluorescent microscopy together with special histological staining practices. In this case (i.e., 4100 ppm Zn), the cells were also proliferating into cytoskeletal stress fibers beyond extending their filopodia. When the Zn-content was increased to 7000 ppm (Fig. 6.4d), the cell attachment and spreading was still at quite high levels. On the surfaces of β-TZP samples, it was not possible to find even a single cell to image by the SEM, confirming the cytotoxicity results of Figure 6.3a.

Although the sample preparation routes of the two studies differed from one another significantly, the findings of the present work enhanced those of Ito *et al*.,[45] especially at the ppm level Zn-doping into β-TCP. In vivo resorbability of the samples of this study must be tested. The search for more reliable ways of Zn-doping in calcium phosphates (HA, TCP or biphasic HA-TCP) and the *in vitro* and *in vivo* characterization of the resultant samples seems to be an exciting field of biomaterials research.[58-62]

6.4. Conclusions

(1) Aqueous co-precipitation was used for synthesizing ppm-level Zn-doped β-TCP precursor nanopowders. This method was suitable to produce 600, 2900, 4100, 7000, 9300 and 10100 ppm Zn-containing β-TCP samples after calcination at 1000°C for 6 hours in air.

(2) Zinc was found to influence the grain growth characteristics and densification of β-TCP samples. 4100 ppm Zn-doped β-TCP sample was observed to have the highest bulk density within the range of dopant levels studied in this work.

(3) *In vitro* cell culture tests performed with mouse osteoblast-like cells showed the significant effect of ppm level presence of Zn in β-TCP samples in enhancing the osteoblastic activity, in direct comparison to pure β-TCP and β-TZP. The

Live/Dead cytotoxicity counts and alkaline phosphatase activity data were collected for all the samples.

(4) Live/Dead counts were peaked for the 2900 ppm Zn-β-TCP samples, whereas the ALP activity was found to be the highest for the 4100 ppm Zn-containing β-TCP samples.

6.5 References

1. A.S. Posner, E.D. Eanes, R.A. Harper, I. Zipkin. X-ray diffraction analysis of the effect of fluoride on human bone apatite. *Arch Oral Biol* **8** (1963) 549-570.

2. S.W. Leung, A.T. Jensen, Factors controlling the deposition of calculus. *Int Dent J* **8** (1958) 613-626.

3. H. Llory, R.M. Frank. Ultrastructure of carious dentin. *Actual OdontoStomat* **23** (1969) 507-522.

4. R.Z. LeGeros. Calcium Phosphates in Oral Biology and Medicine. Karger; New York 1991.

5. R. Tang, W. Wu, M. Haas, G.H. Nancollas. Kinetics of Dissolution of b-Tricalcium Phosphate. *Langmuir* **17** (2001) 3480-3485.

6. W. Wu, R. Tang, M. Haas, G.H. Nancollas. Constant Composition Dissolution Kinetics of Mixed Phases I. Synthetic Calcium Phosphates. *J Coll Interf Sci* **244** (2001) 347-352.

7. H. McDowell, W.E. Brown, J.R. Sutter. Solubility study of calcium hydrogen phosphate: ion-pair formation. *Inorg Chem* **10** (1971) 1638.

8. H.Yuan, J.D. DeBruijn, Y. Li, J. Feng, Z. Yang, K. de Groot, X. Zhang. Bone formation induced by calcium phosphate ceramics in soft tissue of dogs: a comparative study between porous alpha-TCP and beta-TCP. *J Mater Sci Mater M* **12** (2001) 7-13.

9. R.D.A. Gaasbeek, H.G. Toonen, R.J. van Heerwaarden, P. Buma. Mechanism of bone incorporation of beta-TCP bone substitute in open wedge tibial osteotomy in patients. *Biomaterials* **26** (2005) 6713-6719.

10. R.Z. LeGeros. Properties of osteoconductive biomaterials: Calcium phosphates. *Clin Orthop Relat R* **395** (2002) 81-98.

11. J. Wiltfang, H.A. Merten, K.A. Schlegel, S.S. Mosgau, F.R. Kloss, S. Rupprecht, P. Kessler. Degradation characteristics of alpha and beta tri-calcium- phosphate (TCP) in Minipigs. *J Biomed Mater Res B* **63** (2002) 115-121.

12. M. Merialdi, L.E. Caulfield, N. Zavaleta, A. Figuerota, K.A. Costigan, F. Dominici, J.A. Dipietro. Randomized controlled trial of prenatal zinc supplementation and fetal bone growth. *Am J Clin Nutr* **79** (2004) 826-830.

13. E.W. Murphy, B.W. Willis, B.K. Watt. Provisional Tables on the Zinc Content of Foods. *J Am Diet Assoc* **66** (1975) 345-355.

14. S. Cin, E. Unal, A. Pamir, B. Kologlu, A.O. Cavdar. Blood zinc (plasma, red blood cell zinc) and insulin-like growth factor-1 in children from an 'impoverished" area in Ankara. *J Trace Elem Exp Med* **14** (2001) 31-34.

15. D.G. Barceloux. Zinc. *J Toxicol Clin Toxic* **37** (1999) 279-292.

16. M. Hambidge. Human Zinc Deficiency. *J Nutr* **130** (2000) 1344S-1349S.

17. D. Chen, L.C. Waite, W.M. Pierce. *In vitro* bone resorption is dependent on physiological concentrations of zinc. *Biol Trace Elem Res* **61** (1998) 9-18.

18. G. Oner, B. Bhaumick, R.M. Bala. Effect of zinc deficiency on serum somatomedin levels and skeletal growth in young rats. *Endocrinology* **114** (1984) 1860-1863.

19. M. Yamaguchi, H. Oishi, Y. Suketa. Stimulatory effect of zinc on bone formation in tissue culture. *Biochem Pharmocol* **36** (1987) 4007-4012.

20. B.L. Vallee, K.H. Falchuk. The biochemical basis of zinc physiology. *Physiol Rev* **73** (1993) 79-118.

21. A. Togari, S. Arakawa, M. Arai, S. Matsumoto. Alteration of *in vitro* bone metabolism and tooth formation by zinc. *Gen Pharmacol* **24** (1993) 1133-1140.

22. W.R. Holloway, F.M. Collier, R.E. Herbst, J.M. Hodge, G.C. Nicholson. Osteoblast-mediated effects on zinc on isolated rat osteoclasts: Inhibition of bone resorption and enhancement of osteoclast number. *Bone* **19** (1996) 137-142.

23. R.M. Angus, P.N. Sambrook, N.A. Pocock, J.A. Eisman. Dietary intake and bone mineral density. *Bone Miner* **4** (1988) 265-277.

24. M. Hertzberg, J. Foldes, R. Steinberg, J. Menczel. Zinc excretion in osteoporotic women. *J Bone Miner Res* **5** (1990) 251-257.

25. P.D. Saltman, L.G. Strause. The role of trace minerals in osteoporosis. *J Am Coll Nutr* **12** (1993) 384-389.

26. D.L. Bougle, J.P. Sabatier, G.G. Souquieres, F.G. Metz, D. Laroche, P. Jauzac, F. Bureau. Zinc status and bone mineralisation in adolescent girls. *J Trace Elem Med Bio* **18** (2004) 17-21.

27. M. Yamaguchi, A. Igarashi, S. Uchiyama. Bioavailability of Zinc Yeast in Rats: Stimulatory Effect on Bone Calcification *in vivo*. *J Health Sci* **50** (2004) 75-81.

28. M. Yamaguchi, H. Miwa. Stimulatory effect of beta-alanyl-L-histidinato zinc. on bone formation in tissue culture. *Pharmacology* **42** (1991) 230-240.

29. Z.J. Ma, M. Yamaguchi. Alteration in bone components with increasing age of newborn rats: role of zinc in bone growth. *J Bone Miner Metab* **18** (2000) 264-270.

30. Z.J. Ma, M. Yamaguchi. Role of endogenous zinc in the enhancement of bone protein synthesis associated with bone growth of newborn rats. *J Bone Miner Metab* **19** (2001) 38-44.

31. Z.J. Ma, M. Yamaguchi. Stimulatory Effect of Zinc on Deoxyribonucleic Acid Synthesis in Bone Growth of Newborn Rats: Enhancement with Zinc and Insulin-Like Growth Factor-I. *Calcif Tissue Int* **69** (2001) 158-163.

32. P.J. Fraker. Roles for cell death in zinc deficiency. *J Nutr* **135** (2005) 359.

33. T.A. Fuierer, M. LoRe, S.A. Puckett, G.H. Nancollas. A mineralization adsorption and mobility study of hydroxyapatite surfaces in the presence of zinc and magnesium ions. *Langmuir* **10** (1994) 4721-4725.

34. A. Bigi, E. Foresti, M. Gandolfi, M. Gazzano, N. Roveri. Inhibiting effect of zinc on hydroxylapatite crystallization. *J Inor Biochem* **58** (1995) 49-58.

35. A. Bigi, E. Foresti, M. Gandolfi, M. Gazzano, N. Roveri. Isomorphous substitutions in b-tricalcium phosphate: the different effects of zinc and strontium. *J Inorg Biochem* **66** (1997) 259-265.

36. R.Z. LeGeros, Caries Res. 31 (1997) 434-440.

37. R.Z. LeGeros, C.B. Bleiwas, M. Retino, R. Rohanizadeh, J.P. LeGeros. Zinc effect on the *in vitro* formation of calcium phosphates: Relevance to clinical inhibition of calculus formation. *Am J Dent* **12** (1999) 65-71.

38. N. Kanzaki, K. Onuma, G. Treboux, S. Tsutsumi, A. Ito. Inhibitory effect of magnesium and zinc on crystallization kinetics of hydroxyapatite (0001) face. *J Phys Chem B* **104** (2000) 4189-4194.

39. A. Ito, K. Ojima, H. Naito, N. Ichinose, T. Tatseishi. Preparation, solubility, and cytocompatibility of zinc-releasing calcium phosphate ceramics. *J Biomed Mater Res* **50** (2000) 178-183.

40. H. Kawamura, A. Ito, S. Miyakawa, P. Layrolle, K. Ojima, N. Ichinose, T. Tateishi. Stimulatory effect of zinc-releasing calcium phosphate implant on bone formation in rabbit femora. *J Biomed Mater Res* **50** (2000) 184-190.

41. M. Otsuka, S. Marunaka, Y. Matsuda, A. Ito, P. Layrolle, H. Naito, N. Ichinose. Calcium level-responsive in-vitro zinc release from zinc containing tricalcium phosphate (ZnTCP). *J Biomed Mater Res* **52** (2000) 819-824.

42. N. Kanzaki, K. Onuma, G. Treboux, S. Tsutsumi, A. Ito. Effect of impurity on two-dimensional nucleation kinetics: Case studies of magnesium and zinc on hydroxyapatite (0001) face. *J Phys Chem B* **105** (2001) 1991-1994.

43. A. Ito, H. Kawamura, M. Otsuka, M. Ikeuchi, H. Ohgushi, K. Ishikawa, K. Onuma, N. Kanzaki, Y. Sogo, N. Ichinose. Zinc-releasing calcium phosphate for stimulating bone formation . *Mater Sci Eng* C 22 (2002) 21-25.

44. K. Ishikawa, Y. Miyamoto, T. Yuasa, A. Ito, M. Nagayama, K. Suzuki. Fabrication of Zn containing apatite cement and its initial evaluation using human osteoblastic cells. *Biomaterials* **23** (2002) 423-428.

45. A. Ito, H. Kawamura, S. Miyakawa, P. Layrolle, N. Kanzaki, G. Treboux, K. Onuma, S. Tsutsumi, *J Biomed Mater Res* **60** (2002) 224-232.

46. Y. Sogo, T. Sakurai, K. Onuma, A. Ito. The most appropriate (Ca plus Zn)/P molar ratio to minimize the zinc content of ZnTCP/HAP ceramic used in the promotion of bone formation. *J Biomed Mater Res* **62** (2002) 457-463.

47. H. Kawamura, A. Ito, T. Muramatsu, S. Miyakawa, N. Ochiai, T. Tateishi. Long-term implantation of zinc-releasing calcium phosphate ceramics in rabbit femora. *J Biomed Mater Res A* **65** (2003) 468-474.

48. M. Ikeuchi, A. Ito, Y. Dohi, H. Ohgushi, H. Shimaoka, K. Yonemasu, T. Tateishi. Osteogenic differentiation of cultured rat and human bone marrow cells on the surface of zinc-releasing calcium phosphate ceramics. *J Biomed Mater Res A* **67** (2003) 1115-1122.

49. Y. Sogo, A. Ito, M. Kamo, T. Sakurai, K. Onuma, N. Ichinose, M. Otsuka, R.Z. LeGeros. Hydrolysis and cytocompatibility of zinc-containing alpha-tricalcium phosphate powder . *Mater Sci Eng* C **24** (2004) 709-715.

50. M. Otsuka, Y. Ohshita, S. Marunaka, Y. Matsuda, A. Ito, N. Ichinose, K. Otsuka, W.I. Higuchi. Effect of controlled zinc release on bone mineral density from injectable Zn-containing beta-tricalcium phosphate suspension in zinc-deficient diseased rats. *J Biomed Mater Res A* **69** (2004) 552-560.

51. A. Ito, M. Otsuka, H. Kawamura, M. Ikeuchi, H. Ohgushi, Y. Sogo, N. Ichinose. Zinc-containing tricalcium phosphate and related materials for promoting bone formation. *Curr Appl Phys* **5** (2005) 402-406.

52. P. Layrolle, A. Ito, T. Tateishi. Sol-gel synthesis of amorphous calcium phosphate and sintering into microporous hydroxyapatite bioceramics. *J Am Ceram Soc* **81** (1998) 1421-1428.

53. L. Yubao, Z. Xingdong, K. de Groot. Hydrolysis and phase transition of alpha-tricalcium phosphate. *Biomaterials* **18** (1997) 737-741.

54. T. Ivanova, O.V.F. Kamenetskaya, A.B. Koltsov, V.L. Ugolkov. Crystal structure of calcium-deficient carbonated hydroxyapatite. Thermal decomposition. *J Solid State Chem* **160** (2001) 340-349.

55. A.C. Tas, F. Korkusuz, M. Timucin, N. Akkas. An Investigation of the Chemical Synthesis and High-Temperature Sintering Behaviour of Calcium Hydroxyapatite (HA) and Tricalcium Phosphate (TCP) Bioceramics. *J Mater Sci Mater M* **8** (1997) 91-96.

56. I.R. Gibson, I. Rehman, S.M. Best, W. Bonfield. Characterization of the transformation from calcium-deficient apatite to beta-tricalcium phosphate. *J Mater Sci Mater M* **11** (2000) 799-804.

57. B.S. Moonga, D.W. Dempster. Zinc is a potent inhibitor of osteoclastic **bone** resorption *in vitro*. *J Bone Miner Res* **10** (1995) 453-457.

58. S. Loher, W.J. Stark, M. Maciejewski, A. Baiker, S.E. Pratsinis, D. Reichardt, F. Maspero, F. Krumeich, D. Gunther. Fluoro-apatite and calcium phosphate nanoparticles by flame synthesis. *Chem Mater* **17** (2005) 36.

59. F. Miyaji, Y. Kono, Y. Suyama. Formation and Structure of Zinc-Substituted Calcium Hydroxyapatite. *Mater Res Bull* **40** (2005) 209-220.

60. H. Storrie, S.I. Stupp. Cellular Response to Zinc-containing Organoapatite: An *in vitro* study of proliferation, alkaline phosphatase activity and biomineralization." *Biomaterials* **26** (2005) 5492-5499.

61. X. Yin, L. Calderin, M.J. Stott, M.Sayer. Density Functional Study of Structural Electronic and Vibrational Properties of Mg and Zn -doped Tricalcium Phosphate Biomaterial. *Biomaterials* **23** (2002) 4155-4163.

62. E. Chassot, H. Oudadesse, J. Irigaray, E. Curis, S. Benazeth, I. Nicolis. Differentiation of biological hydroxyapatite compounds by infrared spectroscopy, X-ray diffraction and extended X-ray absorption fine structure. *J Appl Phys* **90** (2001) 6440-644.

CHAPTER 7

ENHANCED BIOMIMETIC COATING OF COLLAGEN AND ITS *IN VITRO* EXAMINATION

Abstract

Coating porous collagen membranes via a biomimetic method with a layer of carbonated apatitic calcium phosphates was performed in this study. The biomimetic process involves soaking the substrates in a simulated body fluid (SBF) solution. The goal of this research was to enhance process kinetics of biomimetic coating process by employing novel composition of SBF. For this purpose, an improved version of SBF solution (*tas*-SBF, hereafter referred to as *t*-SBF) was employed and is a TRIS-HCl buffered solution with a HCO_3^- ion concentration of 27 mM. With the use of *t*-SBF, apatitic calcium phosphate coatings homogeneously covered the collagen surface were performed over a 7 day period. This is a significant enhancement in the coating kinetics as opposed to previous attempts. All samples were characterized by X-Ray Diffraction (XRD), Fourier Transformed Infrared (FTIR) spectroscopy, and Field-Emission Scanning Electron Microscopy (FE-SEM). Mouse osteoblasts (7F2) were used to compare *in vitro* response of untreated collagen and SBF-coated collagen membranes via the alkaline phosphatase activity, cell density and cell proliferation tests. These *in vitro* results showed a more favorable response to the apatitic calcium phosphate coating over the untreated collagen membrane.

(This work is submitted to *J Eur Ceram Soc* 2007)

7.1. Introduction

A composite of collagen and apatite is of special interest because of their compositional similarity with bone.[1-4] In recent years, there is an increased effort to produce apatite-collagen composite materials by innovative biomimetic processing.[4-11] Biomimetic coating process is employed to coat collagen substrates to synthesize the apatite-collagen composites.[12-20] This coating process involves soaking the substrate in a supersaturated or metastable solution at human body temperatures (37°C), which in turn forms several-micron-thick bioactive layers of apatitic calcium phosphate nano-aggregates. It has been determined that acellular physiological solutions such as synthetic or simulated body fluid (SBF) solutions are able to induce such bioactive apatitic calcium phosphate layer on metals, ceramics, and polymers (with proper surface treatments).[21-23]

SBF solutions maintain physiological conditions and are able to mimic the ionic concentrations of human plasma. In 1990, Kukubo popularized one such composition known as conventional simulated body fluid or "*c*-SBF".[21] However, one disadvantage of *c*-SBF is that it contains lower carbonate ion concentration than human plasma. In 1999, Tas et al.[24, 25] increased the carbonate ion concentration in a TRIS-HCl buffered SBF solution (*tas*-SBF, hereafter referred to as *t*-SBF) to 27 mM (same as that of human plasma) while Bigi et al.[26] did similar experiments using a HEPES-NaOH buffered SBF solution. Kokubo et al.[27] later increased the carbonate ion concentration of their c-SBF solutions from 4.2 to 27 mM by using HEPES-NaOH buffer and named it "revised-SBF" (*r*-SBF). A detailed historical development of acellular physiological solutions since 1882 has been summarized by the present authors elsewhere.[28] The following sections provide a brief review of biomimetic coating of collagen.

7.1.1 *Biomimetic Coating of Collagen – A Brief Review*

It is reported in the literature that the biomimetic coating kinetics of collagen is very slow.[14] Even after 4 weeks of soaking time, the collagen surface was not fully covered by apatitic calcium phosphates.[13] Several studies indicate that an increase in the bioactivity of collagen can be achieved by modifying the normal soaking procedures.[12-20] These methods include either changing the

chemistry of collagen or adding a compound to *c*-SBF solutions. Rhee et al.[12] performed their experiments by soaking the collagen in SBF solutions with and without citric acid. Although citric acid is known to be an inhibitor of calcium phosphate formation,[29] they determined that carbonated apatitic calcium phosphates formed only on collagen in the SBF solution with an addition of citric acid.[12] The investigation of nucleation of apatite by the same authors indicated that the coating is critically dependent on the carboxylate group of collagen.[13] These results were later substantiated by Zhang et al.,[14] who studied the growth of apatitic calcium phosphates on the collagen membrane by phase-contrast microscopy. They suggested that the charged functional groups of collagen membranes play a key role in the growth of apatitic calcium phosphates.[14] Several theories were proposed to explain the formation of apatite layer on materials soaking in an SBF solution. It was hypothesized that the apatite layer forms when the material surface is negatively charged[13, 30] and/or when silanol groups[1,31] are present on the surface. Chemical treatment by soaking the collagen discs in TEOS at room temperature for 1h was performed by Andrade et al.[15]. This treatment formed a silica coating on the collagen surface resulting in a negative charge upon contact with the SBF solution, thus increasing the bioactivity.[15] In 10 days, the surface was not fully covered and the underlying collagen fibers were still visible.[15] Lickorish et al.[16] deposited apatitic calcium phosphates on collagen by soaking them in SBF in the presence of calcium silicate glass. They used two different solutions, a nucleation solution and a growth solution. The nucleation solution was formed by dissolving calcium silicate in SBF and a growth solution was just SBF solution.[16] The calcium silicate glass played an important role in initiating apatite deposition on collagen substrates because when no glass was present in the nucleating solution, apatite deposition failed to occur even after soaking in the growth solution for 11 days. These findings support the hypothesis of deposition via silanol mechanism. In this process, as reported in ref.,[16] a uniform thin coating of calcium phosphate forms on collagen after approximately a total of 2 weeks of soaking time. The role of phosvitin on the nucleation of apatitic calcium phosphates on collagen was investigated by Kobayashi et al.[17] by

forming a collagen-phosvitin composite. They found that the rate of calcium phosphate nucleation is enhanced in the presence of phosvitin, and also hypothesized that phosvitin controlled the orientation of the precipitated calcium phosphates.[17] Li et al.[18] demonstrated the fabrication of three dimensional collagen/wollastonite composites using freeze-drying methods. These collagen/wollastonite composites exhibited better deposition of apatitic calcium phosphates after soaking in SBF for 7 days and the surface was uniformly covered in 15 days, thus decreasing the coating time.[18] Eglin et al.[19] prepared collagen hydrogel containing bioactive glass (CaO-P_2O_5-SiO_2) and silica sol-gel particles and studied their *in vitro* apatite-forming ability in SBF solution. The silica-collagen hydrogel composite precipitated calcium phosphate whereas silica particles and collagen hydrogel alone did not, indicating a possible synergistic effect between the collagen and silica on the apatite-forming ability.[19] The bioactivity of the nano-HA-collagen composite was also investigated by Lin et al. [20]. Their results show that the composite was coated with apatitic calcium phosphates after 2 weeks of soaking in SBF.[20] From these reported studies, it can be concluded that modification of collagen or addition to SBF increases the kinetics of the coating process and homogeneous coating of the collagen surface in *c*-SBF takes at least 1-2 weeks. Even after modification, this process appears lengthy as the dissolution of collagen in the liquid medium poses a relevant issue.

In view of these findings and the evolution of *r*-SBF[27] with 27 mM HCO_3^- concentration, attempts by Girija et al. were made to coat collagen in *r*-SBF.[32] *r*-SBF showed improvement in coating rate and was able to coat the collagen in just 2 weeks without any modification to either collagen or SBF.[32] The reported SEM micrographs show that the morphology of the apatitic calcium phosphates deposited on the collagen substrate by *r*-SBF differed from those formed by *c*-SBF. The same features are reported by Bigi et al.[26] that showed the spherical aggregates instead of nano-needles or nano-platelets morphology on gelatin films. In order to further increase the coating rate, the presence of polyacrylic acid (PAA) in collagen and in SBF was examined.[33] The results showed that PAA not

only affected the microstructure of apatitic calcium phosphates but their mineralization as well.[33]

7.1.2 *Effects of Various Coating Parameters on Coating Rate and Morphology*

As previously reported, the coating rate was slow when collagen was soaked in *c*-SBF, even with modifications. The reason for the slow apatite inducing ability of *c*-SBF is due to the low HCO_3^- concentration. A study by Dorozhkina et al.[34] emphasized the influence of HCO_3^- concentration in a TRIS-free SBF solution on the morphology and thickness of calcium phosphate coatings formed. They discovered an increase of the HCO_3^- concentration in *c*-SBF from 4.2 to 27 mM resulted in the formation of homogeneous and much thicker carbonated hydroxyapatite layers.[34] Similar results were obtained by Jalota et al.[28] where they compared the coating abilities of TRIS-HCl buffered SBF solutions of 4.2 mM and 27 mM HCO_3^- concentration. They discovered that a *t*-SBF solution with a HCO_3^- concentration of 27 mM was able to coat the titanium strips faster than c-SBF solutions with a concentration of 4.2 mM HCO_3^-.[28] Thus, in order to increase the kinetics of the coating process in collagen, the present authors suggest increasing carbonate ion concentration to 27 mM of the SBF.

A morphological difference was observed in the coatings produced by r-SBF in comparison to those in c-SBF. This difference was also observed on Ti6Al4V substrates in a recent study, where 27 mM HCO_3^- concentrated TRIS-HCl buffered (*c*- and *t*-) and HEPES-NaOH buffered (*r*-) SBF solutions were compared.[28] *c*-SBF and *t*-SBF solutions always produced round globules consisting of intermingled nano-needles of calcium phosphates on Ti6Al4V strips whereas *r*-SBF solutions produced nearly spherical aggregates.[28] This morphological difference between these SBF solutions is possibly due to differences in the buffer used for preparation. Dorozhkina et al.[34] emphasized that HEPES was rather unstable, in comparison to TRIS, and that it easily loses some of the initially present dissolved carbonates. Kokubo et al.,[35] who developed the HEPES-buffered *r*-SBF composition, also reported that *r*-SBF would release CO_2 gas from the fluid. During longer storing periods, there was a decrease in HCO_3^- concentration and an increase in pH value.[35] Furthermore, they stated that *r*-SBF

is unsuitable for long-term use in the biomimetic coating processes due to its instability.[35] Thus, the present authors suggest their preference for the TRIS-buffer over the HEPES-buffer in making the SBF solution.

It was also reported that the rat osteoblast favorably responded to the coating produced by TRIS-HCl buffered SBF solutions.[28] This is due to the resemblance of the thickness of the nanoplatelets or nanoneedles (20-30 nm) produced by biomimetic coatings of TRIS-HCl buffered SBF solutions with the bone mineral.[36] Thus, 27 mM HCO_3^- concentrated TRIS-HCl buffered SBF solutions is the most effective SBF solution in the coating of artificial materials.

7.1.3 *Objectives*

The current literature revealed that biomimetic coating of collagen was attempted using *c*-SBF and *r*-SBF. No attempts were made to increase the coating rate of collagen by increasing the HCO_3^- ion concentration (to 27 mM) in a TRIS-HCl buffered SBF solution (*t*-SBF). The performance of *t*-SBF was determined to be superior than *c*- and *r*-SBF for Ti6Al4V substrates.[28] In this present study, we soaked porous collagen in *t*-SBF to evaluate the characteristics of the formed apatitic calcium phosphate layer. The broad objective of the present work was to establish a crack-free homogeneous coating with enhanced kinetics utilizing *t*-SBF. A second objective was to compare the osteoblast response to the pristine collagen surface with the apatite deposited collagen substrate.

7.2. Experimental Procedure

7.2.1 ***Collagen Preparation*.** Porous membranes of collagen of approximately 1 mm thickness were obtained from Collagen Matrix Inc. (Franklin Lakes, NJ). These membranes were first cut into 10 x 10 mm strips and then thoroughly washed with deionized water. After washing, the strips were directly soaked in 1.5x *t*-SBF at 37±1ºC for a period of 3 and 7 days. The following paragraph describes the procedure for preparing *t*-SBF.

7.2.2 ***t-SBF Preparation*.** The details of preparing the 1x *t*-SBF solution are reported in Chapter 3, Section 3.2.2.

7.2.3 ***Coating Process.*** The coating was performed in 100 mL-capacity glass bottles, which contained 90 mL of SBF solution and the floating clean collagen membrane. Sealed bottles were kept in an oven at 37±1°C for respective 3 and 7 day intervals. After every 48 hours, the used SBF solution was replenished. Both sets of recovered samples for the respective 3 and 7 day periods were thoroughly washed with deionized water, followed by a critical point drying process.

7.2.4 ***Characterization.*** All samples were characterized by powder x-ray diffraction (XRD) (XDS 2000, Scintag, Sunnyvale, CA) using a CuK_{α} radiation at 40 kV and 30 mA, with a step size of 0.03° and preset time of 1 second at each step. Fourier-transform infrared spectroscopy (FTIR) (Nicolet 550, Thermo-Nicolet, Woburn, MA) measurements were performed using a diamond ATR holder over the wave number range of 4000-525 cm^{-1} using 256 scan rate with a resolution of 4 cm^{-1}. The surface topography of untreated collagen membrane and changes acquired upon soaking were analyzed using a field-emission scanning electron microscopy (FESEM) (S-4700, Hitachi, Tokyo, Japan) at 5kV.

7.2.5 ***In Vitro Cell Culture Tests.*** 7F2 rat osteoblast cells (CRL-12557, American Type Culture Collection, Rockville, MD) were grown on 75 cm^2 culture flasks at 37ºC and 50% CO_2 in α-MEM with 2 mM 1-glutamine and 1 mM sodim pyruvate without ribonucleosides and deoxyribonucleosides, augmented by 10% FBS. The culture medium was changed every other day until the cells reached a confluence of 90-95%, as determined visually with an inverted microscope. The cells were then passaged using trypsin (2.5 g/L)/ EDTA (25mM) solution (Sigma-Aldrich Corp., St. Louis, MO, USA). The cells were further seeded at a concentration of 3500 cell/well on 0.14 cm^3 samples for various assays. Cell viability and alkaline phosphatase activity measurements were performed after 72 hours. The cell viability assessment was performed using Live/Dead® Viability/Cytotoxicity Kit (L-3224, Molecular Probes, Eugene, OR). A working solution was prepared by mixing 5µl aliquot of Component A (4 mM calcein AM solution in DMSO) to 10 ml of 4 mM EthD-1 solution (20 µl of the Component B to 10 ml of DPBS). 100 µl of this solution was added to the cell-containing samples along with 100 µl of cell-containing media. Samples were

incubated at room temperature for 30-45 minutes. After the prescribed time period, the fluorescence values were recorded at 494/517 nm for live cells and 528/617 nm for dead cells by using a standard curve obtained by seeding different number of cells in different wells. The alkaline phosphatase (ALP) activity was determined using the ALP concentration and the cell extracted protein concentration. The ALP concentration was calculated using Enzymatic Assay of Phosphatase Alkaline Kit (EC 3.1.3.1, Sigma-Aldrich Corp., St. Louis, MO, USA). A working reagent was prepared by first mixing 2.7 ml of Reagent A (1.0 M Diethanolamine Buffer with 0.50 mM Magnesium Chloride) with 0.30 ml of Reagent B (150 mM p-Nitrophenyl Phosphate Solution (pNPP) and then mixing the solution with 0.10 ml of cell-containing media. 100 µl of this solution was added to each well and thoroughly mixed and incubated at 37ºC for 30 minutes. Following incubation, the absorbance was recorded at 405 nm with the spectrophotometer at room temperature. The standard curve was obtained by plotting the absorbance measured at 405 nm for certain concentration against the concentration in µg/ml. ALP concentration of each sample was then determined using this standard curve and is expressend as µg-pNP/ml. The cell extracted protein concentration was determined in a two-step procedure. The protein was first extracted using M-PER™ Mammalian Protein Extraction reagent and then measured using BCA™ Protein Assay Kit. The cell samples were lysed by adding 200 µl of M-PER™ Reagent to each well plate and then shaken for 5 minutes. Lysate was collected and transferred to microcentrifuge tubes, followed by centrifuging at 4000g for 10 minutes to pellet the cell debris. Supernatant was transferred to clean tubes for analyzing the protein concentration. To measure the protein amount, a working reagent (WR) was prepared by mixing 50 parts of BCA™ Reagent A with 1 part of BCA™ Reagent B (50:1, Reagent A:B). 200 µl of the above mentioned WR was added to each well and thoroughly mixed. Following mixing, the well plate was covered and incubated at 37ºC for 30 minutes. The absorbance at 562 nm was measured with the spectrophotometer at room temperature. A standard curve was prepared by plotting the average blank-corrected 562 nm measurement for each BSA standard versus its concentration in

μg/ml. Cell extracted protein concentration was then determined by using this standard curve and expressed as μg/ml. The ALP activity was then calculated as follows; ALP Activity = [(μg pNP)/139] / μg(cell extracted protein) = μmoles pNPP/ μg cell protein. Osteoblast attachment/proliferation on the pellets was studied using SEM. Cells were first fixed by using 3.5% glutaraldehyde, and then dehydrated through sequential washings in 50%, 70%, 95% ethanol solutions, followed by 2 times in 100% ethanol. Samples were subsequently critical point-dried, prior to sputter-coating with a thin layer of Pt.

7.3. Results

7.3.1 *XRD Analysis*

The phase identification was performed by x-ray diffraction (XRD). The broad peak due to collagen membrane was observed in the 2θ range of 12°-30° in Figure 7.1a. After soaking in 1.5x *t*-SBF for 7 days, peaks of apatitic calcium phosphates were observed at 25.9, 28.7, 32.02, and 39.75 respectively (Fig. 7.1b). The broadening of the apatite peaks is due to the small crystallite size of apatite. Figure 7.1c shows the XRD trace of a rat bone. The XRD pattern formed on collagen after soaking in SBF matched exactly with that of the bone.

7.3.2 *FTIR Analysis*

We used FTIR spectroscopy in order to illustrate the formation mechanism of bone mineral-like apatite and the chemical interaction of apatite with the collagen membrane. The result shows the traces for untreated collagen (Fig. 7.2a), collagen soaked in *t*-SBF for a period of 7 days (Fig. 7.2b) and a rat bone (Fig. 7.2c). The FTIR trace of untreated collagen (Fig. 7.2a) shows the typical bands of N—H stretching at 3310 cm^{-1} for amide A, C—H stretching at 3080 cm^{-1} for amide B, C═O stretching at 1631 cm^{-1} for amide I, N—H deformation at 1549 cm^{-1} for amide II and N—H deformation at 1238 cm^{-1} for amide II bands. After soaking the collagen in SBF for 7 days (Fig. 7.2b), all the absorption bands of collagen disappeared except at 1557 and 1633 cm^{-1}. These two are the most intense bands of collagen and their intensity significantly decreased after soaking

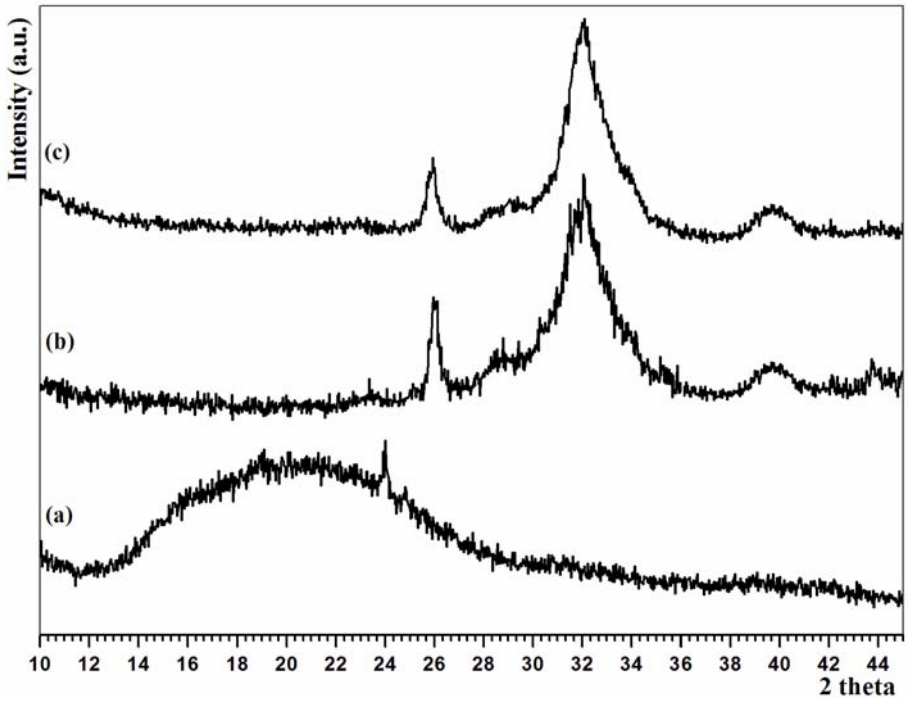

Fig. 7.1 XRD traces of (a) untreated collagen; (b) collagen soaked in *t*-SBF for 7 days; and (c) rat bone.

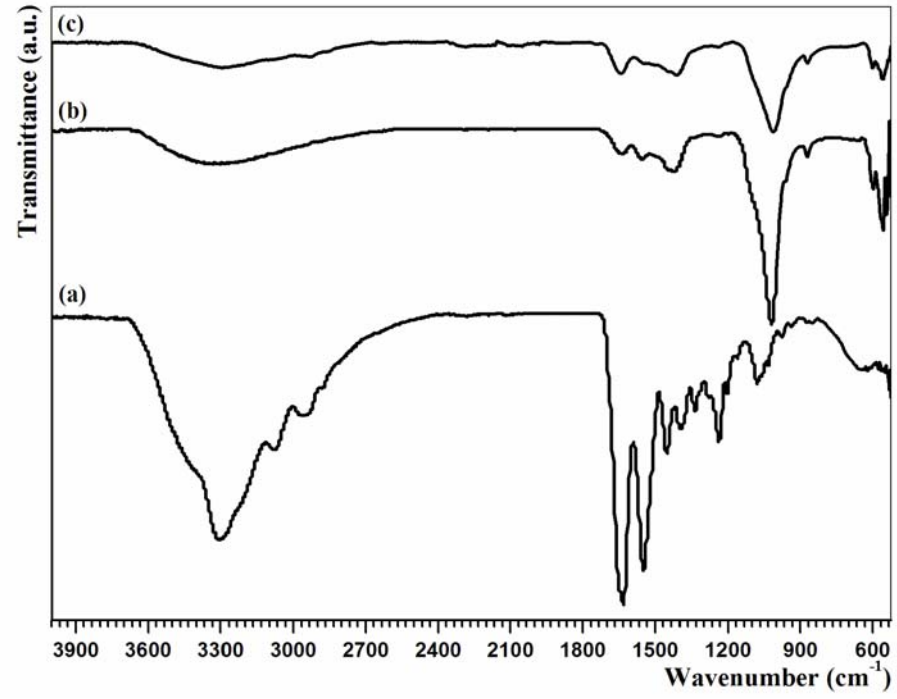

Fig. 7.2 FTIR traces of (a) untreated collagen; (b) collagen soaked in *t*-SBF for 7 days; and (c) rat bone.

in SBF for 7 days. This is considered an evidence of a chemical reaction between calcium phosphate deposited with the collagen and formation of a thick coating layer on collagen. Interestingly, the calcium phosphate formation did not affect the characteristics of collagen. The calcium phosphate coating was confirmed to be apatitic in nature due to the presence of PO_4^{3-} bands at 1021, 608, and 561 cm^{-1}. The crystallinity of this apatite is low because the spectrum is not so sharp as that of well crystallized HA. The absorption bands present at 1420-1470 cm^{-1} and 870 cm^{-1} also revealed the presence of CO_3^{2-}. Some minor peaks are also evident at 961, 1122, and 1230 cm^{-1}, which were due to the presence of HPO_4^{2-} ion in the coating. Therefore, FTIR results confirmed that the apatitic calcium phosphate also contained CO_3^{2-} and HPO_4^{2-} ions. The absence of the stretching and the vibrational modes of O-H group at 3571 and 639 cm^{-1} confirmed that these coatings might not simply be named as hydroxyapatite.

In order to further analyze the coatings, we also collected the FTIR data from rat bone (after cleaning and removing the bone marrow) which is depicted in Figure 7.2c. The similarity of the coating with the bone mineral (rat bone) is shown in Figure 7.2. Bone mineral is not simply "Hydroxyapatite" but is a defective and rather complex material doped with several mono- or divalent cations (Na^+, K^+, Mg^{2+}, Zn^{2+}, Fe^{2+}, etc. upto 1.3 wt.%) as well as with CO_3^{2-} (5.8 wt.%) and HPO_4^{2-} ions with a generic formula of $Ca_{8.3}(PO_4)_{4.3}(HPO_4, CO_3)_{1.7}(OH, CO_3)_{0.3}$. The FTIR pattern of bone mineral also shows the presence of CO_3^{2-} and HPO_4^{2-}, in the coatings of this study. Henceforth, we will refer the apatitic calcium phosphate coating as bone mineral-like apatite.

7.3.3 *Microstructural Analysis*

The pore sizes (200 to 300 μm) and the strut morphology of the as-received collagen foams are shown in the FE-SEM micrographs (Fig. 7.3a, low magnification and Fig. 7.3b, high magnification). The initial progress of the SBF-coating, as a function of soaking time was also studied via FE-SEM (Figs. 7.4a and b). The low magnification (Fig. 7.4a) micrographs show that only a part of the collagen surface is covered with bone mineral such as apatite after soaking in *t*-SBF for 3 days. At higher magnifications, the globules of apatite become clearly

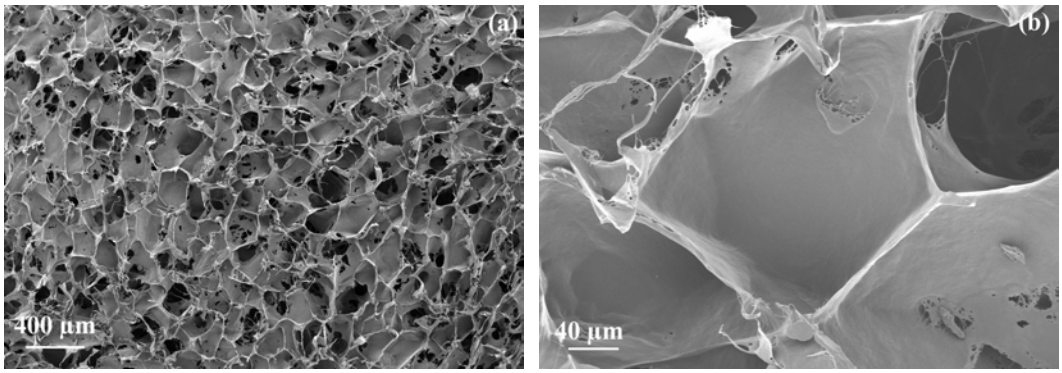

Fig. 7.3 FE-SEM micrographs of porous collagen prior to SBF soaking (a) low and (b) high magnification.

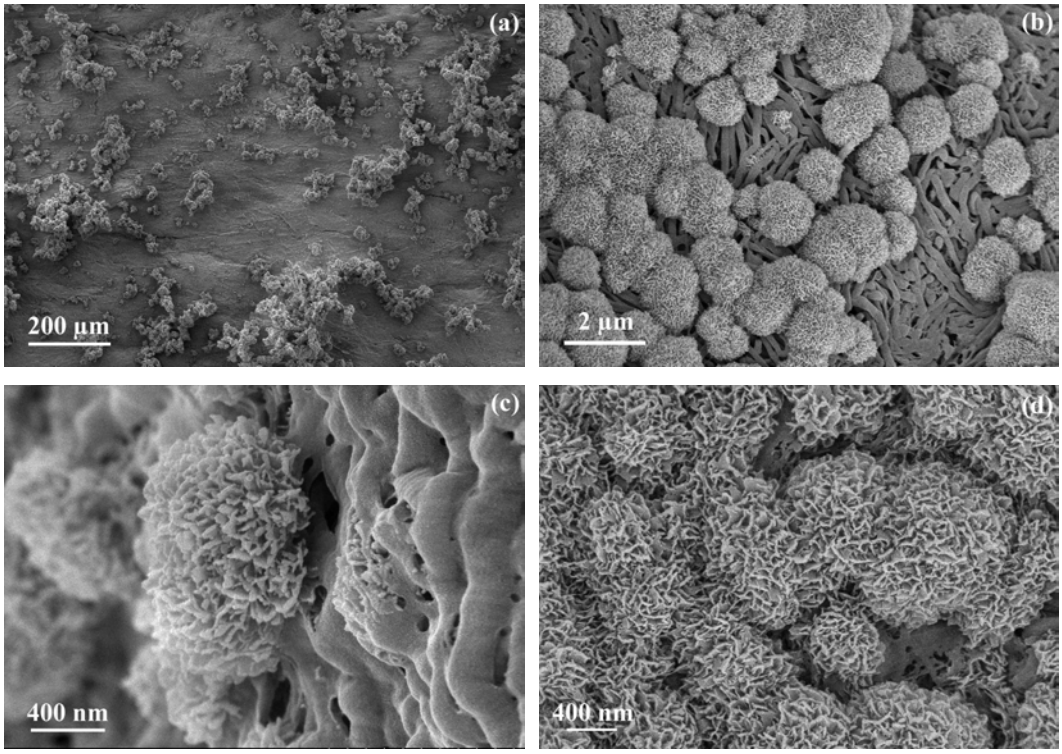

Fig. 7.4 FE-SEM micrographs of collagen membrane soaked in *t*-SBF for a period of 3 days; (a) the collagen surface not fully covered in 3 days, (b) characteristic bone-mineral like apatite globules, (c) their attachment and (d) nanoporous texture of these globules becomes readily visible.

visible along with the underlying collagen fibrils (Fig. 7.4b). At this point, it is hard to predict the nature of attachment of these globules with the collagen. It can be either be a physically or chemically bonded attachment.

In the case of physical attachment, the precipitates that form in the SBF loosely attach to the collagen surface. For chemically bonded attachments, there should be an interaction between bone mineral-like apatite and collagen. Figure 7.4c shows a single globule attached to the surface of the collagen surface. In the same figure, initial growth of SBF produced bone mineral like apatite is evident on the collagen surface. Also, since the strip was floating near the top in the SBF containing bottle, the chances of gravity driven segregation (produced in the SBF) on the surface is minimized. This means that it cannot be a physical attachment process, but a chemically bonded process instead. (Fig. 7.4d) shows a high magnification micrograph of the same area. In this micrograph interlocked nano-needle morphology is seen. A similar kind of morphology is also seen on other materials (Ti, Ti6Al4V, calcium phosphates) when soaked in SBF.[28] At this magnification, we observed that the whole surface is not fully coated. Thus, we conclude that we needed to increase the coatings time so that the whole surface is coated fully and homogeneously.

Based on our observation, we increased the time period of soaking the porous collagen membrane to 7 days. FE-SEM micrographs of Figure 7.5a and d represent our results. The low magnification micrographs show that both the upper struts of foams as well as those underneath are homogeneously coated (Fig. 7.5a and b). Since the gravity effects are minimized, the foams are coated on all sides. This is somewhat different as opposed to coating heavier substrates such as metals and ceramics. As we increased the time of soaking, the strips were fully covered without clogging the pores with bone mineral-like apatite during the coating process. Higher magnification micrographs (Fig. 7.5c and d) show that there is no difference in morphology when the soaking time was increased from 3 to 7 days. Low magnifications showed the globules of apatite and the high

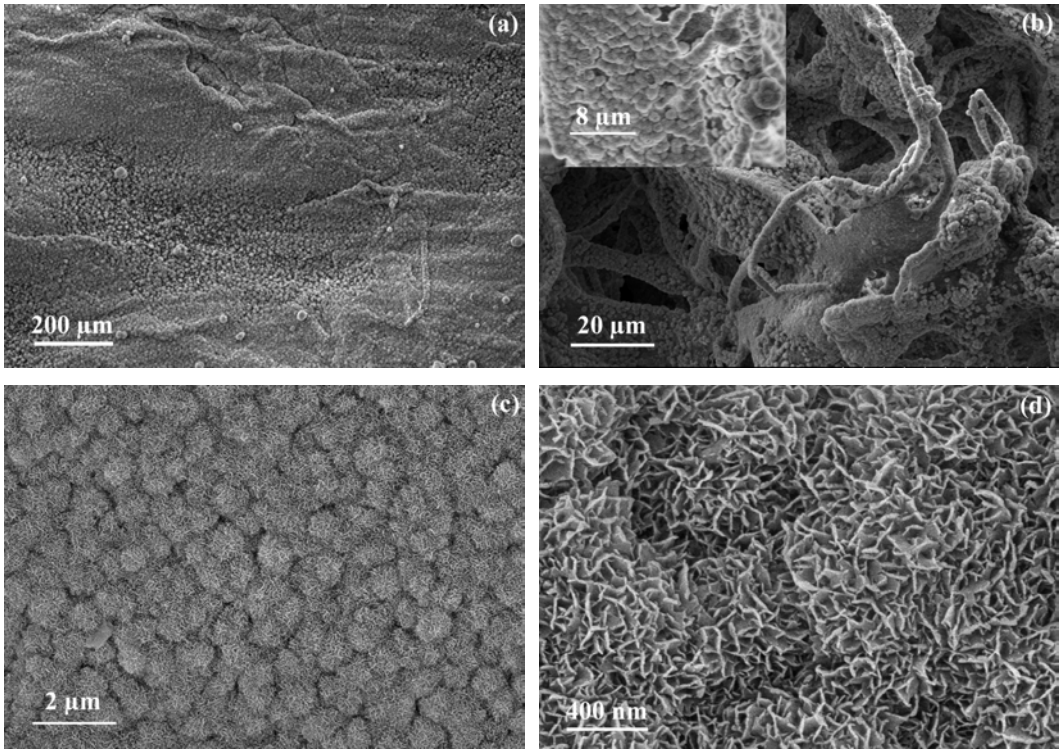

Fig. 7.5 FE-SEM micrographs of collagen membrane soaked in *t*-SBF for a period of 7 days; (a) full surface coverage was observed, (b) the pores were not blocked, (c) the globules become clearly visible, and (d) these globules have the nano-porous morphology.

magnifications showed the nano-sized needles on these globules. Of particular interest was the fact that the surface of the untreated collagen membrane initially had micro-porosities, whereas after coating, the surface exhibited nano-porosities formed by the interlocking of the nano-sized needles.

7.3.4 *In Vitro Results*

Results of *in vitro* examinations with mouse osteoblast are summarized by the histograms in Figures 7.6a (Live/Dead cytotoxicity) and 7.6b (ALP activity). When compared with untreated collagen membranes, the SBF coated collagen resulted in an increase of attached cells and ALP activity. When viewed under FE-SEM, the apatitic surfaces created by *t*-SBF solutions were found to be the more viable surface for osteoblasts to attach and grow than the untreated collagen surfaces. Figures 7.6c and d, represent untreated collagen foams, where the osteoblasts were only able to attach and then extend their filopodia over the available surface. Figures 7.6e and f represent osteoblast cell proliferation and attachment on SBF-coated foams. As evident in these figures, osteoblast cells were able to proliferate to the extent that even the vinculin adhesion plaques, the actin cytoskeleton and the stress fibers became visible. The response of the osteoblast to a given material is regarded as the sum of their ability to attach, proliferate, and differentiate. In the attachment stage, osteoblast filopodia explore the surface topography for areas to which a greater surface area of the cell can adhere. The filopodia are used in sensing the substrate, and extend over significant distances to find an appropriate area to attach. Osteoblast cells produce fewer adhesion plaques while still in the process of migration.

7.4. Discussion

To the best of our knowledge, coating of collagen by soaking in *t*-SBF has never been performed. The collagen membrane was coated fully and homogeneously with bone mineral-like apatite in 7 days. The coated strips were then compared with the untreated strips in terms of osteoblast cell response. This discussion

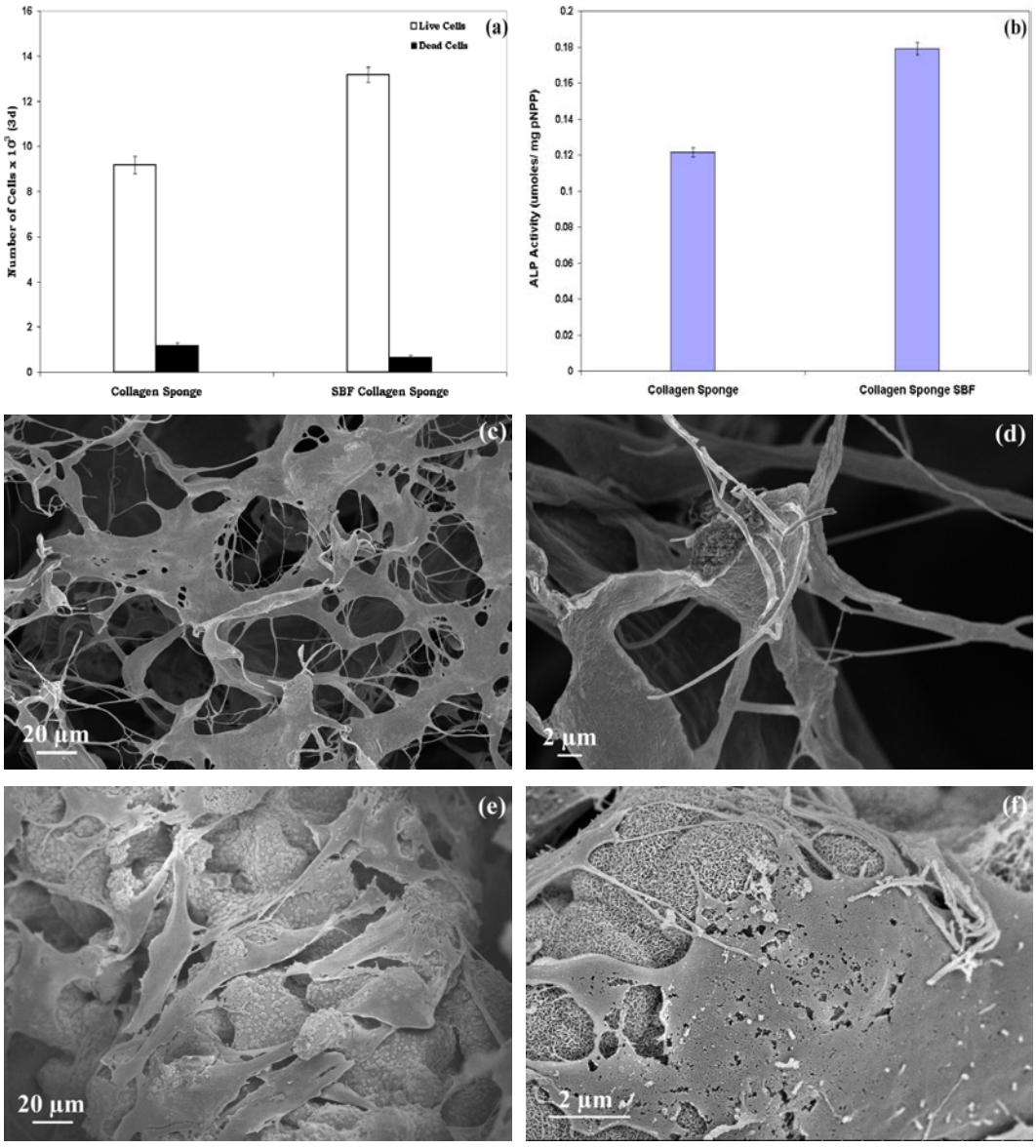

Fig. 7.6 *In vitro* (a) cell viability and (b) protein histograms for untreated and SBF-coated (7 days) collagen; Osteoblast proliferation and attachment on (c)-(d): untreated collagen membrane; (e)-(f): *t*-SBF coated collagen (7 days).

addresses the mechanisms of formation of carbonated apatitic calcium phosphates and the effects of several coating parameters on its formation.

7.4.1 *Formation of Bone Mineral-like Apatite in SBF Solution*

The SBF solution has a Ca/P ratio similar to that of human plasma, 2.50. Different chemical reagents are used to prepare different SBF solutions and reagents used to prepare *t*-SBF are mentioned in Section 3.3.2 Table 3.1. Various chemical reagents and their respective amounts have different effects on the coating phase formed in the solution. The presence of 1mM Na_2HPO_4 along with 2.5 mM $CaCl_2.2H_2O$ in the recipe helps in forming calcium phosphates. The presence of 27mM $NaHCO_3$ plays an important role and assists in the carbonating the coatings. The pH of the solution is another criterion in predicting the phase that will precipitate. If the pH of the solution is in the range of 5 to 6, then the precipitating phase is dicalcium phosphate dihydrate[37] and if the pH is 7.4 or higher, then the solution nucleates carbonated apatitic calcium phosphates. This means that the biomimetic coating process proceeds with the formation of carbonated apatitic calcium phosphates. The precipitation of carbonated apatitic calcium phosphates from the SBF solution may be described by the following reaction[38, 39]:

$$(10\text{-}x\text{-}y)Ca^{2+} + (6\text{-}x\text{-}y)HPO_4^{2-} + yHCO_3^{-} + 2H^{+} + 2OH^{-} = Ca_{10\text{-}x\text{-}y}[(HPO_4)_x(CO_3)_y(PO_4)_{6\text{-}x\text{-}y}](OH)_{2\text{-}x} + (8\text{-}x)H^{+}$$

The PO_4^{2-} sites of the calcium phosphates formed in the SBF solution are substituted with HPO_4^{2-} and CO_3^{2-}. The carbonate ion doping into the phosphate tetrahedral of apatitic calcium phosphates results in the creation of charge compensating Ca- vacancies, which is the reason for the observed Ca-deficiencies of calcium phosphates synthesized in SBF solutions. The addition of 112 mM NaCl into SBF solution leads to the substitution of a certain fraction of Ca-sites with monovalent Na^+ ions. Because the nature of the precipitates formed does not change with the addition of 5 mM K^+ and/or 0.5 mM SO_4^{2-} ions in the SBF solution, the precipitates are similar to the bone mineral. As described earlier, the

bone mineral consists of small sizes of biological apatite crystals containing substantial amounts of 4 to 6 % CO_3^{2-}, 0.5% Mg^{2+}, 0.7% Na^+, and is about 10% Ca-deficient.[1]

7.4.2 *Effect of HCO_3^- Ion Concentration on Coating Rate*

As previously reported, various researchers attempted to coat collagen substrates with bone mineral-like apatite using different SBF solutions.[12-20, 32, 33] The SBF solutions used in the past have been *c*-[12-20] and *r*-SBF[32, 33]. In this study, successful coating of collagen membrane was performed by using *t*-SBF as shown by SEM micrographs in Figure 7.5. Significant differences in the coating rates were observed in the present research in comparison to those performed earlier. It has been shown by various researchers that increasing the HCO_3^- ion concentration in the SBF solution resulted in a much thicker and a homogeneous carbonated apatitic calcium phosphate layer on substrates.[28, 34] Since *t*-SBF has a higher HCO_3^- concentration than *c*-SBF, faster coating rates are expected. By using *t*-SBF we were able to establish homogeneous coatings on collagen surface. It is also reported that *r*-SBF performed faster coating than *c*-SBF,[28, 32] which is due to the higher HCO_3^- concentration in *r*-SBF. Without any modification (being done to either collagen or SBF), collagen was reportedly coated in 2 weeks when soaked in *r*-SBF.[32] Collagen, when soaked in c-SBF, even duration of 4 weeks did not completely cover collagen.[13] The present study reports the coating of collagen by *t*-SBF in 7 days which is faster than the coatings formed by *c*-SBF. Thus, for biomimetic coating processes the usage of *t*- and/or *r*-SBF over *c*-SBF is preferable, since they have higher concentrations of HCO_3^-.

7.4.3 *Effect of Buffering Agent on the Coating Morphology*

Differences were also observed in the coating morphology of the apatitic calcium phosphates of the present study with those reported earlier. *t*-SBF formed round globules consisting of interlocking needle-like nanosize apatitic calcium phosphates (Fig. 7.5c and d) which were similar to those formed by c-SBF[12-20] as reported in previous studies. Girija et al.[32] used *r*-SBF for the coating of collagen fibrils, the precipitates formed on collagen were nearly spherical aggregates and clearly differed to those formed by *c*-SBF. These precipitates resembled those

formed by *Bigi*-SBF[26] (referred to as *b*-SBF), which is known as a HEPES-NaOH buffered 27 mM HCO_3^- SBF solution. Similar morphological differences in the coatings formed by the above-mentioned 3 SBF solutions on Ti6Al4V substrates were reported in a recent study.[28] This difference is possibly due to the different buffers used in the composition of the SBF solutions. While TRIS-HCl buffer was used in the preparation of *c*- and *t*-SBF solution, HEPES-NaOH buffer was used for *r*-SBF preparation. Therefore, the buffer used in preparing a specific SBF solution may have a significant influence on the morphology of the resultant coatings. This could be related to the effect of buffers on the stability of SBF solution which is explained in detail in the following paragraph.

7.4.4 *Effect of Buffering Agent on the Stability of SBF Solution*

The ionic strength of the SBF solution also plays a crucial role. *c*- and *t*-SBF solutions have the same ionic strength values, that is, 160.5 mM whereas *r*-SBF has a significantly lower value of 149.5 mM. CO_2 is released from an aqueous solution at a faster rate if the solution has a low ionic strength.[40] The release of CO_2 from the SBF solution in turn leads to an increase in the pH resulting in a decrease in the level of supersaturation of the solution. It was observed that the pH increase in case of *r*-SBF solutions was higher than those observed in *t*-SBF solutions. It is known that HEPES-NaOH buffered *r*-SBF is unable to retain the HCO_3^- ions to the same extent as those in the TRIS-HCl buffered *t*-SBF solutions. This conclusion is corroborated by other researchers who emphasized that HEPES buffer was unstable and release CO_2 from the solution.[28, 34, 35] Moreover, the pH of 7.4 is the lower end of the buffering capacity of TRIS buffer and this facilitates the formation of calcium phosphate nuclei or clusters in SBF solutions.[41] As compared to that, HEPES buffer has an even lower buffering capacity at a pH of 7.4.[42-44] This explains the instability of the HEPES-NaOH buffer and the *r*-SBF solutions. Moreover, the coatings deposited by *t*-SBF solutions on Ti6Al4V substrates performed much better than those formed by *c*- and *r*-SBF, when rat osteoblasts were cultured on them.[28] Thus, from the view point of coating stability, *t*-SBF was superior to *r*-SBF solution.

7.4.5 *In Vitro Osteoblast Response*

Untreated collagen and SBF-coated collagen membranes were compared via the alkaline phosphatase activity, cell density and cell proliferation tests by using rat osteoblasts (7F2) (Fig. 7.6). Higher cell density (Fig. 7.6a) and alkaline phosphatase activity (Fig. 7.6b) was observed for SBF-coated collagen membranes. This study compares the response of osteoblasts to two parameters: 1) the nano-porous surface of the SBF coating and the original micro-porous surface of the collagen membrane and 2) the chemistry of the materials, collagen vs. apatitic calcium phosphates. Scientists have demonstrated that osteoblast response is extremely sensitive to surface roughness and porosity.[45] It has also been previously reported that the proliferation numbers and alkaline phosphatase (ALP) activities of the osteoblasts improved by approximately 30-40% when comparing the smooth Thermanox control with the rougher calcium phosphate coatings.[46] In addition to differences in roughness, calcium phosphates differed in chemical composition with Thermanox. This study also found that rat osteoblasts were able to easily differentiate between the chemical composition of the surfaces on which they were seeded. In other words, osteoblasts preferred the surface of bone mineral-like apatite over the surface of pristine collagen membrane. It is a well-known fact that the surface chemistry of a material determines the initial *in vitro* interactions of proteins, such as fibronectin with integrin cell-binding domains, which in turn regulate the cell adhesion process. A difference in the osteoblast proliferation was also seen in the SEM micrographs (Fig. 7.6c, d, e and f). The osteoblast spread well on the apatitic calcium phosphate coatings with extending their filopodia and attaching to the nano-sized needles of the bone mineral-like apatite (Fig. 7.6e and f). An overall improved response in terms of osteoblast viability, ALP activity and proliferation was encountered on the apatitic calcium phosphate coating (Fig. 7.6). Thus, the results show that the apatite-coated collagen can be successfully employed as a scaffold material that will prove useful in repairing bone defects.

7.5. Conclusions

Porous collagen membranes with interconnected pores were completely coated biomimetically with apatitic calcium phosphates in 7 days by using 1.5x *t*-SBF solution. This study reports a faster and a more efficient way to coat collagen in comparison to the previous reported studies. SEM confirmed that the biomimetic process was able to cover all the surfaces without clogging the pores. XRD confirmed the nature of the apatitic nature of the coating and showed the strong similarity of the coating to the bone mineral. FTIR corroborated the results obtained by XRD, and showed the closeness in mimicking bone by the coatings. *In vitro* cell culture tests with 7F2 rat osteoblasts were used to compare the untreated collagen to the SBF-coated collagen membrane. The apatitic calcium phosphates formed by the SBF soaking exhibited higher cell attachment and alkaline phosphatase activity in comparison to the untreated collagen membrane. Under SEM it was determined that the osteoblasts on SBF-coated surface were more active and diffused more efficiently than the untreated collagen membrane.

7.6. References

1. L.L. Hench. Bioceramics: From concept to clinic. *J Am Ceram Soc* **74** (1991) 1487-1510.

2. D.D. Lee, C. Rey, M. Aiolova, A. Tofighi. Methods and products related to the physical conversion of reactive amorphous calcium phosphate. US Patent, No. 6117456, 2000.

3. A. Rovira, R. Bareille, I. Lopez, F. Rouais, L. Bordenave, C. Rey, M. Rabaud. Preliminary reports on a new composite material made of calcium phosphate, elastin peptides and collagens. *J Mater Sci Mater M* **4** (1993) 372-380.

4. N.J. Mathers, J.T. Czernuszka. Growth of hydroxyapatite on type 1 collagen. *J Mater Sci Lett* **10** (1991) 992-993.

5. S.-T. Liu. Composite materials for hard tissue replacement. U.S. Patent No. 5320844, 1994.

6. R.Z. Wang, F.Z. Cui, H.B. Lu, H.B. Wen, C.L. Ma, H.D. Li. Synthesis of nanophase hydroxyapatite/collagen composite. *J Mater Sci Lett* **14** (1995) 490-492.

7. Y. Doi, T. Horiguchi, Y. Moriwaki, H. Kitago, T. Kajimoto, Y. Iwayama. Formation of apatite-collagen complexes. *J Biomed Mater Res* **31** (1996) 43-49.

8. M. K. Kwan, S.D. Pacetti, R. K. Yamamoto. Bone grafting matrix. U.S. Patent No. 6187047, 2001.

9. R.K. Yamamoto, M. K. Kwan, S.D. Pacetti. Tissue repair matrix. U.S. Patent No. 6764517, 2004.

10. L.A. Sena, P. Serricella, R. Borojevic, A.M. Rossi, G.A. Soares. Synthesis and characterization of hydroxyapatite on collagen gel. *Key Eng Mater* **254-256** (2004) 493-496.

11. B.-H. Yoon, H.-W. Kim, S.-H. Lee, C.-J. Bae, Y.-H. Koh, Y.-M. Kong, H.-E. Kim. Stability and cellular responses to fluorapatite–collagen composites. *Biomaterials* **26** (2005) 2957–2963.

12. S.-H. Rhee, J. Tanaka. Hydroxyapatite coating on a collagen membrane by a biomimetic method. *J Am Ceram Soc* **81** (1998) 3029-3031.

13. S.-H. Rhee, J.D. Lee, J. Tanaka. Nucleation of hydroxyapatite crystal through chemical interaction with collagen. *J Am Ceram Soc* **83** (2000) 2890-2892.

14. L.-J. Zhang, X.-S. Feng, H.-G. Liu, D.-J. Qian, L. Zhang, X.-L. Yu, F.-Z. Cui. Hydroxyapatite/collagen composite materials formation in simulated body fluid environment. *Mater Lett* **58** (2004) 719-722.

15. A. L. Andrade, J. M. F. Ferreira, R.Z. Domingues. Zeta potential measurement in bioactive collagen. *Mater Res* **7** (2004) 631-634.

16. D. Lickorish, J.A. Ramshaw, J.A. Werkmeister, V. Glattuer, C.R. Howlett. Collagen-hydroxyapatite composite prepared by biomimetic process. *J Biomed Mater Res A* **68** (2004) 19-27.

17. N. Kobayashi, K. Onuma, A. Oyane, A. Yamazaki. The role of phosvitin for nucleation of calcium phosphates on collagen. *Key Eng Mater* **254-256** (2004) 537-540.

18. X. Li, J. Chang. Preparation and characterization of bioactive collagen/wollastonite composite scaffolds. *J Mater Sci Mater M* **16** (2005) 361-365.

19. D. Eglin, S. Maalheem, J. Livage, T. Coradin. *In vitro* apatite forming ability of type I collagen hydrogels containing bioactive glass and silica sol-gel particles. *J Mater Sci Mater M* **17**, 161– 167 (2006).

20. X.Y. Lin, H.S. Fan, X.D. Li, M. Tang, X.D. Zhang. Evaluation of bioactivity and cytocompatibility of nano-HA/collagen composite *in vitro*. *Key Eng Mater* **284-286** (2005) 553-556.

21. T. Kokubo. Surface chemistry of bioactive glass-ceramics. *J Non-Cryst Solids* **120** (1990) 138-151.

22. T. Kokubo. Apatite formation on surfaces of ceramics, metals and polymers in body environment. *Acta Mater* **46** (1998) 2519-2527.

23. T. Kokubo, H.-M. Kim, M. Kawashita, T. Nakamura. Bioactive metals: preparation and properties. *J Mater Sci Mater M* **15** (2004) 99-107.

24. D. Bayraktar, A. C. Tas. Chemical preparation of carbonated calcium hydroxyapatite powders at 37°C in urea-containing synthetic body fluids. *J Eur Ceram Soc* **19** (1999) 2573-2579.

25. A. C. Tas. Synthesis of biomimetic Ca-hydroxyapatite powders at 37°C in synthetic body fluids. *Biomaterials* **21**, 1429-1438 (2000).

26. A. Bigi, E. Boanini, S. Panzavolta, N. Roveri. Biomimetic growth of hydroxyapatite on gelatin films doped with polyacrylate. *Biomacromolecules* **1**, 752-756 (2000).

27. H.-M. Kim, K. Kishimoto, F. Miyaji, T. Kokubo, T. Yao, Y. Suetsugu, J. Tanaka, T. Nakamura. Composition and structure of apatite formed on organic polymer in simulated body fluid with a high content of carbonate ion. *J Mater Sci Mater M* **11** 421-426 (2000).

28. S. Jalota, S.B. Bhaduri, A.C. Tas. Effect of carbonate content and buffer used in SBF solutions on calcium phosphate formation on Ti6Al4V. *J Mater Sci Mater M* **17** (2006) 697-707.

29. J.D. Sallis. Structure/performance relationships of phosphorus and carboxyl containing additives as calcium phosphate crystal growth inhibitors. *Calcium Phosphates in Biological and Industrial Systems*, Edited by Z. Amjad, Kluwer Academic Publishers, Boston, MA 173-191 (1998).

30. K.S. Hwang, J.E. Song, J.W. Jo, H.S. Yang, Y.J. Park, J.L. Ong and H.R. Rawls. Effect of poling conditions on growth of calcium phosphate crystals in ferroelectric $BaTiO_3$ ceramics. *J Mater Sci Mater M* **13** (2002) 133-138.

31. T. Kokubo. Bioactivity of glasses and glass ceramics in bone bonding biomaterials. *Reed Healthcare Communications Netherlands* 31-46 (1992).

32. E. K. Girija, Y. Yokogawa, F. Nagata. Bone-like apatite formation on collagen fibrils by biomimetic method. *Chem Lett* **7** (2002) 702-703.

33. E.K. Girija, Y. Yokogawa, F. Nagata. Apatite formation on collagen fibrils in the presence of polyacrylic acid. *J Mater Sci Mater M* **15** (2004) 593-599.

34. E. I. Dorozhkina, S. V. Dorozhkin. Surface mineralization of hydroxyapatite in modified simulated body fluid (mSBF) with higher amounts of hydrogencarbonate ions. *Coll Surface A* **210** (2002) 41-48.

35. A. Oyane, K. Onuma, A. Ito, H.-M. Kim, T. Kokubo, T. Nakamura. Formation and growth of clusters in conventional and new kinds of simulated body fluids. *J Biomed Mater Res A* **64** (2003) 339-348.

36. Z. Molnar. Additional observation on bone crystal dimentsions. *Clin Orthop* **17** (1960) 38-42.

37. R. Tang, C. A. Orme, G. H. Nancollas. A new understanding of demineralization: The dynamics of brushite dissolution. *J Phys Chem B* **107** (2003) 10653-10657.

38. T. Leventouri, B. C. Chakoumakos, N. Papanearchou, V. Perdikatsis. Comparison of crystal structure parameters of natural and synthetic apatites from neuron powder diffraction. *J Mater Res* **16** (2001) 2600-2606.

39. T.I. Ivanova, O.V. Frank-Kamenetskaya, A.B. Koltsov, V.L. Ugolkov. Crystal structure of calcium-deficient carbonated hydroxyapatite. Thermal decomposition. *J Sol State Chem* **160** (2001) 340-349.

40. F. Barrere, C.A. van Blitterswijk, K. de Groot, P. Layrolle. Influence of ionic strength and carbonate on the Ca-P coating formation from SBF X 5 solution. *Biomaterials* **23** (2002) 1921-1930.

41. J. Pratt, J.D. Cooley, C.W. Purdy, D.C. Straus. Lipase activity from strains of Pasteurella Multocida. *Current Microbiology* **40** (2000) 306-309.

42. W.R. Harris, A.M. Carrferty, S. Abdollahi, K. Trankler. Binding of monovalent anions to human serum transferring. *Biochimica et Biphyisca Acta* **1383** (1998) 197-210.

43. B.R. van Dyke, D.A. Clopton, P. Saltman. Buffer-induced anomalies in the Fenton chemistry of iron and copper. *Inorg Chimica Acta* **242** (1996) 57-61.

44. R.W. Wilson, M. Grosell. Intestinal bicarbonate secretion in marine teleost fish-source of bicarbonate, pH sensitivity, consequences for whole animal acid-base and calcium homeostasis. *Biochimica et Biophysica Acta* **1618** (2003) 163-174.

45. K.J.L. Burg, S. Porter, J.F. Kellam. Biomaterial developments for bone tissue engineering. *Biomaterials* **21** (2000) 2347–2359.

46. H.W. Kim, G. Georgiou, J.C. Knowles, Y.H. Koh, H.E. Kim. Calcium phosphates and glass composite coatings on zirconia for enhanced biocompatibility. *Biomaterials* **25** (2004) 4203-4213.